SIMULATION OF CIRCULATING FLUIDIZED BED COMBUSTORS

A THESIS SUBMITTED TO
THE GRADUATE SCHOOL OF NATURAL AND APPLIED SCIENCES
OF
MIDDLE EAST TECHNICAL UNIVERSITY

BY

YUSUF GÖĞEBAKAN

IN PARTIAL FULFILLMENT OF THE REQUIREMENTS
FOR
THE DEGREE OF DOCTOR OF PHILOSOPHY
IN
CHEMICAL ENGINEERING

SEPTEMBER 2006

Approval of the Graduate School of Natural and Applied Sciences.

Prof. Dr. Canan Özgen
Director

I certify that this thesis satisfies all the requirements as a thesis for the degree of Doctor of Philosophy.

Prof. Dr. Nurcan Baç
Head of Department

This is to certify that we have read this thesis and that in our opinion it is fully adequate, in scope and quality, as a thesis for the degree of Doctor of Philosophy.

Prof. Dr. Nevin Selçuk
Supervisor

Examining Committee Members

Prof. Dr. Nurcan Baç	(METU, CHE)	
Prof. Dr. Nevin Selçuk	(METU, CHE)	
Prof. Dr. İnci Eroğlu	(METU, CHE)	
Prof. Dr. Faruk Arınç	(METU, ME)	
Prof. Dr. Ali Durmaz	(Gazi Unv., ME)	

I hereby declare that all information in this document has been obtained and presented in accordance with academic rules and ethical conduct. I also declare that, as required by these rules and conduct, I have fully cited and referenced all material and results that are not original to this work.

Name, Last name : Yusuf Göğebakan

Signature :

ABSTRACT

SIMULATION OF CIRCULATING FLUIDIZED BED COMBUSTORS

Göğebakan, Yusuf

Ph.D., Department of Chemical Engineering

Supervisor: Prof. Dr. Nevin Selçuk

September 2006, 170 pages

A dynamic mathematical model for simulation of atmospheric circulating fluidized bed combustors has been developed on the basis of first principles and empirical correlations. The model accounts for dense and dilute zone hydrodynamics, volatiles release and combustion, char particles combustion and their size distribution, and heat transfer from/to gas, particles, waterwalls and refractory.

Inputs to the model include configuration and dimensions of the combustor and its internals, air and coal flows, coal analysis, all solid and gas properties, inlet temperatures of air, cooling water, and feed solids, size distribution of feed solids; whereas outputs include transient values of combustor temperatures, gas concentrations, char and inert hold-ups and their size distributions.

The solution procedure employs method of lines approach for the governing non-linear partial differential equations and combined bisection and secant rule for non-linear algebraic equations. The initial conditions required for the model are

provided from the simultaneous solution of governing equations of dynamic model with all temporal derivatives set to zero. By setting all temporal derivatives to zero, model can also be utilized for steady state performance prediction.

In order to assess the validity and predictive accuracy of the model, it was applied to the prediction of the steady state behavior of Technical University of Nova Scotia 0.3 MWt CFBC Test Rig and predictions were compared with measurements taken on the same rig. Comparison of model predictions at steady state conditions revealed that the predictions of the model are physically correct and agree well with the measurements and the model is successful in qualitatively and quantitatively simulating the processes taking place in a circulating fluidized bed combustor.

Keywords: Circulating fluidized bed, dynamic simulation, coal combustion.

ÖZ

DOLAŞIMLI AKIŞKAN YATAKLI YAKICILARIN BENZETİŞİMİ

Göğebakan, Yusuf
Doktora, Kimya Mühendisliği Bölümü
Tez Yöneticisi: Prof. Dr. Nevin Selçuk

Eylül 2006, 170 sayfa

Atmosferik dolaşımlı akışkan yataklı yakıcıların benzetişimi için temel prensiplerden ve deneysel bağıntılardan hareketle bir matematiksel model geliştirilmiştir. Model tanecik yoğun bölge ve tanecik seyreltik bölge hidrodinamiğini, uçucu madde salınımı ve yanmasını, koklaşmış kömür parçacıklarının yanmasını ve boyut dağılımını ile gaz, parçacık, su duvarları ve refrakter arasındaki ısı transferini göz önüne almaktadır.

Modelin girdileri yakıcının konfigürasyonu ve boyutları, hava ve kömür debileri, kömür analizi, tüm katı ve gaz özellikleri, kömür soğutma suyu ve beslenen malzemelerinin sıcaklıları ve boyut dağılımı olup, modelin çıktıları ise zamana bağlı yakıcı sıcaklıkları, gaz konsantrasyonları, kok ve yatak malzemesi miktarları ve boyut dağılımlarıdır.

Çözüm metodunda kısmi diferansiyel denklemlerin çözümü için çizgiler yöntemi, doğrusal olmayan cebirsel denklemlerin çözümü için ise bütünleşik çift bölme ve sekant kuralı kullanmıştır. Model için gereken ilk değerler model denklemlerinin

zamana bağlı türevlerinin sıfıra eşitlenip çözülmesiyle elde edilmiştir. Zamana bağlı türevlerinin sıfıra eşitlenmesi ile model yatışkın durum performansının öngörülmesi için de kullanılabilmektedir.

Matematiksel modelin geçerliliğini ve öngörülerinin doğruluğunu test etmek amacıyla model Nova Scotia Teknik Üniversitesi 0.3 MWt DAYY Test ünitesinin yatışkın durumda çalışırken ki davranışının belirlenmesine uygulanmış ve öngörülerin doğruluğu aynı test ünitesi üzerinde alınan ölçümlerle yapılan karşılaştırma ile değerlendirilmiştir. Yatışkın durumdaki ölçümlerin ve model sonuçlarının karşılaştırılması öngörülerin fiziksel olarak doğru ve ölçümlerle uyum içerisinde olduğunu ve modelin dolaşımlı akışkan yataklı yakıcıda gerçekleşen olayların nicel ve nitel temsilinde başarılı olduğunu göstermiştir.

Anahtar Kelimeler: Dolaşımlı akışkan yatak, dinamik benzetişim, kömür yanması.

To my wife, Zuhal

ACKNOWLEDGMENTS

I have been blessed to receive the support of many wonderful people while producing this work. First and foremost, I would like to express sincere gratitude to my supervisor Prof. Dr. Nevin Selçuk, without whom this thesis would not exist, for her guidance, advice and constant encouragement throughout the development of this work.

I am also grateful to Prof. Dr. İnci Eroğlu and Prof. Dr. Faruk Arınç for their precious discussions and comments during the progress of this work. They helped me in many aspects of this study from the very beginning till the completion of the thesis.

I would like to thank my family, Gülizar and İsmail Göğebakan and Nazife and Mehmet Coşkun, for their continued support and encouragement. I am indebted to my family for their unshakable faith in me.

At last, but not least, a debt of my warmest thanks goes to my wife, Zuhal, for her understanding, endless patience and encouragement when it was most required.

TABLE OF CONTENTS

LIST OF TABLES

LIST OF FIGURES

LIST OF SYMBOLS

a	Decay constant, $1/m$
A	Cross-sectional area, m^2
A_o	Area of distributor plate per orifice, m^2
Ar	Archimedes number, *dimensionless*
b	Rosin-Rammler size distribution function parameter, *dimensionless*
B	Slope parameter in Equation (3.55), *dimensionless*
c	Fraction of unreacted coal on dry-ash-free basis, *dimensionless*
c_p	Specific heat capacity, $J/kg \cdot K$
C	Concentration, mol/m^3
$\overline{C}$	Average concentration, mol/m^3
C_d	Drag coefficient, *dimensionless*
D	Riser diameter, m; Cyclone diameter, m; Diameter, m
D_d	Dust exit diameter of cyclone, m
D_e	Gas exit diameter of cyclone, m
$d_b(z)$	Bubble size, m
$\overline{d}_b$	Mean bubble size, m
D_e	Diameter of vortex finder, m
d_p	Particle diameter, m
d_{p50}	Cut diameter of cyclone, m
$\mathcal{D}$	Diffusivity of oxygen in nitrogen, m^2/s
D_t	Diameter of riser, m
E	Entrainment rate, $kg/m^2 \cdot s$; Activation energy, J/mol
E_o	Mean activation energy, J/mol
f	Parameter in Equation (3.4), *dimensionless*
f_r	CO/CO_2 product ratio, *dimensionless*
$f(E)$	Activation energy distribution function for devolatilization, mol/J
F	Flow rate, kg/s
Fr_D	Froude number based on riser diameter, *dimensionless*
g	Gravitational acceleration, m/s^2

G_s	Net solid circulation flux, $kg/m^2 \cdot s$
h	Individual heat transfer coefficient, $J/m^2 \cdot s \cdot K$
H	Height of riser, m; Height of cyclone inlet, m
H_d	Height of dense zone, m
H_f	Height of dilute zone, m
ΔH^o	Heat of reaction at standard state, J/mol
k	First and n-th order reaction rate constant for devolatilization, $1/s$; Thermal conductivity, $J/m \cdot s \cdot K$
k_{CO}	Reaction rate constant for CO combustion, $mol^n/m^{3n} \cdot s$
k_f	Film mass transfer coefficient, m/s
k_i	Reaction rate constant for ith devolatilization reaction, $1/s$
$k_{1,2}$	First order reaction rate constants for competing reactions model of devolatilization, $1/s$
k_o	Pre-exponential factor for first and nth order devolatilization, $1/s$; Pre-exponential factor for CO/CO_2 product ratio expression, *dimensionless*; Pre-exponential factor for nth order surface reaction rate constant for carbon consumption, $m^{3n-2}/mol^{n-1} \cdot s$; Pre-exponential factor for CO combustion, $mol^n/m^{3n} \cdot s$
k_s	nth order surface reaction rate constant for carbon consumption, $m^{3n-2}/mol^{n-1} \cdot s$
K	Parameter in Equation (3.57), *dimensionless*
$K1$	Parameter in Equation (3.11), *dimensionless*
$K2$	Parameter in Equation (3.11), *dimensionless*
K_{be}	Interphase mass transfer coefficient, $1/s$
L	Length, m
L_b	Length of cylindrical part of cyclone, m
L_c	Length of conical part of cyclone, m
M	Solid hold-up, kg; Molecular weight, kg/mol
n	Molar flow rate, mol/s; Rosin-Rammler size distribution function parameter, *dimensionless*; Reaction rate order, *dimensionless*
n_C	Carbon consumption rate, $mol/m^3 \cdot s$
N_e	Number of effective turns, *dimensionless*
N_H	Number of inlet velocity heads, *dimensionless*
P	Pressure, Pa
Pr	Prandtl number, *dimensionless*
ΔP	Pressure drop, Pa
$P(r)$	Size distribution function, $1/m$

q	Heat flux, $J/m^2 \cdot s$
Q	Volumetric flow rate, m^3/s; Energy generation/loss rate, J/s
R	Ideal gas constant, $J/mol \cdot K$; Radius, m
$\boldsymbol{R}$	Energy generation/loss rate in dilute zone, $J/m^3 \cdot s$
R_{fw}	Thermal resistance across the dilute zone wall, $J/m^2 \cdot s \cdot K$
Re	Reynolds number, *dimensionless*
Re_c	Reynolds number based on transition velocity, *dimensionless*
Re_D	Reynolds number based on riser diameter, *dimensionless*
Re_{mf}	Reynolds number based on minimum fluidization velocity, *dimensionless*
Re_p	Reynolds number based on particle diameter, *dimensionless*
Re_t	Reynolds number based on terminal velocity, *dimensionless*
$\Re(r)$	Shrinkage rate of char particles, m/s
r	Spatial independent variable, m
r_C	Carbon consumption rate on the surface of char particle, $mol/m^2 \cdot s$
r_{CO}	Rate of CO combustion, $mol/m^3 \cdot s$
r_{max}	Maximum particle radius, m
r_{min}	Minimum particle radius, m
S	Length of vortex finder, m
Sc	Schmidt number, *dimensionless*
u	Velocity, m/s
u_0	Superficial gas velocity, m/s
u_b	Bubble rising velocity, m/s
u_c	Transition velocity to turbulent fluidization, m/s
u_{mf}	Minimum fluidization velocity, m/s
u_s	Solid velocity, m/s
u_t	Terminal velocity, m/s
u_{tf}	Throughflow velocity, m/s
v	Fraction of volatiles released, *dimensionless*
v_∞	Fraction of volatiles released at $t = \infty$, *dimensionless*
$v_{\infty,i}$	Fraction of volatiles released at $t = \infty$ for ith devolatilization reaction, *dimensionless*
V	Volume, m^3
V_{in}	Cyclone inlet velocity, m/s
t	Time, s

T	Temperature, K
T_∞	Ambient temperature, K
W	Width of cyclone inlet, m
$W(r)$	Dummy variable used for solution of char PSD, kg/m
x	Spatial independent variable, m; Mass fraction on dry basis, *dimensionless*
x_{vl}	Fraction of volatile matter released to dense zone, *dimensionless*
y	Mole fraction, *dimensionless*
z	Spatial independent variable, m

Greek Letters

α	Thermal diffusivity, m^2/s
$\alpha_{1,2}$	Maximum volatile matter released via devolatilization routes 1 and 2 of competing reactions model of devolatilization, *dimensionless*
δ	Bubble phase volume fraction, *dimensionless*
δ_a	Annular layer thickness, m
ϕ_s	Sphericity, *dimensionless*
ψ	Dummy variable defined in Equation (3.216), K/m
η_{cyc}	Cyclone efficiency, *dimensionless*
ϵ	Emissivity, *dimensionless*
ε	Volume fraction, *dimensionless*
$\overline{\varepsilon}$	Cross-sectional average volume fraction, *dimensionless*
ε_{mf}	Voidage at minimum fluidization, *dimensionless*
$\kappa(r)$	Elutriation rate constant, $1/s$
$\kappa^*(r)$	Elutriation rate constant, $kg/m^2 \cdot s$
$\lambda^o_{H_2O}$	Latent heat of vaporization, J/kg
μ	Viscosity, $N \cdot s/m^2$
σ	Standard deviation of activation energy distribution, J/mol; Stefan-Boltzmann constant, $J/m^2 \cdot s \cdot K^4$
ρ	Density, kg/m^3
ζ	Mechanism factor for CO/CO_2 product ratio, *dimensionless*

Subscripts

0	Feed
1	Bed drain

2	Riser exit
3	Recycle
4	Fly ash
a	Air
ash	Ash
b	Bubble
c	Char
C	Carbon
cyc	Cyclone
$comb$	Combustible
d	Dense zone
dw	Dense zone wall
e	Emulsion, Exit
f	Dilute zone
fc	Fixed carbon
fw	Dilute zone wall
g	Gas
i	Inert; ith devolatilization reaction
j	Species index
max	Maximum
mf	Minimum fluidization
min	Minimum
o	Dense zone surface; Outer surface
p	Particle
pri	Primary
ps	Pressure seal
r	Radiation
rec	Recycle
ref	Reference
rxn	Reaction
s	Solid, Particle surface
sec	Secondary
sp	Stand pipe
sus	Suspension
vm	Volatile matter

w	Wall
x	x-direction
z	z-direction

Abbreviations

BFB	Bubbling Fluidized Bed
CFB	Circulating Fluidized Bed
CFBC	Circulating Fluidized Bed Combustor
CFD	Computational Fluid Dynamics
EDF	Electricitê de France
EFBHE	External Fluid Bed Heat Exchanger
HHV	Higher Heating Value
METU	Middle East Technical University
MOL	Method of Lines
MWe	MegaWatt Electric
MWt	MegaWatt Thermal
ODE	Ordinary Differential Equation
OTU	Once Through Unit
PC	Pulverized Coal-Fired
PDE	Partial Differential Equation
PSD	Particle Size Distribution
TUNS	Technical University of Nova Scotia

CHAPTER 1

INTRODUCTION

1.1 General

Today, demand for electric power continues to rise steeply due to population growth, economic development, and progressive substitution of alternate technology with clean forms of energy generation. Coal has re-emerged as a major energy source for power generation after having played a subsidiary role to oil during the mid 20th century. Today about 40 % of all world electricity is generated from coal, almost double that of its nearest competitor, namely gas (Table 1.1).

Table 1.1: World electricity generation in 2003 [1].

Fuel	GWh	%
Coal	6681339	39.9
Gas	3224699	19.3
Hydro	2725824	16.3
Nuclear	2635349	15.7
Oil	1151729	6.9
Biomass	138207	0.8
Waste	62493	0.4
Others	122244	0.7
Total	**16741884**	**100.0**

As can be seen from Table 1.1, coal is the most important fuel source for electricity generation in the world today and would also continue to dominate the power station fuel scenario in the foreseeable future. Within the available clean coal technologies, atmospheric circulating fluidized bed (CFB) technology has emerged as an environmentally acceptable technology for burning a wide range of coal types to generate steam and electricity.

Development of CFBC boiler technology was initiated in the mid 1970s and its share in the world FBC boiler market has been increasing gradually since 1980s (Figure 1.1) with the trend to circulating fluidized bed combustion prevailing over bubbling fluidized bed combustion.. This was due to its advantages over bubbling FBC, e.g., better combustion efficiency, fewer fuel feed points and therefore simpler fuel feed system, lower limestone requirement due to longer gas/solid contact time.

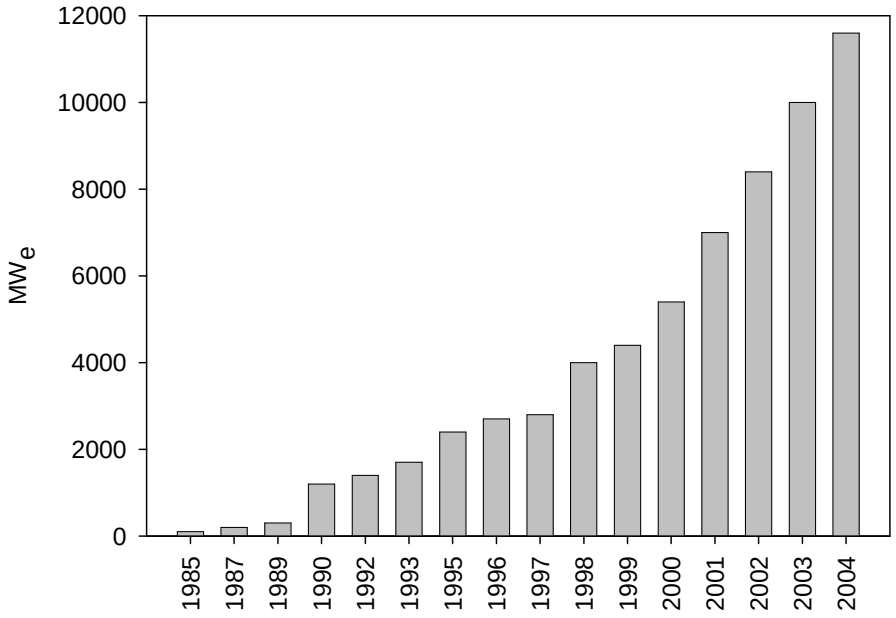

Figure 1.1: Total installed CFB power plant capacity (>100 MWe)

Although less than 30 years old, today CFB has established its position as utility scale boiler technology. The number of installations as well as their size grow rapidly. Plant sizes up to 300 MWe are in operation today and designs for larger boilers (600 - 800 MWe) are being developed. The largest circulating fluidized bed boilers in operation are two 300 MWe CFB boilers at Jacksonville Energy Authority in Jacksonville, Florida, U.S.A and are based on natural circulation with sub-critical steam parameters. The largest circulating fluidized bed boiler under construction, on the other hand, is 460 MWe Lagisza CFB boiler at Poludniowy Koncern Energetyczny SA in Poland with supercritical steam parameters and once-through technology.

1.2 Description of CFB Boiler

A circulating fluidized bed (CFB) boiler is a fluidized bed furnace for generating steam by combustion of fuels under the fast bed regime of fluidization where fine solids are transported through the furnace at a velocity greater than the terminal velocity of individual particles. The major fraction of solids leaving the boiler is captured by a gas-solid separator and returned back to a point near the base of the furnace at a rate sufficiently high to cause a minimum degree of refluxing of solids in the furnace. Flow structure in the CFB boiler is shown schematically in Figure 1.2.

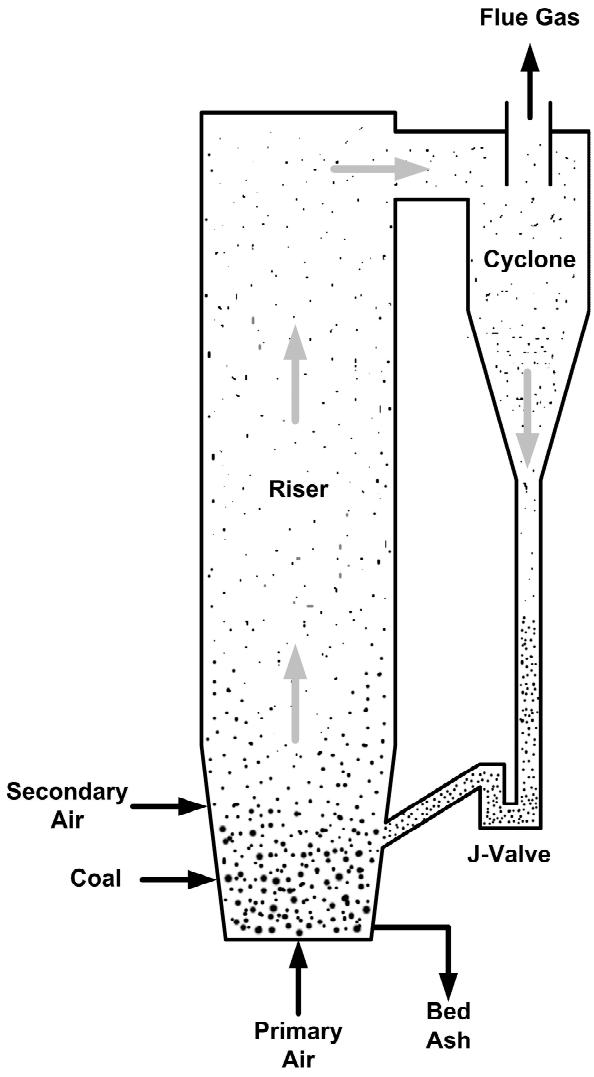

Figure 1.2: Schematic diagram of flow structure in CFB boiler.

A CFB boiler can be divided into two sections. The first section comprises of riser, gas-solid separator (cyclone or impact separator) and solid recycle device (loop seal, seal pot, L-valve or J-valve). These components form a solid circulation loop in which fuel is burned. The furnace enclosure of a CFB boiler is generally made of waterwalls as in pulverized coal-fired (PC) boilers. A fraction of the generated heat is absorbed by these heat-transferring tubes. The second section is the back-pass, where the remaining heat from the flue gas is absorbed by the reheater, superheater, economizer, and air-preheater surfaces. (Figure 1.3).

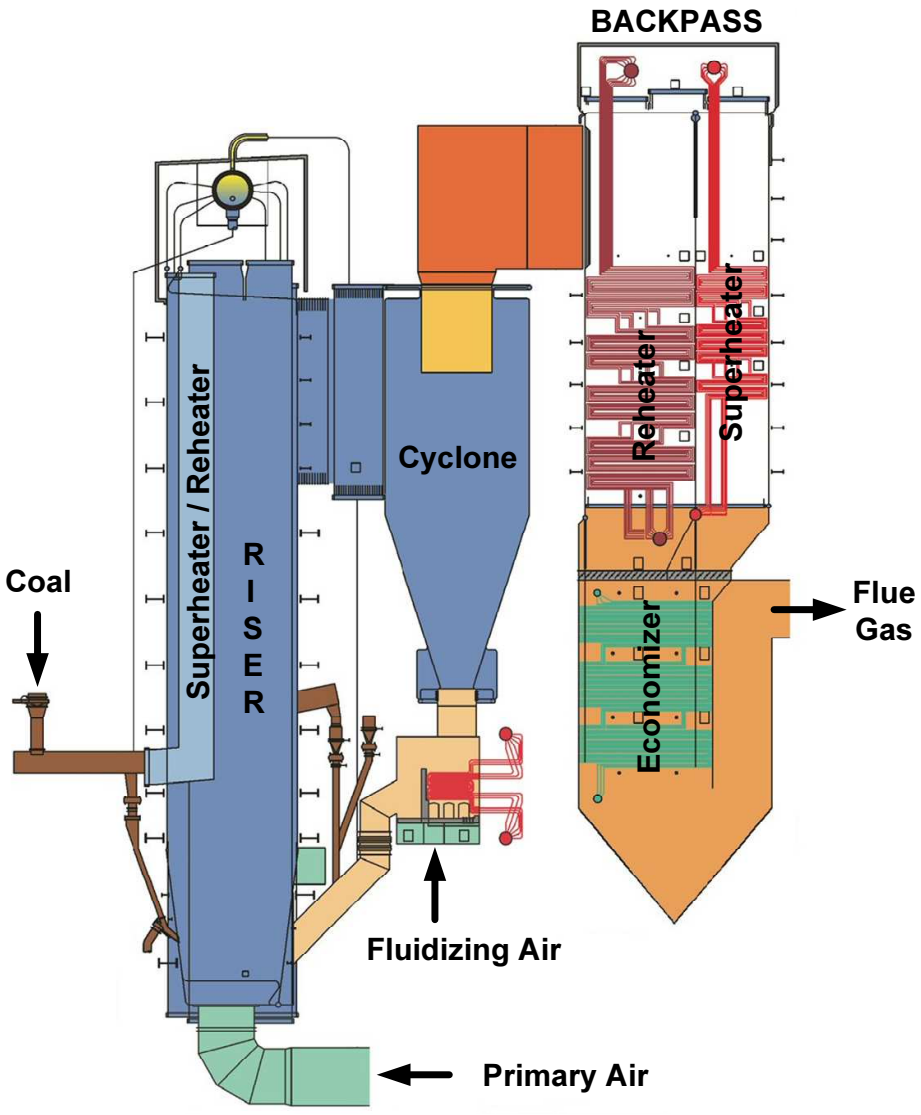

Figure 1.3: Schematic diagram of a CFB boiler.

The lower part of the furnace is smaller and often tapered in cross section. This helps to maintain good fluidization, even with segregated particles. This zone is characterized by a dense gas/solid mixture with rigorous mixing. The walls of the lower section are lined with refractory up to the level of secondary air entry or above so as to protect the tubes from possible corrosion from alternately oxidizing-reducing conditions. Beyond this level the furnace is uniform in cross section and larger than the lower part. The upper part of the furnace is characterized by a dense downward flowing annular region surrounding a dilute upward flowing core. The core-annulus flow structure causes an internal circulation of solids in the furnace.

Coal is generally injected into the lower section of the furnace. It is sometimes fed into the loop-seal, from which it enters the furnace along with returned hot solids. Limestone is fed into the bed in a similar manner. Coal burns when mixed with hot bed solids. Bed ash is extracted from the lower dense through the use of either fluid-bed or water-cooled screw ash coolers.

The primary combustion air enters the furnace through an air distributor at the furnace floor. The secondary air is injected at some height above the nozzles to complete the combustion. The lower part of the riser below secondary air ports is usually an extensively mixed bubbling or turbulent bed with fast fluidization above the secondary air ports. Usually 40 to 60 % of the total air is introduced as primary air.

Solids are well mixed throughout the height of the furnace. Thus, furnace temperature is nearly uniform in the range of 800-900°C, though heat is extracted along the evaporator walls of the furnace. Relatively coarse sorbent and unburned char particles are captured in the cyclone and are recycled back to the furnace. However, finer solid residues generated during combustion and desulfurization leave the furnace through the gas-solid separators, but they are collected by a bag-house or electrostatic precipitator.

1.3 Characteristics of CFB Boilers

Fuel Flexibility

One of the major attractive features of CFB boilers is its fuel flexibility. Fuel particles constitute less than 1-3% by weight of all solids in the furnace. The rest of the solids are noncombustibles: sorbents, fuel-ash or sand. The special hydrodynamic condition in the CFB furnace allows an excellent gas-solid and solid-solid mixing. Thus fuel particles fed to the furnace are quickly dispersed into the large mass of bed-solids, which rapidly heat the fuel particles above their ignition temperature without any significant drop in the temperature of the bed solids. This feature of a CFB furnace would ideally allow it to burn any fuel without the support of an auxiliary fuel, provided its heating value is sufficient to raise the combustion air and the fuel itself above its ignition temperature. Thus, a wide range of fuels can be burned in a CFB boiler without any major change in the design.

To maintain the combustion temperature within an optimum range, it is necessary to absorb a certain portion of the generated heat from the combustion zone. This fraction varies from one fuel to another. A CFB accomplishes this for different types of fuels by controlling the amount of heat absorbed in the furnace by adjusting the heat extraction from the recirculating solids outside the furnace by means of an external heat exchanger. In boilers without the external heat exchanger, the hydrodynamic condition of the furnace can be adjusted such as to change the solids concentration in the furnace; this, in turn, alters the heat absorbed by the furnace.

High Combustion Efficiency

The combustion efficiency of a CFB boiler is higher than that of bubbling fluidized bed boilers. It is generally in the range of 97.5 to 99.5% . The following features contribute to the high combustion efficiency of circulating fluidized bed combustors:

- Better gas-solid mixing

- Higher burning rate (especially for coarser particles)
- Recycling of unburned particles back to the furnace

The primary source of combustible loss in all types of fluidized bed combustors is the escape of fine carbon particles before they are burned. Fresh coal often contains a large amount of fines. In addition, a considerable amount of carbon fines are generated during combustion through attrition. In a bubbling fluidized bed combustor, these fines are easily entrained out of the fluidized bed, which is usually 0.5-1.5 m deep. The free space above the bubbling bed (freeboard), where particles are ejected, is not conducive to efficient combustion because of poor gas-solid mixing and relatively low temperature. Thus an appreciable amount of carbon fines escaping into the freeboard of a bubbling fluidized bed combustor leaves the system unburnt.

In a CFB boiler the combustion zone extends up to the top of the furnace and further beyond into the hot cyclone. Thus, carbon fines generated in the furnace have a greater time to burn during their travel through the height of the furnace and then through the rest of the circulating loop. The only combustible loss is due to the escape of carbon fines generated in the upper section of the furnace. In some boilers, re-injection of these fines from downstream sections (economizer hopper, precipitator, for example) of the cyclone are also used to minimize the carbon loss. Unlike bubbling beds, CFB boilers retain their efficiency over a wide range of operating condition, even when firing fuels with a considerable amount of fines.

Efficient Sulfur Removal

Sulfur capture in a CFB is more efficient than in a bubbling fluidized bed. A typical CFB boiler can capture 90% of the sulfur dioxide with only 1.5 to 2.5 times the stoichiometric amount of sorbent, while a bubbling fluidized bed boiler may require 2.5 to 3 or more for 90% capture [2].

Unlike combustion, the sulfur capture reaction is slow. Sulfur dioxide in the flue gas must remain in contact with calcined sorbents for a sufficient period of time

for complete conversion into calcium sulfate. The interior of sorbent particles is not readily available for sulfation reaction. In a bubbling fluidized bed, the average residence time of gas in the combustion zone is of the order of 1-2 seconds, while it is 3-4 seconds in a CFB. Furthermore, the average size of sorbents in a bubbling bed is about 1 mm, while that in a circulating fluidized bed is 0.1 mm. The specific reaction surface of a 0.1 mm particle is 10 times that of a 1.0 mm particle. Thus both utilization of sorbent particles and conversion of SO_2 in CFB are superior to that in bubbling beds.

Low NO_x Emission

The low emission of nitrogen oxides is a major attractive feature of both bubbling and circulating fluidized bed boilers as combustion takes place at relatively low temperatures (800-900 °C). Data collected in commercial CFB boilers suggest NO_x emission in the range of 50-150 ppm [3]. Such low levels of NO_x have been observed consistently in all commercial CFB boilers . At such temperatures nitrogen in the combustion air is not normally oxidized to NO_x.

Smaller Furnace Cross Section

A high heat release rate per unit furnace cross section is a major advantage of the CFB boiler. The CFB firing system has a grate heat release rate of about 3.5 to 4.5 MW/m^2 which is close to or higher than that of pulverized coal-firing [2]. Moreover, for a given thermal output, a bubbling fluidized bed boiler requires a furnace grate area 2 to 3 times larger than that of a CFB boiler. The high heat release rate of CFB boilers arises from the high superficial gas velocity (4-7 m/s). The intense gas-solid mixing promotes a high rate of heat liberation through rapid generation and dispersion of heat in the bed.

Fewer Feed Points

The fuel feed system is simplified in a CFB boiler due to its relatively small number of feed points. It requires less grate area for a given thermal output due to vigorous mixing resulting from higher gas velocities. Furthermore, good mixing and the extended combustion zone allow one feed point to serve a grate

area much larger than that in a bubbling bed. For example, a 100 MWt CFB boiler requires only one feed point, compared with 20 to 30 in a bubbling bed boiler of the same capacity [2].

1.4 Aim and Scope of the Thesis

Circulating fluidized bed boilers offer fuel flexibility, broad turn down ratio, relatively fast response to load changes and lower SO_2 and NO_x emissions. Thus, several hundred CFB boilers are in use in process and utility industries worldwide. Many of these commercial units spend a significant portion of their operating lives following the load changes when the fuel rate changes introducing a chain of transient events. Therefore, investigation of dynamic behavior of CFB combustors is of vital importance. Although a number of studies exists on the simulation of atmospheric CFB combustors under steady-state conditions, number of studies on predicting the complete transient behavior is limited.

Therefore, the objectives of the proposed study are:

- Development of a comprehensive code for dynamic simulation of CFB combustors,
- Application of the dynamic code to the prediction of steady state behavior of a CFB combustor,
- Assessment of the steady state performance of the code by comparing its predictions with experimental data available in the literature.

CHAPTER 2

REVIEW OF CFBC MODELS

2.1 General

Advantages of circulating fluidized bed combustion (CFBC) technology such as the ability to burn wide variety of fuels efficiently and to control pollutant emissions without flue gas treatment systems have led to a steady increase in its commercial use over the past decades. Increasing number of CFB boiler installations has led to the development of mathematical models in order to analyze new design, to optimize the process and to predict the emission and thermal performances over a broad range of operating conditions.

In the last two decades, substantial effort has been devoted to the development of a steady-state comprehensive mathematical models for circulating fluidized bed boilers [4–32]. However, number of studies on the understanding of the dynamic behavior of CFB boilers [33–43] is limited.

2.2 Previous Studies on Dynamic CFBC Modeling

Many of commercial CFB boilers spend a significant portion of their operating lives under off-design conditions due to either load changes or changing fuel quality due to complex and heterogenous nature of solid fuel. These changes usually lead to disruption of steady-state conditions, hence dynamic modeling becomes an essential requirement for the prediction of thermal and emission performances. Despite extensive research carried out on steady-state modeling [4–32], only a limited number of studies [33–43] has been carried out for dynamic modeling of CFB boilers. These studies are reviewed below.

Zhang *et al.* [33] performed one of the earliest studies on the dynamic modeling of CFB boilers and have developed a 1-D dynamic model on the basis of first principles while considering the wide size distribution of particles. Model includes riser, cyclone, hopper, L-valve and superheater bed, *i.e.*, external fluid bed heat exchanger(EFBHE). The combustor is divided into two zones. The bottom section of the bed, from the distributor plate to the secondary air injection point, is assumed to be a dense zone similar to a bubbling bed. The upper section above the secondary air injection level is assumed to be the dilute zone. The dilute zone is divided into several lumped-parameter blocks in series, within which gas and solids are assumed to be well-mixed in each block, and with no backmixing of gas between the blocks. The riser hydrodynamics is considered to be at steady-state as the gas and solid dynamics are assumed to be instantaneous. Dynamic changes of gas concentrations are directly related to the reaction rates. Change of char particles size distribution due to combustion and attrition also considered in the model. The only model validation provided is a comparison of the simulated dense zone temperature against measured data from a 20 t/h CFB boiler for a 16% step increase in the coal feeding rate and satisfactory agreement was reported.

Following Zhang *et al.* [33], Mori *et al.* [34] proposed a simplified dynamic model for a 70 t/h multisolid CFB boiler in order to develop an advanced control system. Model includes solid circulation line, *i.e.*, riser, cyclone, stand-pipe and L-valve, and external heat exchanger with consideration of combustion, heat generation and transfer. The riser is considered in three zones; a dense zone, a reducing zone and an oxidizing zone. Both gas and solids are considered to be well mixed in each of these zones and back flow of solids between these zones is taken into account. Volatiles release and combustion is assumed to be instantaneous in the dense zone. Neither SO_2 generation and capture nor NO_x formation and reduction is considered in the model. Solid hold-up through the riser is assumed to vary in the axial direction only and is obtained from steady-state pressure drop measurements taken from 70 t/h boiler. Transient hold-up is considered to change linearly between initial and final steady-state conditions. The model utilizes a

fudge factor, i.e. solids downflow ratio, representing backmixing between the three riser zones and this parameter is selected as 15 in order to match the measured and predicted temperature profiles of initial and final steady-state conditions. No dynamic model validation was presented by the authors.

Hyppanen *et al.* [35] presented a dynamic model for development of a dynamic process simulator to simulate energy balances of power plants and to analyze dynamic changes in water/steam cycles such as step changes in load. Therefore, model of Hyppanen *et al.* [35] incorporates not only the boiler, but also the water/steam cycle. CFB boiler model takes into account hydrodynamics, water vaporization, volatiles release and combustion, char combustion and heat transfer to steam cycle but neglects the dynamic behavior of emissions. The riser is divided into numerous compartments in series, each assumed to be well-mixed. The axial suspension density profile is determined using an empirical correlation, while the dynamics of these profiles are estimated with the aid of an experimentally determined time constant. The circulating mass flow rate is assumed to be constant through the riser and calculated from an empirical correlation. Volatiles release, burning and mixing are combined in a single expression and fitted to experimental data. Solid mixing between the cells has been described by using a dispersion model, details of which are not discussed. An empirical correlation for heat transfer coefficient is utilized in the model. Experimental data from the 125 MWe power plant were used to determine the parameters of empirical correlations and verification of dynamic model. Comparison between predictions and measurements shows reasonably good agreement. The authors also developed an advanced control structure based on the proposed dynamic model and reported improved load following capability based on the new control structure.

Similar to the objective of Mori *et al.* [34] and Hyppanen *et al.* [35], *i.e.* development of a process control structure based on a dynamic CFB model, Muir *et al.* [37] developed a global model to predict the transient response of the temperature, flue gas oxygen concentration and heat removed from an in-bed heat

exchanger in a CFB combustor. The model also includes an overlaying control structure which adjusts the model inputs in response to model outputs for process control purposes. In the model, suspension density is assumed to vary in the axial direction only and particles are represented by single effective mean particle diameter. Instantaneous devolatilization and subsequent volatiles combustion is assumed in the model. Variation of particle size due to combustion, fragmentation and attrition does not considered in the model. Moreover, it is assumed that gas and solids in the riser are at the same temperature and that particles introduced to the combustor are instantaneously heated to the combustion temperature. The temperature distribution in the furnace is neglected and whole CFB loop is represented by a single temperature obtained from a global energy balance. Unlike previous models, this model considers the thermal inertia of walls. The model is validated by comparing its predictions with step-response tests carried out on a pilot CFB combustor and generally very good agreements were reported.

To simulate the processes within the CFB combustor, Park and Basu [36] developed a dynamic model which predicts the transient temperature response of CFB combustor as well as the corresponding transient carbon and oxygen concentrations. The model includes mass balances of oxygen and carbon, energy balances, as well as sub-models for hydrodynamics, combustion and heat transfer to both refractory and waterwalls. Riser is divided into two parts, a turbulent dense zone and a fast bed. Fast bed section is broken down into homogeneous, fully-mixed cells. In order to account for radial variations, core-annulus model is utilized in the fast bed section. Particles are represented by single effective mean particle diameter. Thermal inertia of the refractory walls is also taken into consideration. Based on the assumption that hydrodynamic changes occurs much faster than thermal or concentration changes, steady-state hydrodynamics is utilized in the model. All volatiles are assumed to be released and burned in the turbulent zone whereas char is considered to burn throughout the CFB combustor loop. Performance of the proposed model is tested with measurements taken from a 0.3 MWt CFB combustor by performing experiments with step disturbance to

coal feed rate and good agreement between measured and predicted values of temperatures was observed.

An overall power plant model similar to Hyppanen *et al.* [35] is also presented by Remberg and Fett [38] whose model can consider subsystems for gas turbine, atmospheric or pressurized CFB boiler and water/steam cycle. In the CFB boiler subsystem, riser, lateral gas pass, cyclone, EFBHE and second pass is considered and these components are represented by well-mixed, homogeneous cells connected in series. CFB boiler model considers particle size distributions, fluid dynamics, drying, devolatilization, gas and solid phase reactions and heat transfer details of which are not given. Thermal inertia of the refractory walls is also taken into consideration. The only model validation is the steady-state furnace temperature prediction against measurements obtained from an atmospheric combined heat and power plant and sufficient agreement was reported.

To reflect the dynamic characteristics of a 220 t/h CFB boiler, Li *et al.* [39] developed a one-cell global dynamic CFB boiler model considering global mass and energy balances only. The proposed model neglects many physical aspects of CFB boiler and tries to form a basic engineering approach for modeling of dynamic behavior of CFB boiler. Authors present model predictions for load changes from 70% to 110% but do not provide experimental validation.

Following Li *et al.* [39], Costa *et al.* [40] developed a dynamic CFB boiler model to quantify plant flexibility and to determine transient behavior of the boiler. Model describes hydrodynamics, combustion, heat transfer in the circulation loop and also consider water/steam side. In the model, CFB boiler is divided into three zones. The first zone extends from the base of furnace to the secondary air injection ports. The second zone extends from the secondary air injection ports to the top of refractory lining zone. The third zone covers the rest to the top of the furnace. The external recirculation of the bed material through cyclone is described as the internal recirculation between the zones of the boiler.

Hydrodynamics of the boiler is described by a 1-D simplified model with two fluxes (one ascending and the other descending) for solids and with only one ascending flux for the gas. Size distributions in each zone is assumed to be uniform and all solids are represented by a single mean diameter. Volatiles release and combustion is assumed to be instantaneous. For heat transfer, correlations developed by Electricitè de France (EDF) are utilized. Proposed model was validated against data obtained from 250 MWe boiler and predictions were found to be in satisfactory agreement with the measurements.

Chen *et al.* [41] presents a dynamic model for large scale CFB boilers with water/steam cycle. The model uses cell approach to simulate the axial gas and solid distributions and core-annulus approach to describe the radial distribution of solids while taking into account wide size distribution of solids. Riser is divided into two parts, a turbulent dense zone and a fast bed consisting of cells in series. Mass and energy balances are performed for each cell, which is assumed to be homogeneous and well mixed. It is assumed that all the gas going upward in the dilute zone passes through core region only, *i.e.*, no gas flow in the annulus region. Moreover, size distributions of particles in the core and annulus regions are assumed to be identical. Similar to approach of Park and Basu [36], steady-state hydrodynamics is utilized in the model. No experimental validation of the dynamic model is provided. Instead, model predictions of 410 t/h pyroflow CFB boiler to step changes in coal feed rate is given.

Following their previous work, Kettunen *et al.* [42] presents a model based analysis of dynamic behavior of large scale CFB boiler by using a tailored dynamic CFB boiler simulator. Model parameters are obtained from a transient process tests. The fine-tuned model is then used to design the control systems of 262 MWe CFB units and control system development of a supercritical OTU CFB boiler. It is stated that the model consists of several sub-models based on fundamental laws of conservation of mass, energy and momentum and on empirical correlations. Model considers both CFB boiler and complete water/steam cycle including steam turbine and generator. As the model is developed by a commercial

boiler manufacturer, namely Foster Wheeler Finland, details of the model is not available due to the know-how. Model is tested against data obtained from a 235 MWe CFB boiler during changes in fuel feed rate, primary and secondary air flow rates, primary to secondary air ratio and load and good agreement was reported.

The last study carried on dynamic simulation of CFB boilers is done by Hongwei *et al.* [43]. In their study, they present a dynamic model of a 450 t/h CFB boiler. The model considers sub-models for gas-firing duct, CFB combustor, cyclone and J-valve and utilizes lump-parameter approximation. The combustor is divided into dense and dilute zones in which dense zone is represented by a bubbling bed whereas dilute zone is represented by core-annulus flow structure. For solution, dense and dilute zones are represented by series of cells having uniform properties. Particles are assumed to be spherical and represented by a mean particle size. Performance of the dynamic model was not tested against measurements.

2.3 Overview of the Models

Prominent features of studies carried out to model the dynamic response of a CFB boiler described above are briefly summarized in Table 2.1. As can be seen from the table, models are generally 1-D in nature and consider hydrodynamics, char combustion, volatiles release and combustion and heat transfer. They utilize steady-state hydrodynamics based on the assumption of fast hydrodynamic changes. Particles are represented by an average particle size in hydrodynamics and combustion calculations. Only some studies considered the thermal inertia of walls. Furthermore, some of the studies did not validated against experimental data or very limited validations were made.

Present study, on the other hand, provides a new model based on conservation equations for energy and chemical species in conservative form for both dense and dilute zones considering hydrodynamics, volatiles release and combustion, char combustion, char particles temperature and size distribution and heat transfer to both waterwalls and refractory for dynamic simulation of CFBCs.

Table 2.1: A summary of dynamic CFB models in the open literature.

Reference	Year	Dimension	Sub-models Included								Validation
			A	B	C	D	E	F	G	H	
Zhang *et al.* [33]	1991	1-D	YES	YES	YES	NO	YES	YES	NO	NO	YES
Mori *et al.* [34]	1991	1-D	YES	NO	YES	NO	YES	NO	NO	NO	NO
Hyppanen *et al.* [35]	1993	1-D	YES	NO	YES	YES	YES	NO	NO	YES	YES
Park and Basu [36]	1997	1.5-D	YES	NO	YES	NO	YES	NO	NO	NO	YES
Muir *et al.* [37]	1997	1-D	YES	NO	YES	NO	YES	NO	NO	NO	YES
Remberg and Fett [38]	1999	1-D	YES	YES	YES	NO	YES	NO	NO	YES	NO
Li *et al.* [39]	1999	0-D	NO	NO	YES	NO	YES	NO	NO	NO	NO
Costa *et al.* [40]	2001	1-D	YES	NO	YES	NO	YES	YES	NO	YES	YES
Chen *et al.* [41]	2001	1.5-D	YES	YES	YES	NO	YES	NO	NO	YES	NO
Kettunen *et al.* [42]	2003	N/A	N/A	N/A	N/A	N/A	N/A	N/A	N/A	N/A	YES
Hongwei *et al.* [43]	2003	0-D	YES	NO	YES	YES	YES	NO	NO	NO	NO

NOMENCLATURE

A : Hydrodynamics
B : Particle Size Distribution
C : Char Combustion
D : Volatiles Release and Combustion
E : Heat Transfer
F : SOx Retention
G : NOx Reduction
H : Water/Steam Cycle

CHAPTER 3

MODEL DESCRIPTION

3.1 Physical System

The physical system to be considered is a continuously operated atmospheric circulating fluidized bed combustor fed with coal of wide size distribution and equipped with a cyclone, J-valve and bed ash removal system. Excess heat generated within combustor is removed by means of waterwalls and heat transfer through combustor walls, respectively. Schematic diagram of the physical system is illustrated in Figure 3.1

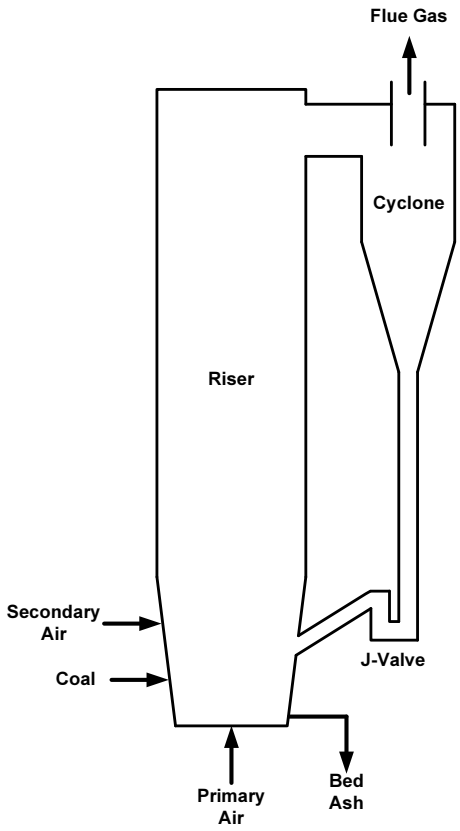

Figure 3.1: Schematic diagram of a CFB combustor.

3.2 Hydrodynamics

Understanding of the solids distribution and flow behavior in circulating fluidized bed (CFB) boilers is the key to successful design, scale-up and modeling of CFB systems. The solid distribution governs the pressure drop occurring along the CFB boiler and is directly related to the solids residence time within the boiler. It also determines the gas-solid interfacial area per unit volume of the mixture, which directly affects the gas-solid contact efficiency, heat and mass transfer rates and the extent of chemical reactions. Therefore accurate prediction of solids holdups through the CFB boiler is an essential requirement in CFB modeling.

To model the voidage and solid flow pattern in a circulating fluidized bed boiler, different simplifying assumptions were adapted by different authors. However, one common assumption to all modeling studies is that the CFB boiler consists of two distinct regions, the lower dense zone and the upper dilute zone, respectively [44–48]. A transition zone may exist in between the dense and dilute zones. The intersection point between the dense and dilute zone depends on the overall pressure balance of CFB boiler. Basu and Fraser [2] reported that intersection point between the dense and dilute zone is the secondary air injection level in most of the CFB boilers. Therefore, intersection point between the dense and dilute zone is assumed to be the secondary air injection level.

3.2.1 Dense Zone

Dense zone of CFB boilers is of particular importance despite its comparatively small height within the riser. It contains high amounts of solids hold-up and therefore many experimental work has been carried out to characterize the flow structure of dense zone. However, experimental studies carried out to identify the flow structure of dense zone show that up to now no general agreement about the flow structure in the dense zone has yet been reached.

In the open literature, there is a consensus in two flow structure for characterization of dense zone. In the former view, it is claimed that dense zone of CFB

Table 3.1: Correlations for transition velocity.

Lee and Kim [59]	$Re_c = 0.700Ar^{0.485}$
Leu *et al.* [60]	$Re_c = 0.568Ar^{0.578}$
Horio [61]	$Re_c = 0.936Ar^{0.472}$
Nakajima *et al.* [62]	$Re_c = 0.663Ar^{0.467}$
Bi and Grace [63]	$Re_c = 1.243Ar^{0.447}$
Bi and Grace [63]	$Re_c = 0.565Ar^{0.461}$

Table 3.2: Parameters used in the calculation of u_c.

Gas density (ρ_g), kg/m^3	0.31
Gas viscosity (μ_g), $N \cdot s/m^2$	4.6×10^{-5}
Particle density (ρ_p), kg/m^3	2600
Average particle size (d_p), μm	350

shows the characteristics of a bubbling bed [49–53]. On the other hand, in the latter view, it is argued that dense zone of CFB is a turbulent bed [54–57].

The turbulent fluidization flow regime is commonly considered to lie between bubbling fluidization and the fast fluidization regime [58]. The gas velocity, u_c, at which the standard deviation of pressure fluctuations reached a maximum is said to mark the beginning of the transition to turbulent fluidization. A number of empirical equations have been developed to predict the transition velocity as listed in Table 3.1.

To decide on fluidization regime of dense zone, transition velocities to turbulent fluidization are calculated for typical operating conditions of a CFB boiler. Parameters utilized in the calculations are given in Table 3.2 whereas calculated transition velocities are displayed in Table 3.3.

As can be seen from Table 3.3, calculated transition velocities show great deviation ranging between 2.49 to 5.09 m/s. Considering that average of calculated turbulent fluidization transition velocity (3.82 m/s) is higher than the typical dense zone gas velocities encountered in CFB boilers ($\sim$ 3 m/s) and that there are comparatively few papers available in the open literature that deal

Table 3.3: Calculated transition velocities.

Correlation	$u_c, m/s$
Lee and Kim [59]	3.48
Leu *et al.* [60]	4.53
Horio [61]	4.35
Nakajima *et al.* [62]	3.01
Bi and Grace [63]	5.09
Bi and Grace [63]	2.49

with the modeling of flow structure in the turbulent fluidization regime on either pilot or large scale, dense zone of the CFB boiler is assumed to be a bubbling bed. However, in order to account for higher gas velocities encountered in the dense zone of CFBs compared to that of BFBs, empirical correlations based on CFB conditions are utilized in the development of dense zone hydrodynamic model.

Dense zone is represented by an emulsion phase and a bubble phase by a modified two-phase model of Johnsson *et al.* [64] developed for high gas throughflow typically encountered in CFBs for Geldart group B and D particles.

$$u_0 = (1 - \delta)u_{mf} + \delta\, u_b + u_{tf} \tag{3.1}$$

Equation (3.1) expresses the total gas flow as the sum of three constituent flows: the flow in the emulsion phase (u_{mf}), the visible bubble flow ($\delta\, u_b$) and a gas flow through and between bubbles called throughflow (u_{tf}). Emulsion phase is assumed to be in minimum fluidization conditions. Solids in emulsion phase is assumed to be well-mixed whereas gas in both emulsion and bubble phases are assumed to be in plug flow, respectively.

The rise velocity of bubbles is obtained from Davidson and Harrison [65],

$$u_b = 0.711(g\,\overline{d}_b)^{1/2} + u_0 - u_{mf} \tag{3.2}$$

and bubble fraction in the dense zone is calculated by using the empirical correlation of Johnsson *et al.* [64] where bubble fraction is given by

$$\delta = \frac{1}{1 + \frac{1.3}{f}(u_0 - u_{mf})^{-0.8}} \tag{3.3}$$

with

$$f = \left[0.26 + 0.70exp(-3300\, d_p)\right]\left[0.15 + (u_0 - u_{mf})\right]^{-0.33} \tag{3.4}$$

The bubble size can be predicted from the correlation of Darton *et al.* [66],

$$d_b(z) = 0.54(u_0 - u_{mf})^{0.4}(z + 4\sqrt{A_o})^{0.8} g^{-0.2} \tag{3.5}$$

In this thesis study, bubbles are assumed to be free of solids and a mean bubble size calculated by averaging the bubble size predicted over the height of the bed was utilized. The mean bubble size is then calculated as,

$$\overline{d}_b = \frac{1}{H_d}\int_0^{H_d} d_b(z)dz \tag{3.6}$$

The relation between the local, time-averaged values of dense zone voidage and the bubble density is given as

$$\varepsilon_{g,d} = (1 - \delta)\varepsilon_{mf} + \delta \tag{3.7}$$

Then solid volume fraction becomes

$$\varepsilon_{s,d} = 1 - \varepsilon_{g,d} \tag{3.8}$$

As can be seen from Equation (3.7), calculation of bed voidage requires the value of bed voidage at minimum fluidization conditions. Therefore, empirical correlation proposed by Broadhurst and Becker [67] given below is utilized for the calculation of bed voidage at minimum fluidization conditions.

$$\varepsilon_{mf} = 0.586\,\phi_s^{-0.72} Ar^{-0.029} \left(\frac{\rho_g}{\rho_s}\right)^{0.021} \tag{3.9}$$

in which Archimedes number is defined as,

$$Ar = \frac{\rho_g\,(\rho_s - \rho_g)\,d_p^2\,g}{\mu_g^2} \tag{3.10}$$

Minimum fluidization velocity required in Equations (3.1) and (3.2) can be obtained from the well-known Ergun equation [68],

$$K_1 \mathrm{Re}_{mf}^2 + K_2 \mathrm{Re}_{mf} - Ar = 0 \tag{3.11}$$

where

$$K_1 = \frac{1.75}{\varepsilon_{mf}^3\,\phi_s} \tag{3.12}$$

$$K_2 = \frac{150\;(1-\varepsilon_{mf})}{\varepsilon_{mf}^3\,\phi_s^2} \tag{3.13}$$

Solution of Equation (3.7) yields

$$\mathrm{Re}_{mf} = \sqrt{\frac{1}{4}\left(\frac{K_2}{K_1}\right)^2 + \left(\frac{1}{K_1}\right)\,Ar} - \frac{1}{2}\left(\frac{K_2}{K_1}\right) \tag{3.14}$$

The minimum fluidization velocity is then calculated once Re_{mf} is solved from Equation (3.14) as follows:

$$u_{mf} = \frac{\mathrm{Re}_{mf}\,\mu_g}{d_p\,\rho_g} \tag{3.15}$$

The flow division at the base of the dense zone is calculated by using the definitions of visible bubble flow, Q_b,

$$Q_b = A_d\,\delta\,u_b \tag{3.16}$$

and flow in emulsion phase, Q_e:

$$Q_e = A_d(1-\delta)\varepsilon_{mf}\, u_{mf} \tag{3.17}$$

Dividing Equation (3.16) by (3.17) yields,

$$\frac{Q_b}{Q_e} = \frac{u_b\,\delta}{u_{mf}(1-\delta)\varepsilon_{mf}} \tag{3.18}$$

and noting that,

$$\frac{n_b}{n_e} = \frac{Q_b}{Q_e} \tag{3.19}$$

results in,

$$\frac{n_b}{n_e} = \frac{u_b\,\delta}{u_{mf}(1-\delta)\varepsilon_{mf}} \tag{3.20}$$

Combining the total mass conservation equation at the base of the bed, *i.e.*,

$$n_{a,pri} = n_b + n_e \tag{3.21}$$

and Equation (3.20) and rearranging results in the molar flow in the bubble phase at the base of the bed,

$$\text{at } z = 0 \qquad n_b = n_{a,pri}\frac{1}{1 + \dfrac{u_{mf}}{u_b}\dfrac{1-\delta}{\delta}\varepsilon_{mf}} \tag{3.22}$$

Flow in the emulsion phase at the base of the bed can similarly be obtained as,

$$\text{at } z = 0 \qquad n_e = n_{a,pri}\frac{1}{1 + \dfrac{u_b}{u_{mf}}\dfrac{\delta}{(1-\delta)\varepsilon_{mf}}} \tag{3.23}$$

The distinction between a bubble and an emulsion phase in the dense zone necessitates the introduction of lateral gas exchange between the two phases. Gas exchange between bubbles and emulsion is important because on one side bubbles cause the bypassing of gas which is not available for combustion while on the other hand, further oxidation of intermediate compounds takes place in the bubbles. The exchange of gas between bubble and emulsion phases in bubbling beds depends on the ratio of gas flow rate in emulsion phase to bubble volume, however in CFBs it depends on the ratio of gas throughflow rate to bubble volume due to high gas through flow encountered in CFBs [19]. Therefore, neglecting the diffusive effects interphase mass transfer coefficient can be written as

$$K_{be} = 4\frac{u_{tf}}{\overline{d}_b} \tag{3.24}$$

Having calculated all the hydrodynamic parameters of the dense zone, dense zone solid hold-up, $M_{s,d}$, and dense zone pressure drop, ΔP_d, can be calculated from the following equations,

$$M_{s,d} = (\varepsilon_{c,d}\rho_c + \varepsilon_{i,d}\rho_i)V_d \tag{3.25}$$

$$\Delta P_d = (\varepsilon_{c,d}\,\rho_c + \varepsilon_{i,d}\,\rho_i)g\;H_d \tag{3.26}$$

3.2.2 Dilute Zone

Knowledge of solids distribution in the dilute zone is essential for design, operation and modeling purposes as it governs pressure drop along the CFB and is directly related to the mean solid residence time within the dilute zone. Moreover, solid concentration of dilute zone not only effects combustion or SO_2 capture but also contributes to physical phenomena such as heat transfer. Therefore, in order to model physical and chemical phenomena in the dilute zone, it is necessary to model solids distribution and flow structure in this region.

Local measurements of solids distribution and velocities in the dilute zone demonstrated that this zone is formed by transient strands or clusters of relatively

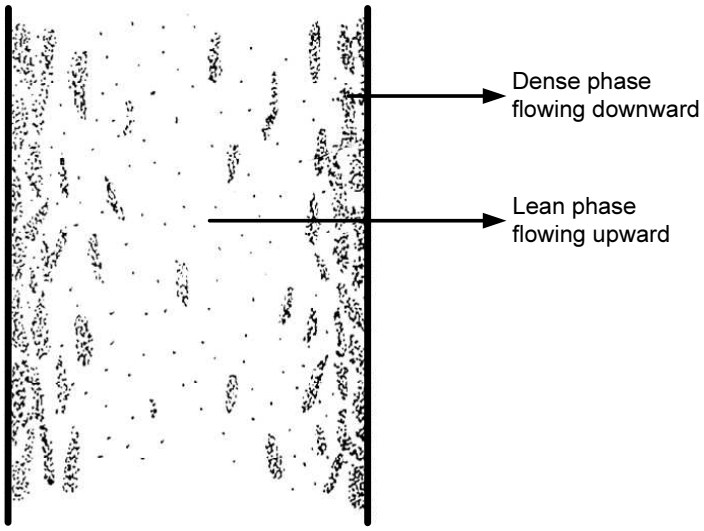

Figure 3.2: Flow structure in the dilute zone.

dense particle agglomerates dispersed in a dilute continuum of discrete particles resulting in two-phase structure as shown in Figure 3.2, with each phase consisting of both gas and solids [69]. The two phases are *i*) an upflowing lean suspension of low solids concentration and *ii*) a dense phase of relatively high solids concentration which moves downwards in the forms of strands or clusters [70, 71]. During a period of time, both phases can be found anywhere in the riser. However, the probability of observing a specific phase at certain instant strongly depends on location. Measurements showed that lean suspension of solids generally flow upward in the core whereas, the dense phase of solids move downwards on the walls, *i.e.*, core-annulus flow structure [56, 70, 72, 73].

Many hydrodynamic models have been proposed to characterize the solids distribution and flow in the dilute zone. Harris and Davidson [74] classified and grouped available dilute zone hydrodynamic models into three categories: *i*) Type I models which predict only axial variation of suspension density or solids volume fraction [45, 47, 75–78]; *ii*) Type II models which characterize both radial and axial variation of solids volume fraction by assuming two or more regions, such as core-annulus or clustering annular flow models [74, 79–84] and *ii*) Type III models that employ fundamental equations of fluid dynamics to predict the

two-phase gas-solid flow [85–88]. Type I and II models may be best employed as design tools to investigate the effect of operating conditions and riser dimensions on the riser flow structure and they may be easily coupled with reaction kinetics models to simulate performance of CFB reactors [89]. Type III models, however, are well suited to investigations of the local flow structure in CFB risers and of the impact of geometry [87].

There is a controversy amongst the various researchers over which type of modeling philosophy is the most valid. Of the three classifications of hydrodynamic models described, Type III models are not widely applied because of the difficulty in describing the variety of interactions , *i.e.*, interparticle collisions, collisions/interactions of particles with walls, drag and lift forces, for particles of different shapes, sizes and densities, each with its own motion in CFBs. Modelers have adopted a wide range of different approaches, *i.e.*, Eularian, Lagrangian or combinations of the two; interpenetrating two-fluid approach or discrete particles; 2-D or 3-D codes; solution via finite difference, finite element or finite volume approaches to overcome such difficulties [90]. Therefore, no agreement on either appropriate closure models or even on the governing equations had been reached [91]. In addition, proposed constitutive models for the solid-phase stresses and the interphase momentum transfer are partially empirical. Although computational fluid dynamics has evolved substantially in recent years, Type III models fail to give accurate predictions of flow structure in CFBs so far [32,92,93]. Today, the main challenge of CFB modeling using Type III models lies in the complexity of flow behavior rather than the limitation of computational capacity. Type III models may be the most rigorous, but the required simplifying assumptions, when balanced against their mathematical complexity, limit their usefulness from a practical perspective [89].

Type I and and Type II models, on the other hand, require correlations based on experimental data or a combination of empirical correlations and fundamental relationships. Type II models well predict time-averaged radial flow structure in the dilute zone, but they require many experimental input parameters, *i.e.*,

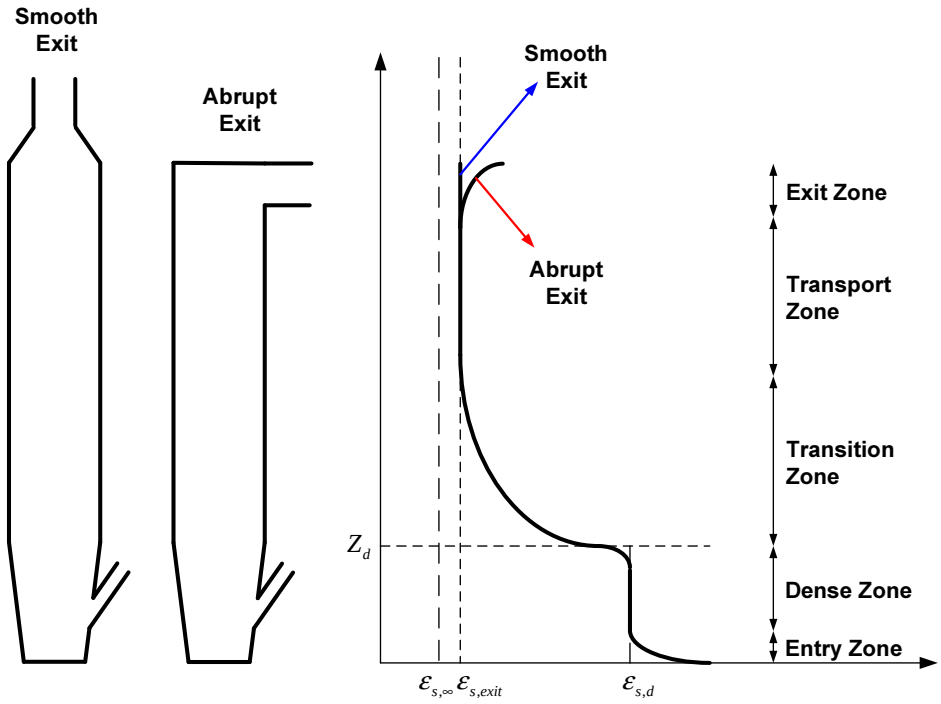

Figure 3.3: Axial profile of a CFB riser.

external solids circulation rate, downward solids velocity, solid volume fraction of strands or clusters *etc.*, which are not generally available and since the parameters will be difficult to quantify, this restricts their use as either design tools or as part of performance prediction model [89,92]. Type I models, however, are simple and empirical in nature but they show very good agreement with the experimental data and they are mathematically straightforward [89]. The only disadvantage of Type I models is that empirical or semi-empirical constants utilized in Type I models may not always comply with the experimental conditions of the system to be modeled. In such cases, however, it is the usual practice to adjust some of these constants until a compromise is found to reproduce the measured data as accurately as possible [19].

In order to make a decision on the type of model, *i.e.*, Type I or Type II, to be used for description of dilute zone hydrodynamics in this thesis study, a brief description of the models is given below. Type I models predict the axial variation of solid volume fraction or so called cross-sectional average solid volume fraction by dividing the riser axially to a number of zones as shown in Figure 3.3. Nearly

Table 3.4: Correlations for calculation of annular layer thickness.

Patience & Chaouki [94]	$\delta_a = 0.5D\left[1 - \frac{1}{\sqrt{1+1.1Fr_D\left(\frac{G_s}{\rho_p u_g}\right)^{0.083\,Fr_D}}}\right]$
Werther [95]	$\delta_a = 0.5D{Re_D}^{-0.22}\left(\frac{H}{D}\right)^{0.21}\left(\frac{H-z}{H}\right)^{0.73}$
Zhang *et al.* [96]	$\delta_a = 0.05D^{0.74}$
Bai *et al.* [97]	$\delta_a = 0.403D{\overline{\varepsilon}_s}^{0.7}$
Bi *et al.* [98]	$\delta_a = 0.5D\left[1 - \sqrt{1.34 - 1.30{\overline{\varepsilon}_s}^{0.7} + {\overline{\varepsilon}_s}^{0.7}}\right]$
Tian *et al.* [99]	$\delta_a = 24.343\,{u_g}^{0.4996}{G_s}^{-1.0251}\left(\frac{D}{H}\right)^{1.501}\left(\frac{z}{H}\right)^{-0.4919}$
Harris *et al.* [100]	$\delta_a = 0.5D\left[1-0.4014{\overline{\varepsilon}_s}^{-0.0247}{Re_D}^{0.0585}\left(\frac{H-z}{H}\right)^{-0.0663}\right]$

all of the published Type I models of CFB risers consists of combinations of these five or less zones shown in the figure. However, one common assumption to all modeling studies is that the CFB boiler consists of two distinct regions, the lower dense zone with constant solid volume fraction and the upper dilute zone with exponential decay of solids, respectively.

Type II models, however, follow the same approach with Type I models for axial variation of solids volume fraction but in order to account for lateral variations further divide riser cross-section into two or more zones laterally. The most popular Type II model in the literature is called as *"core-annulus model"* in which rapid dilute suspension flows upward in the core, whereas dense clusters of particles intermittently flow downward in the annular wall region. Both core and annulus are represented by averaged solids volume fractions. Moreover, exchange of particles is generally assumed from core to annulus hence thickness of annular wall layer decreases as you go upward in the riser. The thickness of annular wall layer, δ_a, is defined as the region adjacent to the riser wall within which the net

Table 3.5: Parameters used in the calculation of annular layer thickness.

Riser diameter (D), m	0.23
Riser overall height (H), m	6.35
Superficial gas velocity in the riser (u_g), m/s	5.00
Particle density (ρ_p), kg/m^3	2600
Net solids circulation flux (G_s), $kg/m^2 \cdot s$	31.50
Reynolds number based on riser diameter (Re_D), $-$	7764
Froude number based on riser diameter (Fr_D), $-$	3.33

Table 3.6: Calculated average annular layer thicknesses.

Correlation	δ_a, m
Patience and Chaouki [94]	0.0266
Werther [95]	0.0168
Zhang *et al.* [96]	0.0169
Bai *et al.* [97]	0.0084
Bi *et al.* [98]	0.0156
Tian *et al.* [99]	0.0146
Harris *et al.* [100]	0.0211

flow of solids is downwards. This corresponds to the distance to the wall from the point of zero particle flux or zero particle velocity in core-annulus flow. A number of empirical equations have been developed to predict the thickness of annular layer as listed in Table 3.4. In order to evaluate the effect of annular layer thickness on the performance of hydrodynamic model, these empirical correlations were used to calculate the thickness. Parameters utilized in the calculations are given in Table 3.5 whereas calculated annular layer thicknesses are displayed in Table 3.6.

As can be seen from Table 3.6, calculated average annular layer thicknesses vary within the range 0.0084 to 0.0266 m. Considering that diameter of the test rig to be modeled (0.23 m) is much higher than the average of calculated annular layer thickness (0.0171 m) in the dilute zone and that thickness of annular layer decreases with height from the surface of dense zone, effect of radial variation of solid volume fraction in the dilute zone on the performance prediction will

be minimum. Furthermore, it is not considered necessary to add this level of complexity to an already challenging dynamic system model of fluidized bed combustion systems. Therefore, it is assumed that the interchange of both gas and solids is fast enough so that radial variation can be neglected. In other words, suspension density or the solids volume fraction is assumed to vary in the axial direction only.

It was shown that solids volume fraction in the dilute zone decreases exponentially as a function of distance from the surface of the dense zone or height in dilute zone [47, 48]. Therefore, model of Kunii and Levenspiel [101] is utilized as it has minimum number of adjustable parameters compared to the other models available in the literature [75, 76, 102].

$$\varepsilon_{s,f}(z) = \varepsilon_{s,d} \exp(-az) \tag{3.27}$$

where a is the decay constant and $\varepsilon_{s,d}$ is the solids volume fraction of just above the surface of dense zone. The decay constant is usually correlated with superficial gas velocity and particle diameter [47, 103, 104]. However, the solids profile in dilute zone is also effected by combustor diameter [49] and gas properties [105]. In a recent study of Choi *et al.* [106] an empirical correlation was presented to predict decay constant which was found by using experimental data obtained with variations in column size, gas velocity, temperature, particle size, and density;

$$a = \frac{1}{d_p} \exp\left(-11.2 + 210\frac{d_p}{D_t - d_p}\right)\left[\frac{d_p\,\rho_g(u_0 - u_{mf})}{\mu_g}\right]^{-0.492}$$

$$\times \left[\frac{\rho_p\, g\, d_p}{\rho_g(u_0 - u_{mf})^2}\right]^{0.725}\left(\frac{\rho_p - \rho_g}{\rho_g}\right)^{0.731} C_d^{-1.47} \tag{3.28}$$

where drag coefficient C_d is given by,

$$C_d = \begin{cases} 24/Re_p & \text{for } Re_p \leq 5.8 \\ 10/Re_p^{0.5} & \text{for } 5.8 < Re_p \leq 540 \\ 0.43 & \text{for } 540 < Re_p \end{cases} \tag{3.29}$$

and particle Reynolds number, Re_p, is defined as,

$$Re_p = \frac{d_p\, u_0\, \rho_g}{\mu_g} \tag{3.30}$$

Equation (3.28) covers riser diameters from 0.05 to 0.4 m, particle diameters from 46 to 720 μm, particle densities from 930 to 3050 kg/m^3, gas velocities from 0.3 to 6.2 m/s, and temperatures from 24 to 600 ^oC.

The solids volume fraction distribution in the dilute zone was calculated by using Equation (3.27) together with decay constant, a, from Equation (3.28). The total solids volume fraction at the dense zone surface is taken equal to the dense zone solid volumes fraction with consideration of influence of secondary air injection following the line thought of Rhodes and Geldart [107], *i.e.*,

$$\varepsilon_{s,o} = \varepsilon_{s,d} \frac{u_{0,d}}{u_{0,f}} \tag{3.31}$$

Volume fractions of char and inert particles of size r at dense zone surface are given by the following equations, respectively,

$$\varepsilon_{c,o}(r) = \varepsilon_{s,o} \frac{M_{c,d} P_{c,d}(r) \Delta r / \rho_c}{M_{c,d}/\rho_c + M_{i,d}/\rho_i} \tag{3.32}$$

$$\varepsilon_{i,o}(r) = \varepsilon_{s,o} \frac{M_{i,d} P_{i,d}(r) \Delta r / \rho_i}{M_{c,d}/\rho_c + M_{i,d}/\rho_i} \tag{3.33}$$

Volume fractions of char and inert particles of size r at any height z in the dilute zone is then calculated by combining Equation (3.27) with Equations (3.32) and (3.33) as follows,

$$\varepsilon_{c,f}(r,z) = \varepsilon_{c,o}(r) \exp(-a_c z) \tag{3.34}$$

$$\varepsilon_{i,f}(r,z) = \varepsilon_{i,o}(r) \exp(-a_i z) \tag{3.35}$$

Char and inert particles fluxes for a particle of size r at any height z in the dilute zone is then calculated by using the following equations with the approximation that particles upflow velocity is equal to the slip between the gas and particle velocity, *i.e.*, $u_s = (u_g - u_t)$,

$$E_{c,f}(r,z) = \varepsilon_{c,f}(r,z)\rho_c(u_g - u_{t,c}) \tag{3.36}$$

$$E_{i,f}(r,z) = \varepsilon_{i,f}(r,z)\rho_i(u_g - u_{t,i}) \tag{3.37}$$

Terminal velocity required in Equations (3.36) and (3.37) is calculated by using the correlation given by Kunii and Levenspiel [108],

$$u_t = \begin{cases} \dfrac{g(\rho_p - \rho_g)d_p^2}{18\mu_g} & \text{for } Re_t \leq 0.4 \\ \left[\dfrac{4}{225}\dfrac{(\rho_p - \rho_g)^2 g^2 d_p^3}{\rho_g \mu_g}\right]^{1/3} & \text{for } 0.4 < Re_t \leq 500 \\ \left[\dfrac{3.1 g(\rho_p - \rho_g)d_p}{\rho_g}\right]^{0.5} & \text{for } 500 < Re_t \leq 200\,000 \end{cases} \tag{3.38}$$

where Re_t is defined as

$$Re_t = \frac{d_p\, u_t\, \rho_p}{\mu_g} \tag{3.39}$$

Size distribution of char and inert particles at any height in the dilute zone is calculated by assuming that probability of finding particles of size r at any height is proportional to their presence in bed,

$$F_c(z)P_{c,f}(r,z) = E_{c,f}(r,z)A_f P_{c,d}(r) \tag{3.40}$$

$$F_i(z)P_{i,f}(r,z) = E_{i,f}(r,z)A_f P_{i,d}(r) \tag{3.41}$$

Multiplying both sides of Equations (3.40) and (3.41) by dr and integrating yields the flow rate of char and inert particles in dilute zone:

$$F_c(z) = A_f \int_{r_{min}}^{r_{max}} E_{c,f}(r,z) P_{c,d}(r) dr \tag{3.42}$$

$$F_i(z) = A_f \int_{r_{min}}^{r_{max}} E_{i,f}(r,z) P_{i,d}(r) dr \tag{3.43}$$

Then size distributions of char and inert particles becomes

$$P_{c,f}(r,z) = \frac{A_f E_{c,f}(r,z) P_{c,d}(r)}{F_c(z)} \tag{3.44}$$

$$P_{i,f}(r,z) = \frac{A_f E_{i,f}(r,z) P_{i,d}(r)}{F_i(z)} \tag{3.45}$$

Once all hydrodynamic parameters of dilute zone are calculated, average dilute zone solid volume fractions, $\overline{\varepsilon}_{c,f}$ and $\overline{\varepsilon}_{i,f}$, dilute zone solids hold-up, $M_{s,f}$, and pressure drop, ΔP_f, can be calculated from the following equations, respectively

$$\varepsilon_{c,f}(z) = \int_{r_{min}}^{r_{max}} \varepsilon_{c,f}(r,z) dr \tag{3.46}$$

$$\varepsilon_{i,f}(z) = \int_{r_{min}}^{r_{max}} \varepsilon_{i,f}(r,z) dr \tag{3.47}$$

$$\overline{\varepsilon}_{c,f} = \frac{1}{H_f} \int_0^{H_f} \varepsilon_{c,f}(z) dz \tag{3.48}$$

$$\overline{\varepsilon}_{i,f} = \frac{1}{H_f} \int_0^{H_f} \varepsilon_{i,f}(z) dz \tag{3.49}$$

$$M_{s,f} = (\overline{\varepsilon}_{c,f}\, \rho_c + \overline{\varepsilon}_{i,f}\, \rho_i) V_f \tag{3.50}$$

$$\Delta P_f = (\overline{\varepsilon}_{c,f}\, \rho_c + \overline{\varepsilon}_{i,f}\, \rho_i) g H_f \tag{3.51}$$

3.2.3 External Equipments

3.2.3.1 Cyclone

Generally, cyclones are used to separate particles from the gas exiting the riser. Cyclones are very simple devices that use centrifugal force to separate particles from a gas stream while causing minimum pressure drop. They commonly are constructed of sheet metal or sometimes steam-cooled tubes. They have a low capital cost, small space requirement, and no moving parts. They are lined with castable refractory material or fire bricks to resist abrasion and also to insulate the metal body from high-temperature gas. A typical cyclone is illustrated in Figure 3.4.

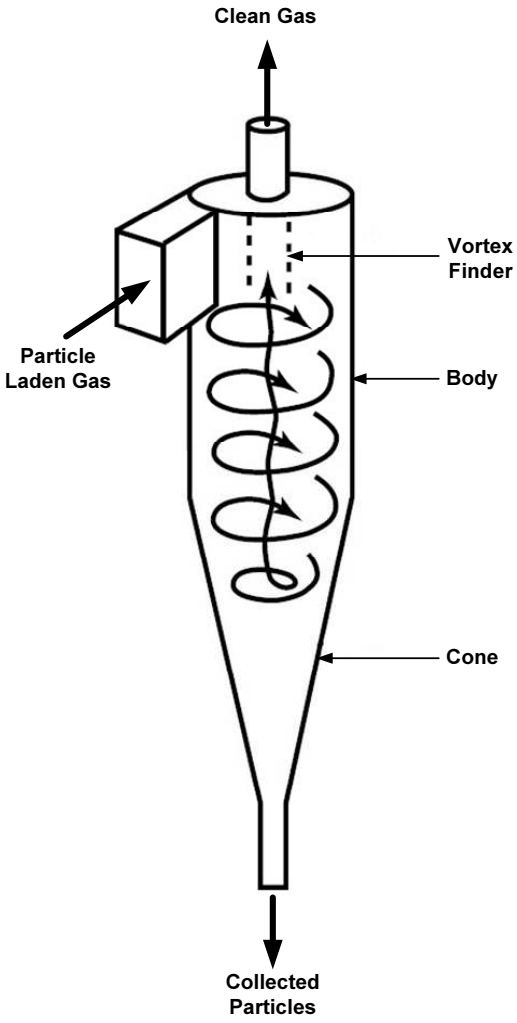

Figure 3.4: Schematic diagram of a cyclone.

Cyclone has a tangential inlet to a cylindrical body, causing the gas stream to be swirled around. Particles are thrown toward the wall of the cyclone body. As the particles reach the stagnant boundary layer at the wall, they leave the flowing gas stream and presumably slide down the wall, although some particles may be re-entrained as they bounce off of the wall back into the gas stream. As the gas loses energy in the swirling vortex, it starts spinning inside the vortex and exits at the top. The vortex finder tube does not create the vortex or the swirling flow. Its function is to prevent short-circuiting from the inlet directly to the outlet.

Changes in geometrical ratios can influence efficiency and pressure drop significantly. Increasing the inlet velocity increases the centrifugal force, and therefore the efficiency, but it also increases the pressure drop. Decreasing the cyclone diameter also increases centrifugal force, efficiency, and pressure drop. Figure 3.5 and Table 3.7 illustrate typical cyclone dimensions [109]. Relative dimensions are based upon the diameter of the body of the cyclones. High-efficiency cyclones tend to have long, narrow bodies, while high-throughput cyclones with large diameters generate less pressure.

The theoretical efficiency of a cyclone can be calculated by balancing the terminal velocity with the residence time resulting from a distance traveled in the cyclone with the utilization of Stokes' law as

$$\eta_{cyc}(d_p) = \frac{\pi N_e V_{in} {d_p}^2 (\rho_p - \rho_g)}{9\mu_g W} \tag{3.52}$$

However, it is reported that theoretical efficiency relationship based on this approach does not correlate well with the real data but correlates reasonably well for determining the 50 % cut diameter (the diameter of the particle that is collected with 50 % efficiency) [109]. Substitution of this definition into Equation (3.52) gives the expression for 50 % cut diameter of cyclones, *i.e.*

$$d_{p50} = \left[\frac{9\mu_g W}{2\pi N_e V_{in}(\rho_p - \rho_g)}\right]^{0.5} \tag{3.53}$$

Table 3.7: Typical cyclone dimensions.

		Standard	Stairmand	Swift
Inlet height	H/D	0.50	0.50	0.44
Inlet width	W/D	0.25	0.20	0.21
Gas exit diameter	D_e/D	0.50	0.50	0.40
Body length	L_b/D	2.00	1.50	1.40
Cone length	L_c/D	2.00	2.50	2.50
Vortex finder	S/D	0.625	0.50	0.50
Dust exit diameter	D_d/D	0.25	0.375	0.40

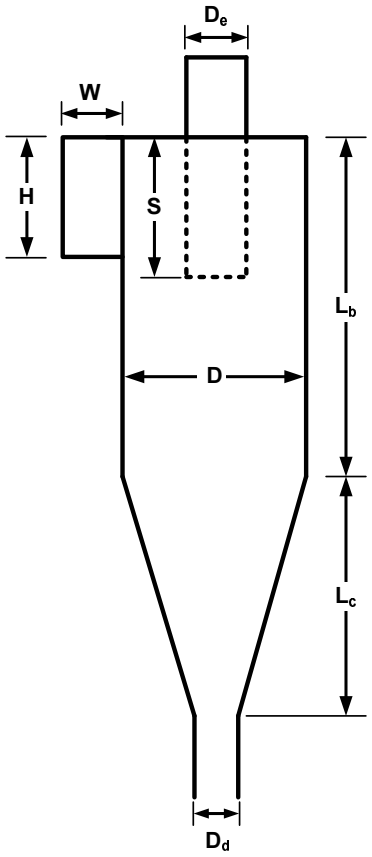

Figure 3.5: Cyclone dimensions.

Number of effective turns, N_e, can be calculated by using the following expression if the dimensions of the cyclone is known. Otherwise, it is reported that a value of $N_e = 5$ best represents the experimental data [110].

$$N_e = \frac{1}{H}\left(L_b + \frac{L_c}{2}\right) \tag{3.54}$$

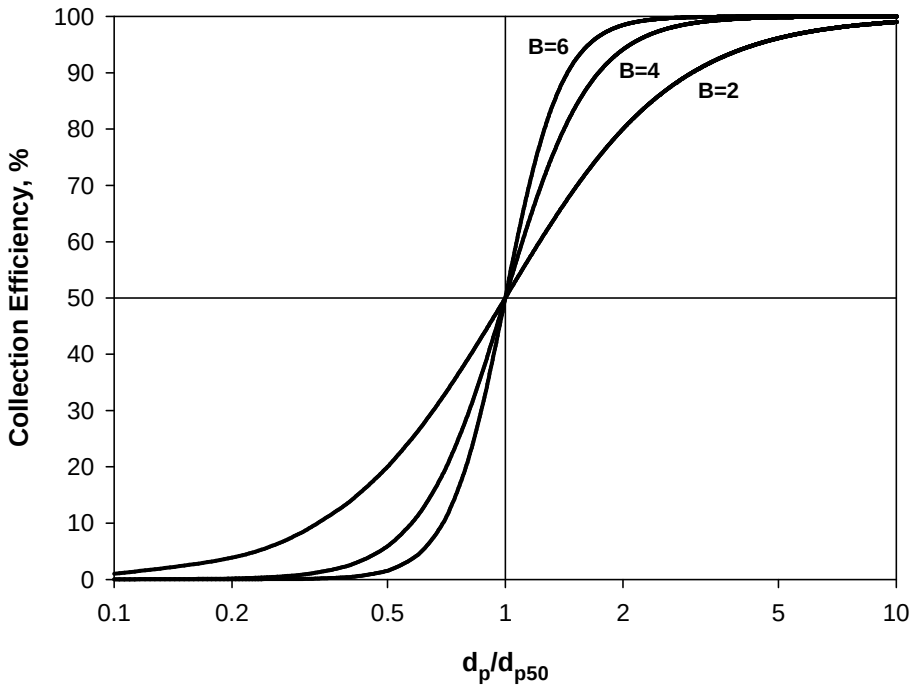

Figure 3.6: Effect of slope parameter on cyclone efficiency.

The particles larger than 50 % cut diameter have a greater probability of being captured by the cyclone whereas particles finer than this size have a lower probability of being collected. Thus for a cyclone, the collection efficiency will depend on the size distribution of solids entering to the cyclone. The efficiency of cyclone for other particle sizes can be determined from Lapple's empirical efficiency correlation given below.

$$\eta_{cyc}(d_p) = \frac{1}{1 + \left[\frac{d_{p50}}{d_p}\right]^B} \tag{3.55}$$

where B is a slope parameter of the collection efficiency curve, typically ranging from 2 to 6. The larger value for B results in a sharper cut. Since more mass is associated with larger particles, the sharper cut results in higher overall mass removal efficiency. Effect of slope parameter B on cyclone efficiency is illustrated in Figure 3.6.

Pressure drop provides the driving force that generates gas velocity and centrifugal force within a cyclone. Pressure drop across the cyclone can be

calculated from the following correlation which is based on the number of inlet velocity heads as shown below,

$$\Delta P_{cyc} = \frac{1}{2}\rho_g {V_{in}}^2 N_H \tag{3.56}$$

$$N_H = K\frac{HW}{{D_e}^2} \tag{3.57}$$

where K is a parameter ranging between 12 to 18. Number of inlet velocity heads, N_H, is reported to be 8 for standard cyclone dimensions, 6.4 for the Stairmand cyclone design, and 9.24 for the Swift cyclone design [109].

3.2.3.2 Standpipe

The purpose of the standpipe is to transfer solids from the cyclone exit to the pressure seals and to create necessary pressure drop for returning the solids into the riser. Solids in the standpipe are in a state between the fixed bed and minimum fluidization. The fluidization air introduced into the pressure seal rises partially in the standpipe and overcomes friction. The mass in the standpipe causes the necessary pressure drop for returning the solids into the riser. The standpipe pressure drop is assumed to depend only upon the static pressure of the solid inventory in standpipe and is calculated as follows.

$$\Delta P_{sp} = \frac{g\, M_{s,sp}}{A_{sp}} \tag{3.58}$$

3.2.3.3 Pressure Seal

One unique characteristic of CFB operation is to obtain a constant and desired solid circulating rate. At given gas velocity, the circulating rate determines the solid load and overall pressure drop in the combustor, which in turn affects hydrodynamics, chemical reactions, heat transfer and fan power. Due to high operating temperature of a CFB combustor, solids circulation rate is usually controlled by non-mechanical valves such as L-valves, J-valves or other kind of seal

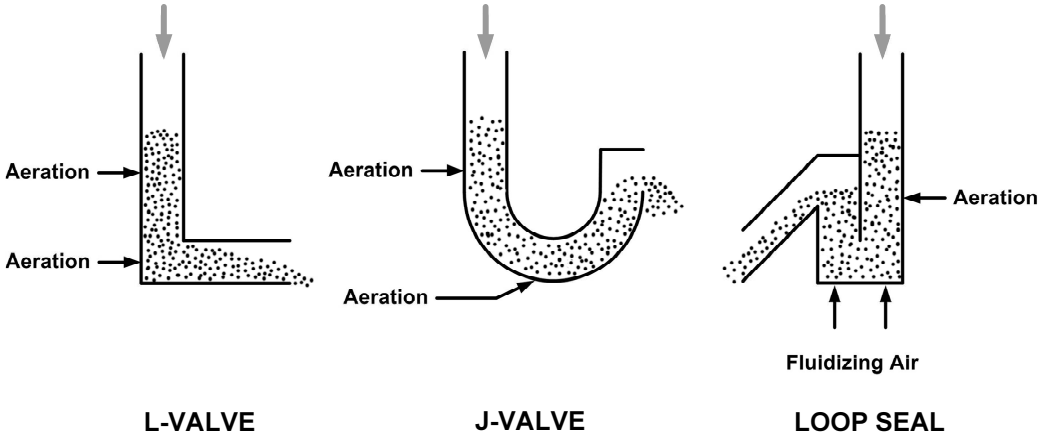

Figure 3.7: Schematic illustration of pressure seals.

pots. The circulating fluidized bed loop is very similar to the water-steam loop of natural circulation boilers. In both cases, the dense phase in the downcomer imposes a pressure drop high enough to force the fluid to move toward the riser to reach an equilibrium state.

Pressure seals are generally realized as L-valves, J-valves or loop seals as shown in Figure 3.7. These non-mechanical valves allow the flow of solids between the standpipe and riser. Air facilitates the movement of solids in these valves. An advantage of the L-valve is its simple design, while the J-valve allows finer adjustment of solids flow into the riser through the changing aeration rate in the vertical leg. Solids in the L-valves and J valves are generally in a state between fixed bed and moving bed whereas solids in loop seal in a state of bubbling fluidization. The pressure drop of a pressure seal depends on its type. Geldart and Jones [111] suggest the following expression for calculation of pressure drop across the L-valve.

$$\Delta P_{ps} = \frac{216 {G_s}^{0.17} L_{ps}}{{D_{ps}}^{0.63} {d_p}^{0.15}} \tag{3.59}$$

where

$$D_{ps} = \sqrt{\frac{4A_{ps}}{\pi}} \tag{3.60}$$

3.2.4 Pressure Loop

In CFB systems, it is desirable to have reliable estimates of riser pressure drop, solids hold-up and solids inventory to maintain stable operation at a given gas velocity and solids circulation rate. The solids hold-up is related to the pressure drop across the riser, which in turn depends on the pressure drop across the cyclone, standpipe and pressure seal. The overall pressure balance therefore establishes the pressure driving force needed for solids circulation, as well as the required blower capacity. Schematic illustration of pressure distribution in a CFB is illustrated in Figure 3.8.

Since the static pressure in the standpipe causes the driving force for circulation, the pressure drop in the standpipe must equal to the pressure drops of the other parts, *i.e.*,

$$\Delta P_{sp} = \Delta P_{riser} + \Delta P_{cyc} + \Delta P_{ps} \tag{3.61}$$

where ΔP_{riser} is the sum of dense and dilute zone pressure drops,

$$\Delta P_{riser} = \Delta P_d + \Delta P_f \tag{3.62}$$

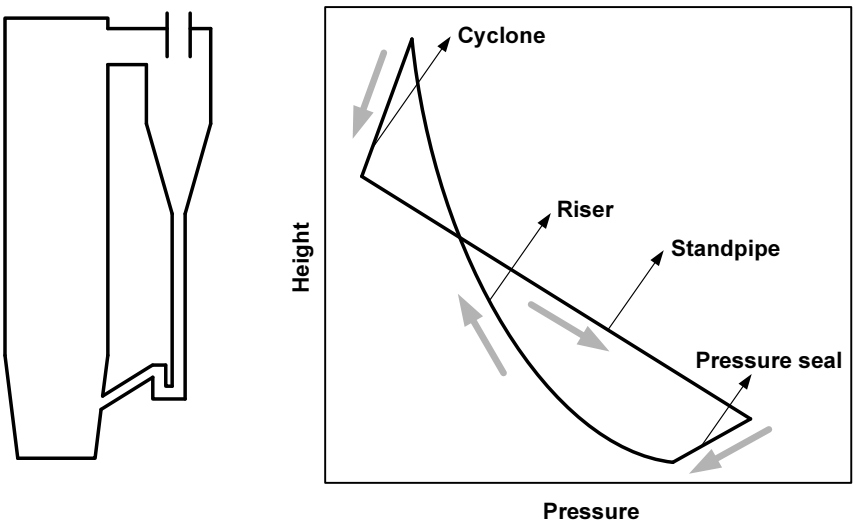

Figure 3.8: Schematic illustration of pressure distribution in a CFB.

3.3 Combustion

Combustion of coal is a very complex process. This partly due to the fact that coal is not a homogeneous material, *i.e.*, different portions (both microscopic and macroscopic) of a single coal sample exhibit widely differing chemical compositions and physical properties. Composition of coal is expressed by two kinds of analysis as shown in Figure 3.9. According to origin and age of coal its composition may vary widely. Therefore, an elementary description of the coal combustion process is not possible.

Using coal analysis and heating value, it is possible to categorize coals by rank as shown in Table 3.8. Coal rank expresses the progressive metamorphism of coal from lignite (low rank) to anthracite (high rank). Rank is based on heating value, for low-rank coals and on percentage of fixed carbon for higher-rank coals, both calculated on a dry and ash-free basis. The heating value and percentage of fixed carbon increase whereas volatile matter content decreases as the rank moves from lignite to anthracite.

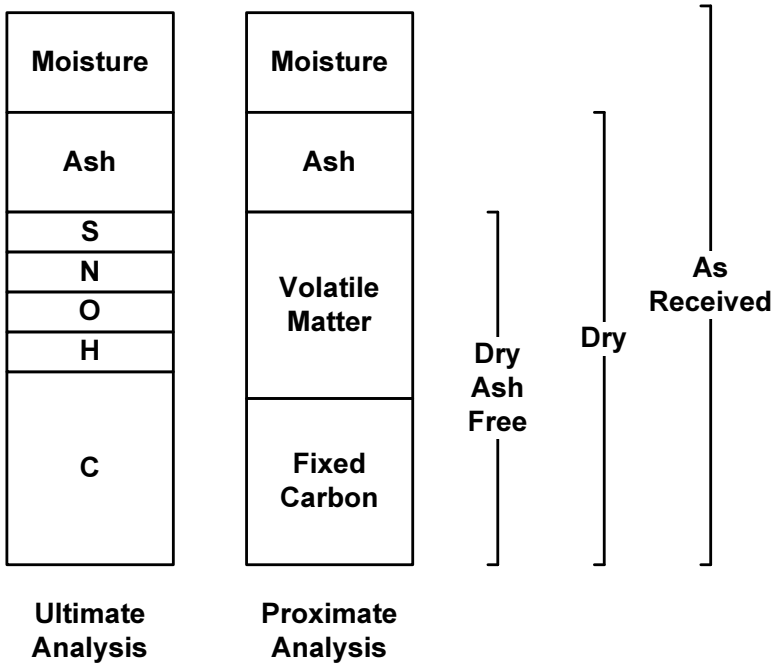

Figure 3.9: Composition of coal.

Table 3.8: ASTM Classification of coals by rank (dry-ash-free).

	Fixed Carbon, %	HHV, MJ/kg
Meta-anthracite	$>$ 98	
Anthracite	92 - 98	
Semianthracite	86 - 92	
Low volatile bituminous	78 - 86	
Medium volatile bituminous	69 - 78	
High volatile A bituminous		$>$ 32.56
High volatile B bituminous		30.24 - 32.56
High volatile C bituminous		26.75 - 30.24
Subbituminous A		24.42 - 26.75
Subbituminous B		22.10 - 24.42
Subbituminous C		19.30 - 22.10
Lignite A		14.65 - 19.30
Lignite B		$<$ 14.65

When a coal particle is fed to a fluidized bed combustor, initially moisture will be driven off and the temperature of the coal particle rises as it is heated by inert particle convection, gas convection and radiation. The temperature of the coal particle rapidly reaches a value at which volatile matter in the coal commences to be liberated, escaping in the form of combustible vapors into the bed. The residue left after devolatilization is char, which is essentially porous carbon with ash bound in it; the degree of porosity depends upon the type of coal. Once the ignition temperature is reached, the char commences to burn, but, the time required to burn it out is much longer, one to two orders of magnitude longer than that taken to evolve the volatiles [112–114].

3.3.1 Volatiles Release and Combustion

Devolatilization is a chemical decomposition of coal and begins at a temperature of 350 - 400°C [115]. Volatiles are the primary gaseous decomposition products, some of which will be liquids or even solids at ambient temperature and pressure. Devolatilization of coal has been noted to be an extremely complex phenomena due to the large number of chemical reactions and physical changes occurring during the process.

The volatile fraction of coals normally contributes a significant proportion of the total energy released during combustion and thus should not be ignored. Volatiles may also contribute significantly to the CO emission as well as NO_x formation in fluidized beds. Although, time scale for devolatilization is small, compared to that for the combustion of char, the distribution of volatile matter throughout the system affects the combustor performance and pattern of heat release.

Devolatilization rates of coals are complex functions of the experimental conditions, under which the devolatilization proceeds, and the overall devolatilization process is open to manipulation. The most important factors are:

- coal rank and composition
- pore structure of coal
- particle size
- temperature
- pressure
- heating rate
- atmosphere (oxidizing or reducing)
- type of reactor (fixed bed, fluidized bed, *etc.*)

The relatively few experimental data available, as well as the inherent difficulty in developing a comprehensive model, have required theoreticians to make many simplifying assumptions. The most general ones are approximation of irregular coal particles by spheres, using an average particle size and defining composition in terms of volatile matter, fixed carbon and ash to avoid the complex chemistry of coal. To date, description of the gaseous products produced and the kinetics of their formation have been more extensively dealt with.

There exists a number of models for kinetic interpretation of devolatilization process. The simplest model for the process of volatiles evolution is based on a single decomposition reaction occurring uniformly through the particle:

$$coal \xrightarrow{k} volatiles + char \tag{R1}$$

The rate of reaction R1 is either approximated by a first order rate expression,

$$\frac{dv}{dt} = k(v_\infty - v) \tag{3.63}$$

or an nth order rate expression,

$$\frac{dv}{dt} = k(v_\infty - v)^n \tag{3.64}$$

where v is the yield of volatiles at time t, v_∞ is the ultimate yield of volatiles at $t = \infty$ and k is the rate constant. The rate constant is generally correlated with temperature by an Arrhenius expression,

$$k = k_o \exp\left(-\frac{E}{RT}\right) \tag{3.65}$$

The parameters v_∞, k_o, E and n in Equations (3.63) and (3.64) depend upon coal type, heating rate and experimental technique utilized and must be determined experimentally.

Although first and nth order models are frequently used in describing coal decomposition due to their simplicity, they lack the flexibility to represent much of the data available in literature [116]. The most serious shortcoming of these models is the failure to account for apparently asymptotic yield, v_∞, observed at the final temperature [115]. In addition, activation energies predicted by these models are much lower than expected from studies on model compounds [117]. Consequently more complex models have been proposed to describe devolatilization process. These models consider devolatilization to occur via a number of independent parallel reactions [115] or competing ones [118].

Parallel reaction model considers devolatilization to occur via a large number of independent parallel first order reactions [115]. The rate of volatiles production

by a particular reaction within the coal structure is then described in a manner similar to Equation (3.63) with a subscript i used to denote one particular reaction:

$$\frac{dv_i}{dt} = k_i(v_{\infty,i} - v_i) \tag{3.66}$$

Integration of Equation (3.66) for non-isothermal conditions yields the amount of of volatile matter released due to a particular reaction:

$$v_i = v_{\infty,i}\left[1 - \exp\left(-\int_0^t k_i dt\right)\right] \tag{3.67}$$

The rate constants, k_i, are assumed to follow Arrhenius relation with a common pre-exponential factor, k_o,

$$k_i = k(E) \ = k_o \exp\left(-\frac{E}{RT}\right) \tag{3.68}$$

but different activation energies varying in the range E_{min} to E_{max} according to a probability density function $f(E)$. Most often a Gaussian distribution is used to describe $f(E)$ [115],

$$f(E) = \left[(2\pi)^{1/2}\sigma\right]^{-1} \exp\left[-\frac{(E - E_o)^2}{2\sigma^2}\right] \tag{3.69}$$

with,

$$\int_0^\infty f(E)dE = 1 \tag{3.70}$$

where E_o and σ are the mean and standard deviation of the activation energy distribution, respectively.

As can be seen from the resulting model equations, *i.e.* Equations (3.67), (3.68) and (3.69), parallel independent reaction model requires four parameters to be

estimated from the experimental data: v_∞, k_o, E_o and σ, only one more than the primitive single first order reaction model represented by Equation (3.63). Hence, this model is sufficiently simple for combustion calculations. A single set of experimentally determined parameters, k_o, E_o and σ, can be used to correlate experimental data obtained under different heating conditions whereas first and nth order models require different set of parameters for each heating condition. The value of v_∞ may vary for different coals as well as for different temperatures and heating rates.

An alternative to the multiple parallel reaction model is to assume the existence of multiple competing reactions by which the devolatilizing coal may follow any of a number of reaction paths depending on the temperature-time history [118]. This concept was introduced as it provides a simple empirical explanation of the effects on yield of both temperature and heating rate. The simplest model of this kind postulates two competing overall reactions [118]:

$$coal \xrightarrow{k_1} \alpha_1\ volatiles_1 + (1-\alpha_1)\ char_1 \tag{R2}$$

$$coal \xrightarrow{k_2} \alpha_2\ volatiles_2 + (1-\alpha_2)\ char_2 \tag{R3}$$

with rate equations,

$$\frac{dc}{dt} = -(k_1 + k_2)c \tag{3.71}$$

and

$$\frac{dv}{dt} = (\alpha_1 k_1 + \alpha_2 k_2)c \tag{3.72}$$

where c is the mass fraction of initial coal to be reacted. The rate constants k_1 and k_2 are of Arrhenius form with the important feature that $E_1 < E_2$:

$$k_n = k_{o,n} \exp\left(-\frac{E_n}{RT}\right), \qquad n = 1, 2 \tag{3.73}$$

At low temperatures, the first reaction, R2, is dominant leading to the asymptotic volatile yield α_1. At high temperatures, the second reaction becomes faster than the first, resulting in higher volatiles yields (asymptotically α_2). The ultimate yield of volatiles lies between α_1 and α_2 depending upon the final temperature, heating rate and residence time.

Both parallel independent reaction and parallel competing reaction models have been reported to give good results [116]. However, it is suggested that two competing reactions model can be used at moderate and higher temperatures whereas the parallel independent reactions model is recommended at low temperatures typically encountered in fluidized bed combustors [119].

As highlighted above, up to date, there is still no generalized kinetic model for description of devolatilization process. Furthermore, enhanced heat and mass transfer taking place in CFBs due to high gas flow rates and intense mixing [120] increases the probability of instantaneous devolatilization in the dense zone as confirmed by previous modeling studies [8, 13, 27, 28, 30]. Therefore, it is assumed that volatiles are released instantaneously as the coal particles enter the combustor and mixed with hot bed of particles. Furthermore, devolatilization process is considered to take place only in the dense zone and volatiles are assumed to be uniformly distributed along the height of the combustor.

The released volatile matter is assumed to immediately undergo the following set of reactions in the emulsion phase;

$$C + 1/2\ O_2 \rightarrow CO \tag{R4}$$

$$2\ H + 1/2\ O_2 \rightarrow H_2O \tag{R5}$$

$$S + O_2 \rightarrow SO_2 \tag{R6}$$

$$2\ N \rightarrow N_2 \tag{R7}$$

$$2\ O \rightarrow O_2 \tag{R8}$$

$$H_2O \rightarrow H_2O \tag{R9}$$

The net effect of devolatilization is, thus, the same as that of additional gaseous feed stream added solely to the emulsion phase. The composition of volatile matter released to emulsion phase is then calculated as,

$$x_{C,vm} = (x_C - x_{fc})/x_{vm} \tag{3.74}$$

$$x_{O,vm} = x_O/x_{vm} \tag{3.75}$$

$$x_{H,vm} = x_H/x_{vm} \tag{3.76}$$

$$x_{S,vm} = x_{S,comb}/x_{vm} \tag{3.77}$$

$$x_{N,vm} = x_N/x_{vm} \tag{3.78}$$

Combustion of volatiles in fluidized beds is not well understood. Laboratory scale investigations on the combustion of pre-mixed gases in fluidized beds of sand have shown that homogeneous reactions are inhibited in the emulsion phase due to radical-quenching on the inert solids [121–124] and that below some critical temperature ($\sim$ 800°C) the combustion of gases does not take place in the emulsion phase. As the operating temperatures of fluidized bed combustors (850-900 °C) is above that critical temperature, it was concluded that combustion of volatiles is assumed to take place in both the emulsion and bubble phases in this thesis study.

3.3.2 Char Combustion

The combustion processes are similar in a bubbling or circulating fluidized beds, but the burning rates of chars are different [125]. The burning rate of char in

circulating fluidized bed is higher than that in bubbling fluidized beds due to higher mass transfer rates encountered in CFBs [126]. The higher degree of mixing in CFBs contributes to the higher burning rates in CFBs.

The heterogeneous reaction between oxygen and char occurs, to a large extent, in the emulsion phase only. Within this phase, oxygen transfers through the interstices of the ash particles to the burning char particle, where reaction may take place on the surface and inside pores. Therefore, overall reaction may involve steps such as mass transfer through the gas film surrounding the particle, diffusion through the pore structure and chemical reaction. Depending on which steps are rate controlling, one of these standard models may be used to describe carbon consumption: The uniform reaction model (constant diameter/decreasing density), the shrinking particle model (constant density/decreasing diameter), or the shrinking core model (ash layer enveloping a shrinking size unreacted core). The relative importance of each of the various processes is a complicated function of bed temperature, fluid mechanics, oxygen concentration, particle size and char reactivity.

Char combustion is generally believed to proceed with one or more of the following heterogeneous reactions,

$$C(s) + 1/2\ O_2 \rightarrow CO \tag{R10}$$

$$C(s) + O_2 \rightarrow CO_2 \tag{R11}$$

$$C(s) + CO_2 \rightarrow 2\ CO \tag{R12}$$

and subsequent oxidation of CO to CO_2 in the boundary layer surrounding the particle or in the free stream,

$$CO + 1/2\ O_2 \rightarrow CO_2 \tag{R13}$$

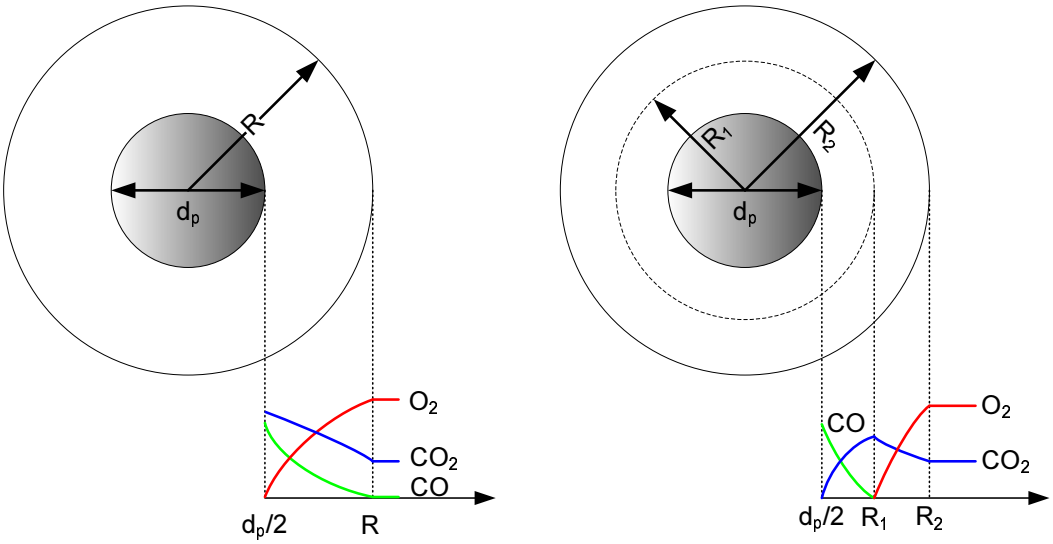

Figure 3.10: Char combustion mechanisms.

Generally, penetration of oxygen into the unburnt char is limited to a short distance compared to the particle dimensions, so that reaction is confined to the outer thin layer of the remaining char particle [127] and due to the vigorous agitation in fluidized bed combustors, the residue of ash on the burning char surface is usually flaked off and presents no resistance to diffusion.

Elimination of intraparticle effects necessitates the examination of reactions taking place in the boundary layer surrounding the particle. There are two basic boundary layer reaction models for char combustion which are illustrated in Figure 3.10. They may be classified according to their priori assumptions regarding where CO burns [128]. In the single film model, the oxidation of char particle is assumed to be controlled by diffusion of O_2 through a stationary film to the surface of the char particle and/or by the kinetics of surface reaction, R10 or R11. Carbon monoxide oxidation does not occur in the boundary layer. In the double film model, it is assumed that CO is produced on the surface of the char particle by the reaction R12 and the CO produced is burned in a thin flame front in the boundary layer. No oxygen will reach the char surface and no CO will reach

the external edge of the boundary layer. However, the carbon dioxide reduction reaction, R12, is now generally not considered since the rate of carbon gasification is not high enough to be the dominant reaction at FBC temperatures [129] and high particle temperatures predicted with CO oxidation in the boundary layer is contrary to experimental findings in fluidized bed conditions [130].

There is much controversy in the literature whether both CO and CO_2 are primary products of combustion of char particles. The product ratio CO/CO_2 was investigated by several authors experimentally and it was related to particle temperature by an Arrhenius expression,

$$\frac{[CO]}{[CO_2]} = f_r \;=\; k_o \exp\left(-\frac{E}{R\,T_p}\right) \tag{3.79}$$

and measured values was found to be between 0.2 and 12 as reported in the study of Linjewile and Agarwal [131]. In the important size range for fluidized bed combustors ($\sim 500\ \mu m$ to $\sim 2\ mm$), the major product measured was CO.

By defining a mechanism factor in terms of the product ratio, f_r, as [131]

$$\zeta = \frac{(1+2f_r)}{(1+f_r)} \tag{3.80}$$

reactions R10 and R11 can be expressed with a single reaction as given below:

$$C(s) + \frac{1}{\zeta}\,O_2 \rightarrow 2\left(1-\frac{1}{\zeta}\right)CO + \left(\frac{2}{\zeta}-1\right)CO_2 \tag{R14}$$

The mechanism factor can take values between 1 and 2, as $\zeta = 1$ when the product is only CO_2 and $\zeta = 2$ when the product is only CO.

With the simplification of a shrinking particle model, the reaction rate controlling steps of char combustion are reduced to only two, external mass transfer and surface reaction. In order to determine which mode is more important, extensive experimental studies have been carried out and limiting case models have been

formulated. It has been shown that as mass transfer coefficient decreases with increasing particle size, the combustion of large char particles ($d_p \geq 2\ mm$) is dominated by mass transfer control, whereas chemical kinetics becomes important for the burning of smaller diameter particles [132]. However, for systems which are utilizing feed of wide size distribution limiting case models may not be satisfactory [133] as there will be a smooth transition between the two possibilities in the particle size range under consideration.

Therefore a shrinking particle, single film model with CO oxidation in the free stream which considers both mass transfer-reaction resistances at the particle surface seems to be appropriate for modeling char combustion in circulating fluidized beds.

The combustion rate of a carbonaceous particle is usually expressed as the mass of carbon consumed per unit time per unit external surface area of the particle and it was found to be proportional to the partial pressure of oxygen at the surface [127, 134, 135]. The processes of pore diffusion and internal chemical reaction are lumped together in the apparent rate constant and order based on external surface area. The rate of carbon oxidation reaction per unit external surface area can then be expressed as

$$r_{C,s} = k_s C_{O_2,s}^n \tag{3.81}$$

where $C_{O_2,s}$ is the oxygen concentration at the particle surface and, k_s and n are the apparent reaction rate coefficient and reaction order respectively. The variation of chemical kinetic reaction rate coefficient with temperature is expressed by an Arrhenius type equation:

$$k_s = k_o \exp\left(-\frac{E}{R T_p}\right) \tag{3.82}$$

where k_o is an apparent rate constant based on particle outer surface area and E is an apparent activation energy.

Table 3.9: Apparent rate constants for char combustion.

Reference	k_o (m/s)	E (J/mol)
Field *et al.* [127]	$595T_p$	17976
Hoy and Gill [134]	$5.5T_p$	90000

The most widely utilized apparent reaction rate coefficients in the literature are of Field *et al.* [127] and Hoy and Gill [134] which were obtained by the compilation of extensive experimental data reported in the literature. The apparent rate constants and activation energies reported in these studies are listed in Table 3.9. In this thesis study rate expression of Field *et al.* [127] is utilized.

The reaction orders reported in the literature shows a range between 0 to 1 [136], but $n = 1$ has usually been assumed to simplify the calculations in modeling studies. Smith [136] has examined the consequences of assuming $n = 1$ and reported that assuming an order of unity above a particle temperature of 1000 K, which is lower than temperatures encountered in FBCs, gives moderately good approximations to measured combustion rates whereas for temperatures less than 1000 K he suggested that reaction order should be taken as $n = 0.5$.

Assuming an apparent order of unity for char combustion rate and noting that the surface reaction rate must equal the rate at which oxygen diffuses inward through the boundary layer to the particle surface, *i.e.*,

$$k_f(\overline{C}_{O_2,e} - C_{O_2,s}) = \frac{k_s}{\zeta} C_{O_2,s} \tag{3.83}$$

the oxygen concentration at the char particles surface can be obtained in terms of the average oxygen concentration in emulsion phase;

$$C_{O_2,s} = \frac{\overline{C}_{O_2,e}}{\dfrac{k_s}{\zeta k_f} + 1} \tag{3.84}$$

The rate of carbon oxidation at the particles surface can then be expressed in terms of bulk oxygen concentration by combining Equations (3.81) and (3.84)

and rearranging;

$$r_{C,e} = \frac{\zeta}{1/k_f + \zeta/k_s}\overline{C}_{O_2,e} \tag{3.85}$$

Mass transfer coefficient for oxygen, k_f, is calculated by using the expression suggested by Basu and Subbarao [137],

$$k_f = \frac{\mathcal{D}}{d_p}\left[2 + 0.6(Re_t)^{1/2}Sc^{1/3}\right] \tag{3.86}$$

in which Re_t and Sc are defined as

$$Re_t = \frac{d_p\, u_t\, \rho_p}{\mu_g} \tag{3.87}$$

$$Sc = \frac{\mu_g}{\mathcal{D}\,\rho_g} \tag{3.88}$$

Diffusivity of oxygen in nitrogen, $\mathcal{D}$, is approximated from the equation suggested by Field *et al.* [127], *i.e.*,

$$\mathcal{D} = \mathcal{D}_{ref}\left[\frac{T}{T_{ref}}\right]^n \frac{P_{ref}}{P} \tag{3.89}$$

where $\mathcal{D}_{ref}$ is $2.01 \times 10^{-5}\ m^2/s$, T_{ref} is $298.15\ K$, P_{ref} is $1.01325 \times 10^5\ Pa$ and n is 1.5, respectively. The unit of $\mathcal{D}$ is given in m^2/s.

Shrinkage rate of char particles, which is required for the calculation of char particle size distribution, can be determined by noting that rate of carbon removal from the surface of char particle must equal the rate of combustion of carbon at the particle surface,

$$\frac{d}{dt}\left[\frac{4}{3}\pi\, r^3 \rho_c \frac{x_{fc}}{x_{fc} + x_{ash}}\right] = -4\pi r^2 M_C\, r_{C,e} \tag{3.90}$$

Rearranging Equation (3.90) yields the working form of the char particles shrinkage rate:

Table 3.10: Coefficients for CO oxidation rate expression.

Reference	k_o $(mol^n/m^{3n}.s)$	E/R (K)	α	β	γ
Hottel *et al.* [138]	4.75×10^5	8052	1	0.3	0.5
Howard *et al.* [139]	1.3×10^8	15106	1	0.5	0.5
Yetter *et al.* [140]	7.2×10^{14}	34743	1	0.25	0.5

$n = 1 - \alpha - \beta - \gamma$

$$\Re(r) = \frac{dr}{dt} = -\frac{3}{\rho_c}\frac{x_{fc} + x_{ash}}{x_{fc}} M_C \, r_{C,e} \tag{3.91}$$

After devolatilization and char combustion, the primary product CO is further oxidized in the gas phase with oxygen. The main influence on CO emission is exerted by homogeneous oxidation of CO to CO_2. Low temperatures, short residence times and insufficient mixing of CO and O_2 may limit this effect. Furthermore, especially under extreme air staging conditions large amount of CO remains unoxidized in the reducing dense zone of the combustor.

With regard to the oxidation of CO produced from volatiles (R4) and char combustion (R10), there are several kinetic laws in the open literature in the following form,

$$r_{CO} = k_{CO} C_{CO}^{\alpha} C_{O_2}^{\beta} C_{H_2O}^{\gamma} \tag{3.92}$$

with

$$k_{CO} = k_o \exp\left(-\frac{E}{RT}\right) \tag{3.93}$$

The widely used kinetic rate constants and activation energies reported in these studies are listed in Table 3.10. There is general agreement in the literature that the CO oxidation reaction is first order in carbon monoxide and half order with respect to water vapor. Therefore, α and γ are usually taken as 1.0 and 0.5, respectively. The order in oxygen ranges from 0 to 1 depending on the concentration of oxygen. In this study the rate of CO oxidation was predicted by using the expression of Hottel *et al.* [138].

3.4 Char Particle Size Distribution

Since carbon consumption rate depends on the surface area provided by the burning char particles, calculation of particle size distribution (PSD) and hold-up of char particles is of fundamental importance in the prediction of behavior of fluidized bed combustors.

Levenspiel *et al.* [141] developed general equations in terms of mass balances to relate particle size distributions and flow rates of entering and leaving streams for particles undergoing size change in a fluidized bed. This work was extended later by others to account for either density change in particles [142–144] or to incorporate communition of particles by fragmentation and attrition [144–147]. Up to date, the time dependent behavior of char PSD was only studied by Weimer and Clough [148, 149] and Saastamoinen *et al.* [150]. However, their study was limited to temporal variation of char PSD for prespecified gas phase temperature and concentrations.

In order to deduce an equation based on the mass fractions in size intervals for shrinking char particles the following assumptions are made:

- Particle size distribution of feed char particles, $P_0(r)$, is expressed by Rosin-Rammler size distribution function (See Appendix A for derivation).
- As solids in the dense zone is assumed to be well-mixed, bed drain char size distribution represents the dense zone char size distribution.
- Elutriation rate of char particles of size r is directly proportional to their concentration in the dense zone.
- Densities of char particles do not change during combustion.
- Fragmentation and attrition of char particles is negligible.
- Char particles are considered to shrink by combustion only.

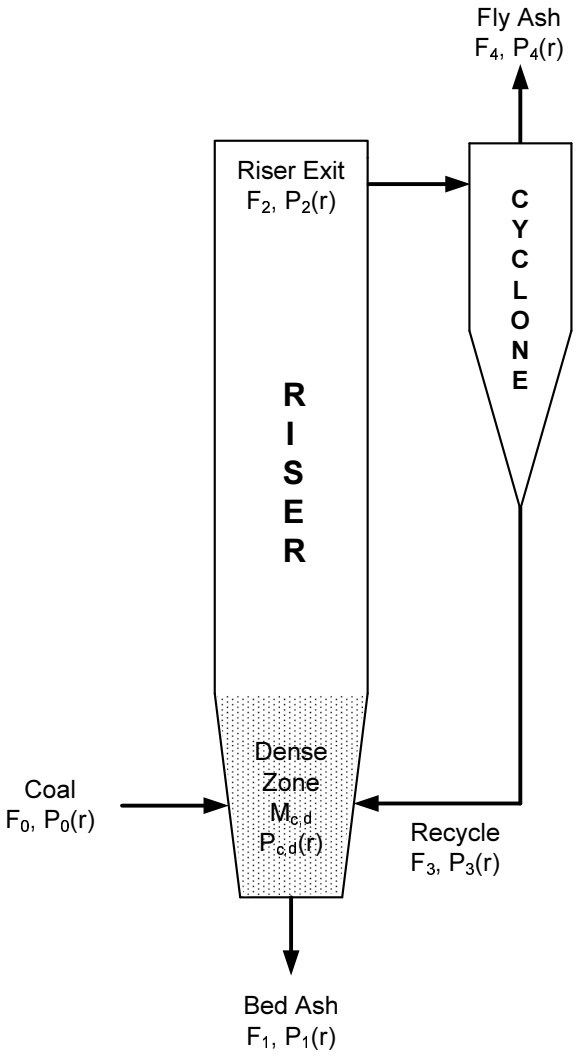

Figure 3.11: Streams considered in char population balance.

Considering the streams given in Figure 3.11, the unsteady-state mass balance for char particles of sizes between r and $r+\Delta r$ for the entire range of particles in the dense zone at a particular instant can be expressed in verbal form as,

$$\left\{ \begin{array}{c} char\ of\ size\ r \\ accumulated \\ in\ the\ interval\ \Delta r \end{array} \right\} = \left\{ \begin{array}{c} char\ of\ size\ r \\ entering \\ in\ feed \end{array} \right\} + \left\{ \begin{array}{c} char\ of\ size\ r \\ entering \\ in\ recycle \end{array} \right\}$$
$$- \left\{ \begin{array}{c} char\ of\ size\ r \\ leaving \\ in\ bed\ drain \end{array} \right\} - \left\{ \begin{array}{c} char\ of\ size\ r \\ leaving \\ in\ carryover \end{array} \right\} + \left\{ \begin{array}{c} char\ shrinking\ into \\ the\ interval\ \Delta r \\ from\ a\ larger\ size \end{array} \right\}$$
$$- \left\{ \begin{array}{c} char\ shrinking\ out \\ of\ the\ interval\ \Delta r \\ to\ a\ smaller\ size \end{array} \right\} - \left\{ \begin{array}{c} char\ mass \\ depleted\ in\ the \\ interval\ \Delta r \end{array} \right\} \quad (3.94)$$

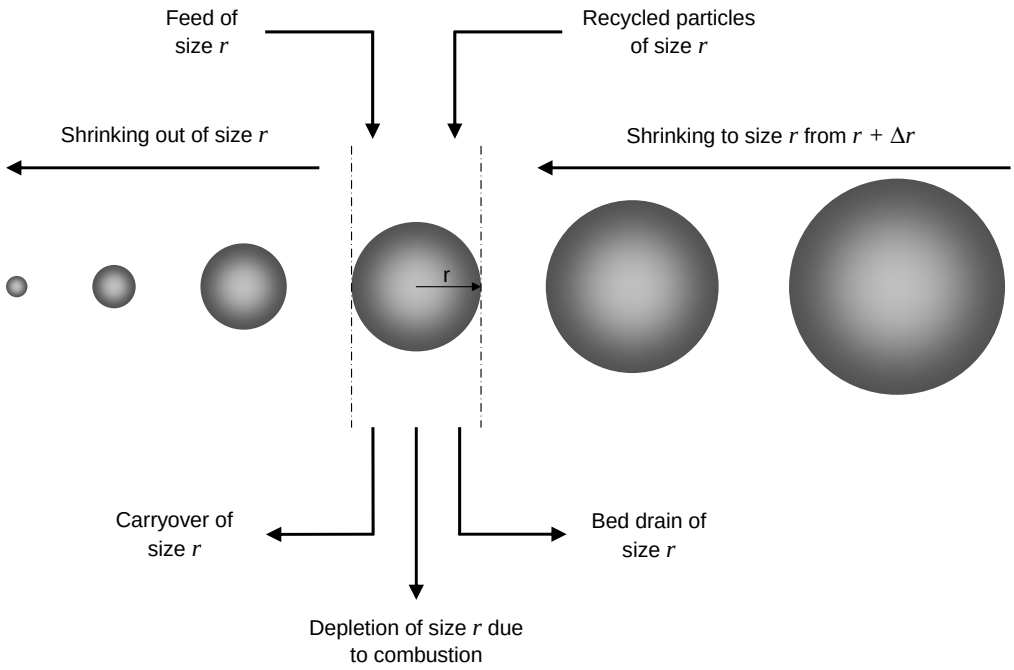

Figure 3.12: Schematic representation of char population balance.

Verbal form of unsteady-state mass balance for shrinking char particles is shown schematically in Figure 3.12. This balance can be written in symbols as

$$\left[M_{c,d}P_{c,d}(r)\Delta r\right]_{t+\Delta t} - \left[M_{c,d}P_{c,d}(r)\Delta r\right]_{t} = F_0P_0(r)\Delta r\Delta t + F_3P_3(r)\Delta r\Delta t$$
$$- F_1P_1(r)\Delta r\Delta t - F_2P_2(r)\Delta r\Delta t + \left[M_{c,d}P_{c,d}(r)\left(\frac{dr}{dt}\right)\Delta t\right]_{r}$$
$$- \left[M_{c,d}P_{c,d}(r)\left(\frac{dr}{dt}\right)\Delta t\right]_{r+\Delta r} + \frac{3M_{c,d}P_{c,d}(r)}{r}\left(\frac{dr}{dt}\right)\Delta t \quad (3.95)$$

where, time dependency of parameters has not been shown in formulations for the sake of simplicity in notation. Dividing both sides of Equation (3.95) by $\Delta r\Delta t$ and taking $lim_{\Delta r,\Delta t\to 0}$ one gets:

$$\frac{\partial}{\partial t}\left[M_{c,d}P_{c,d}(r)\right] = F_0P_0(r) + F_3P_3(r) - F_1P_1(r) - F_2P_2(r)$$
$$- \frac{\partial}{\partial r}\left[M_{c,d}P_{c,d}(r)\left(\frac{dr}{dt}\right)\right] + \frac{3}{r}M_{c,d}P_{c,d}(r)\left(\frac{dr}{dt}\right) \quad (3.96)$$

Recalling the assumption that solids are well mixed, *i.e.*,

$$P_1(r) = P_{c,d}(r) \tag{3.97}$$

and noting that the rate of elutriation of particles of size r is directly proportional to their concentration in the bed, *i.e.*,

$$F_2 P_2(r) = \kappa(r) M_{c,d} P_{c,d}(r) \tag{3.98}$$

where the proportionality constant, $\kappa(r)$, is named as elutriation rate constant, Equation (3.96) can be modified to yield,

$$\begin{aligned} \frac{\partial}{\partial t}\left[M_{c,d}P_{c,d}(r)\right] &= F_0 P_0(r) + F_3 P_3(r) - F_1 P_d(r) - \kappa(r) M_{c,d} P_{c,d}(r) \\ &\quad - \frac{\partial}{\partial r}\left[M_{c,d}P_{c,d}(r)\left(\frac{dr}{dt}\right)\right] + \frac{3}{r} M_{c,d} P_{c,d}(r)\left(\frac{dr}{dt}\right) \end{aligned} \tag{3.99}$$

The mechanism of particle elutriation is so complicated that no generalized model is yet available, though extensive studies on the subject have been carried out theoretically. Therefore, many empirical correlations have been proposed as a result of the extensive studies on elutriation [106, 147, 151–157]. In this thesis study, elutriation rate constant required in Equation (3.99) is calculated by using the definition of elutriation rate constant together with elutriation rate expression of Geldart *et al.* [154] as it was reported by Hannes [19] that expression of Geldart *et al.* shows the best performance when its predictions compared with measurements. The elutriation rate constant is defined as

$$\kappa(r) = \frac{A_d}{M_{c,d}} \kappa^*(r) \tag{3.100}$$

where $\kappa^*(r)$ is given by Geldart *et al.* [154] as

$$\kappa^*(r) = 23.7 \rho_g u_0 \exp\left(-5.4 \frac{u_t}{u_0}\right) \tag{3.101}$$

One can relate the flow rate of recycled particles with the elutriation rate of particles of size r by using the cyclone efficiency, $\eta_{cyc}(r)$ as

$$F_3 P_3(r) = \eta_{cyc}(r) F_2 P_2(r) \tag{3.102}$$

Combining Equations (3.98) and (3.102), substituting into Equation (3.99) and rearranging gives

$$\begin{aligned}\frac{\partial}{\partial t}\Big[M_{c,d}P_{c,d}(r)\Big] &= F_0 P_0(r) - F_1 P_d(r) - \big[1-\eta_{cyc}(r)\big]\kappa(r) M_{c,d}P_{c,d}(r) \\ &\quad - \frac{\partial}{\partial r}\left[M_{c,d}P_{c,d}(r)\left(\frac{dr}{dt}\right)\right] + \frac{3}{r}M_{c,d}P_{c,d}(r)\left(\frac{dr}{dt}\right)\end{aligned} \tag{3.103}$$

In order to express Equation (3.103) in more compact form, the unknowns, *i.e.* M_d and $P_d(r)$, are combined in a dummy variable defined as,

$$W(r) = M_{c,d}P_{c,d}(r) \tag{3.104}$$

and inserted to Equation (3.103) to yield the working form of the char population balance:

$$\begin{aligned}\frac{\partial W(r)}{\partial t} &= F_0 P_0(r) - \frac{W(r)}{M_d}F_1 - \big[1-\eta_{cyc}(r)\big]\kappa(r)W(r) \\ &\quad - \frac{\partial}{\partial r}\Big[W(r)\Re(r)\Big] + \frac{3}{r}W(r)\Re(r)\end{aligned} \tag{3.105}$$

where $\Re(r) = dr/dt$ is the shrinkage rate defined in Equation (3.91) and $P_0(r)$ is the size distribution of feed particles, represented by a Rosin-Rammler size distribution function given below:

$$P_0(r) = n\, b\, r^{n-1} \exp(b\, r^n) \tag{3.106}$$

Equation (3.105) is subject to the following boundary condition

$$\text{at } r = r_{max} \qquad W(r) = 0 \tag{3.107}$$

as the probability of having solid particles of size r_{max} in the dense zone is practically zero, due to the shrinkage of maximum particle size in the dense zone.

Once the solution for $W(r)$ becomes available, dense zone char hold-up, $M_{c,d}$, dense zone char size distribution, $P_d(r)$, riser exit char flow rate, F_2, riser exit char size distribution, $P_2(r)$, recycle char flow rate, F_3, recycle char size distribution, $P_3(r)$, fly ash char flow rate, F_4 and fly ash char size distribution, $P_4(r)$ are obtained from Equations (3.108) to (3.115) derived from descriptions given in Equations (3.98), (3.102) and (3.104).

$$M_{c,d} = \int_{r_{min}}^{r_{max}} W(r)dr \tag{3.108}$$

$$P_d(r) = \frac{W(r)}{M_{c,d}} \tag{3.109}$$

$$F_2 = \int_{r_{min}}^{r_{max}} \kappa(r)W(r)dr \tag{3.110}$$

$$P_2(r) = \frac{\kappa(r)W(r)}{F_2} \tag{3.111}$$

$$F_3 = \int_{r_{min}}^{r_{max}} \eta_{cyc}(r)F_2P_2(r)dr \tag{3.112}$$

$$P_3(r) = \frac{\eta_{cyc}(r)F_2P_2(r)}{F_3} \tag{3.113}$$

$$F_4 = \int_{r_{min}}^{r_{max}} \left[1 - \eta_{cyc}(r)\right]F_2P_2(r)dr \tag{3.114}$$

$$P_4(r) = \frac{\left[1 - \eta_{cyc}(r)\right]F_2P_2(r)}{F_4} \tag{3.115}$$

3.5 Gaseous Species Conservation Equations

Species conservation equations in both dense and dilute zone are formulated using conservative equations so that the axial variation of the velocities of bubble and emulsion phases and also the gas velocity in the dilute zone are inherently included. In the foregoing derivations species considered in the model will be denoted as shown in Table 3.11.

Table 3.11: Species considered in the model.

Species index, j	Species
1	O_2
2	CO
3	CO_2
4	H_2O
5	SO_2

3.5.1 Dense Zone

3.5.1.1 Bubble Phase

Under the assumption of plug flow of gas in bubble phase, a transient mass balance on species j between heights z and $z + \Delta z$ can be expressed in verbal form as,

$$\left\{ \begin{array}{c} species\ j \\ accumulated\ in \\ control\ volume \end{array} \right\} = \left\{ \begin{array}{c} species\ j\ in \\ by\ convection \\ at\ z \end{array} \right\} - \left\{ \begin{array}{c} species\ j\ out \\ by\ convection \\ at\ z + \Delta z \end{array} \right\} + \left\{ \begin{array}{c} species\ j \\ generated/depleted \\ by\ chemical\ reactions \end{array} \right\} + \left\{ \begin{array}{c} species\ j \\ transferred\ from/to \\ emulsion\ phase \end{array} \right\} \quad (3.116)$$

Using the definition of the gas interchange coefficient between bubble and emulsion phases given in Equation (3.24), above mentioned verbal form of species balance for component j can be rewritten in symbols as,

$$A_d \Delta z \delta \big[C_{j,b}|_{t+\Delta t} - C_{j,b}|_t \big] = \Delta t n_{j,b}|_z - \Delta t n_{j,b}|_{z+\Delta z} + A_d \delta \Delta z \Delta t \, \Re_{j,b} + A_d \delta \Delta z \Delta t \, K_{be} \big(C_{j,e} - C_{j,b} \big) \tag{3.117}$$

dividing both sides of Equation (3.117) by $A_{bed} \delta \Delta z \Delta t$ and taking $lim_{\Delta z, \Delta t \to 0}$ yields,

$$\frac{\partial C_{j,b}}{\partial t} = -\frac{1}{A_d \delta} \frac{\partial n_{j,b}}{\partial z} + \Re_{j,b} + K_{be} \big(C_{j,e} - C_{j,b} \big) \tag{3.118}$$

Ideal gas assumption can be utilized to express left hand side of Equation (3.118) in terms of molar flow rates. Under this assumption one may write,

$$C_{j,b} = \frac{P_j}{R T_d} \tag{3.119}$$

or,

$$C_{j,b} = \frac{P}{R T_d} \frac{n_{j,b}}{n_b} \tag{3.120}$$

Taking the derivative of Equation (3.120) with respect to time yields the term $\partial C_{j,b} / \partial t$:

$$\frac{\partial C_{j,b}}{\partial t} = \frac{P}{R} \left[-\frac{n_{j,b}}{n_b T_d^2} \frac{dT_d}{dt} + \frac{1}{n_b T_d} \frac{\partial n_{j,b}}{\partial t} - \frac{n_{j,b}}{n_b^2 T_d} \frac{\partial n_b}{\partial t} \right] \tag{3.121}$$

Combining Equations (3.118) and (3.121), and rearranging yields the working form of the species balance in bubble phase:

$$\frac{\partial n_{j,b}}{\partial t} = \frac{R T_d \, n_b}{P \, A_d \, \delta} \left[A_d \delta \Re_{j,b} + A_d \delta K_{be} (C_{j,e} - C_{j,b}) - \frac{\partial n_{j,b}}{\partial z} \right] + \frac{n_{j,b}}{T_d} \frac{dT_d}{dt} + \frac{n_{j,b}}{n_b} \frac{\partial n_b}{\partial t} \tag{3.122}$$

Equation (3.22) can be used to set the boundary condition of Equation (3.122) as,

$$\text{at } z = 0 \qquad n_{j,b} = y_{j,b} \frac{n_{a,pri}}{1 + \dfrac{u_e}{u_b} \dfrac{1-\delta}{\delta} \varepsilon_{mf}} \tag{3.123}$$

Species generation/depletion term in Equation (3.122), $Re_{j,b}$, takes the following forms for each species considered,

$j = 1 \quad (O_2)$

$$\Re_{1,b} = -0.5 r_{CO,b} \tag{3.124}$$

$j = 2 \quad (CO)$

$$\Re_{2,b} = -r_{CO,b} \tag{3.125}$$

$j = 3 \quad (CO_2)$

$$\Re_{3,b} = r_{CO,b} \tag{3.126}$$

$j = 4 \quad (H_2O)$

$$\Re_{4,b} = 0 \tag{3.127}$$

$j = 5 \quad (SO_2)$

$$\Re_{5,b} = 0 \tag{3.128}$$

3.5.1.2 Emulsion Phase

Under the assumption of plug flow of interstitial gas in emulsion phase, a transient mass balance on species j between heights z and $z+\Delta z$ can be expressed in verbal form as,

$$\left\{ \begin{array}{c} species\ j \\ accumulated\ in \\ control\ volume \end{array} \right\} = \left\{ \begin{array}{c} species\ j\ in \\ by\ convection \\ at\ z \end{array} \right\} - \left\{ \begin{array}{c} species\ j\ out \\ by\ convection \\ at\ z + \Delta z \end{array} \right\} + \left\{ \begin{array}{c} species\ j \\ generated/depleted \\ by\ chemical\ reactions \end{array} \right\} + \left\{ \begin{array}{c} species\ j \\ transferred\ from/to \\ emulsion\ phase \end{array} \right\} \tag{3.129}$$

Using the definition of the gas interchange coefficient between bubble and emulsion phases given in Equation (3.24), above mentioned verbal form of species balance for component j can be rewritten in symbols as,

$$\begin{aligned} A_d\Delta z(1-\delta)\varepsilon_{mf}\left[C_{j,e}|_{t+\Delta t} - C_{j,e}|_t\right] &= \Delta t n_{j,e}|_z - \Delta t n_{j,e}|_{z+\Delta z} \\ &+ A_d(1-\delta)\varepsilon_{mf}\Delta z\Delta t\Re_{j,e} \\ &+ A_d\delta\Delta z\Delta t K_{be}\big(C_{j,b} - C_{j,e}\big) \end{aligned} \tag{3.130}$$

dividing both sides of Equation (3.130) by $A_d(1-\delta)\varepsilon_{mf}\Delta z\Delta t$ and taking $lim_{\Delta z,\Delta t\to 0}$ yields,

$$\frac{\partial C_{j,e}}{\partial t} = -\frac{1}{A_d(1-\delta)\varepsilon_{mf}}\frac{\partial n_{j,e}}{\partial z} + \Re_{j,e} + \frac{\delta}{(1-\delta)\varepsilon_{mf}}K_{be}\big(C_{j,b} - C_{j,e}\big) \tag{3.131}$$

In order to express the left hand side of Equation (3.131) in terms of molar flow rates through ideal gas law, Equation (3.121) can be rewritten for emulsion phase as,

$$\frac{\partial C_{j,e}}{\partial t} = \frac{P}{R}\left[-\frac{n_{j,e}}{n_e T_d^2}\frac{dT_d}{dt} + \frac{1}{n_e T_d}\frac{\partial n_{j,e}}{\partial t} - \frac{n_{j,e}}{n_e^2 T_d}\frac{\partial n_e}{\partial t}\right] \tag{3.132}$$

and combined with Equation (3.131) to produce the working form of the species balance in the emulsion phase;

$$\begin{aligned} \frac{\partial n_{j,e}}{\partial t} = \frac{RT_d n_e}{PA_d(1-\delta)\varepsilon_{mf}}\Bigg[&A_d(1-\delta)\varepsilon_{mf}\Re_{j,e} \\ &+ A_d\delta K_{be}(C_{j,b} - C_{j,e}) - \frac{\partial n_{j,e}}{\partial z}\Bigg] + \frac{n_{j,e}}{T_d}\frac{dT_d}{dt} + \frac{n_{j,e}}{n_e}\frac{\partial n_e}{\partial t} \end{aligned} \tag{3.133}$$

Equation (3.22) can be used to set the boundary condition of Equation (3.122) as,

$$\text{at } z = 0 \qquad n_{j,e} = y_{j,e}\frac{n_{a,pri}}{1 + \dfrac{u_b}{u_{mf}}\dfrac{\delta}{(1-\delta)\varepsilon_{mf}}} \tag{3.134}$$

The expression for species generation/depletion term, $Re_{j,e}$, appearing in Equation (3.133) takes the following forms for each species considered,

$j = 1 \quad (O_2)$

$$\Re_{1,e} = -\frac{F_{vm}x_{vl}}{V_{bed}(1-\delta)\varepsilon_{mf}}\left[0.5\frac{x_{C,vm}}{M_C} + 0.5\frac{x_{H,vm}}{M_{H_2}} + \frac{x_{S,vm}}{M_S}\right] - 0.5n_{C,e} - 0.5r_{CO,e} \tag{3.135}$$

$j = 2 \quad (CO)$

$$\Re_{2,e} = \frac{F_{vm}x_{vl}}{V_{bed}(1-\delta)\varepsilon_{mf}}\left[0.5\frac{x_{C,vm}}{M_C}\right] + n_{C,e} - r_{CO,e} \tag{3.136}$$

$j = 3 \quad (CO_2)$

$$\Re_{3,e} = r_{CO,e} \tag{3.137}$$

$j = 4 \quad (H_2O)$

$$\Re_{4,e} = \frac{1}{V_{bed}(1-\delta)\varepsilon_{mf}}\left[F_{vm}x_{vl}\frac{x_{H,vm}}{M_{H_2}} + F_{coal}\frac{x_{H_2O}}{M_{H_2O}}\right] \tag{3.138}$$

$j = 5 \quad (SO_2)$

$$\Re_{5,e} = \frac{F_{vm}x_{vl}}{V_{bed}(1-\delta)\varepsilon_{mf}}\left[\frac{x_{S,vm}}{M_S}\right] \tag{3.139}$$

where volatile matter flow rate, F_{vm}, is calculated as

$$F_{vm} = F_{coal}x_{vm} \tag{3.140}$$

$n_{C,e}$ in Equations (3.135) and (3.136) is the solid carbon consumption rate in emulsion phase and given by the following equation (See Appendix B for derivation),

$$n_{C,e} = \frac{3M_{c,d}}{V_d(1-\delta)\varepsilon_{mf}}\frac{1}{M_C}\frac{x_{fc}}{x_{fc}+x_a}\int_{r_{min}}^{r_{max}}\frac{P_{c,d}(r)\,\Re(r)}{r}dr \tag{3.141}$$

3.5.2 Dilute Zone

The gases from the emulsion and bubble phases are assumed to mix instantaneously at the top of the dense zone and then enter dilute zone. Therefore, dilute zone consists of a single gas phase with solids dispersed in it. The gas is assumed to be in plug flow. A transient mass balance on species j between heights z and $z + \Delta z$ can be expressed in verbal form as,

$$\left\{ \begin{array}{c} species\ j \\ accumulated\ in \\ control\ volume \end{array} \right\} = \left\{ \begin{array}{c} species\ j\ in \\ by\ convection \\ at\ z \end{array} \right\} - \left\{ \begin{array}{c} species\ j\ out \\ by\ convection \\ at\ z + \Delta z \end{array} \right\} + \left\{ \begin{array}{c} species\ j \\ generated/depleted \\ by\ chemical\ reactions \end{array} \right\} \quad (3.142)$$

Above mentioned verbal form of species balance for component j can be written in symbols as,

$$A_f \Delta z (1 - \varepsilon_{s,f}) \left[C_{j,f}|_{t+\Delta t} - C_{j,f}|_t \right] = \Delta t n_{j,f}|_z - \Delta t n_{j,f}|_{z+\Delta z} + A_f (1 - \varepsilon_{s,f}) \Delta z \Delta t \Re_{j,f} \quad (3.143)$$

Dividing both sides of Equation (3.143) by $A_f(1-\varepsilon_s)\Delta z \Delta t$ and taking $lim_{\Delta z, \Delta t \to 0}$ yields,

$$\frac{\partial C_{j,f}}{\partial t} = -\frac{1}{A_f(1 - \varepsilon_{s,f})} \frac{\partial n_{j,f}}{\partial z} + \Re_{j,f} \quad (3.144)$$

Following the same approach applied to derivation of Equation (3.121), $\partial C_{j,f}/\partial t$ term takes the following form,

$$\frac{\partial C_{j,f}}{\partial t} = \frac{P}{R} \left[-\frac{n_{j,f}}{n_f T_f^2} \frac{\partial T_f}{\partial t} + \frac{1}{n_f T_f} \frac{\partial n_{j,f}}{\partial t} - \frac{n_{j,f}}{n_f^2 T_f} \frac{\partial n_f}{\partial t} \right] \quad (3.145)$$

Equation (3.145) is then combined with Equation (3.144) to produce the working form of the species balance in the dilute zone;

$$\frac{\partial n_{j,f}}{\partial t} = \frac{R\,T_f\,n_f}{P\,A_f(1-\varepsilon_{s,f})}\left[A_f(1-\varepsilon_{s,f})\Re_{j,f} - \frac{\partial n_{j,f}}{\partial z}\right] + \frac{n_{j,f}}{T_f}\frac{\partial T_f}{\partial t} + \frac{n_{j,f}}{n_f}\frac{\partial n_f}{\partial t} \tag{3.146}$$

Boundary condition for Equation (3.146) can be expressed as,

$$\text{at } z_f = 0 \qquad n_{j,f} = n_{j,e} + n_{j,b} + n_{a,sec}\,y_{j,a} \tag{3.147}$$

The expression for species generation/depletion term, $\Re_{j,f}$, appearing in Equation (3.146) takes the following forms for the species considered,

$j = 1 \quad (O_2)$

$$\Re_{1,f} = -\frac{F_{vm}(1-x_{vl})}{V_f(1-\varepsilon_{s,f})}\left[0.5\frac{x_{C,vm}}{M_C} + 0.5\frac{x_{H,vm}}{M_{H_2}} + \frac{x_{S,vm}}{M_S}\right] - 0.5n_{C,f} - 0.5r_{CO,f} \tag{3.148}$$

$j = 2 \quad (CO)$

$$\Re_{2,f} = \frac{F_{vm}(1-x_{vl})}{V_f(1-\varepsilon_{s,f})}\left[0.5\frac{x_{C,vm}}{M_C}\right] + n_{C,f} - r_{CO,f} \tag{3.149}$$

$j = 3 \quad (CO_2)$

$$\Re_{3,f} = r_{CO,f} \tag{3.150}$$

$j = 4 \quad (H_2O)$

$$\Re_{4,f} = \frac{F_{vm}(1-x_{vl})}{V_f(1-\varepsilon_{s,f})}\left[\frac{x_{H,vm}}{M_{H_2}}\right] \tag{3.151}$$

$j = 5 \quad (SO_2)$

$$\Re_{5,f} = \frac{F_{vm}(1-x_{vl})}{V_f(1-\varepsilon_{s,f})}\left[\frac{x_{S,vm}}{M_S}\right] \tag{3.152}$$

where $n_{C,f}$, the solid carbon consumption rate at any height in the dilute zone is the sum of carbon consumption rates for entrained and elutriated particles, as shown below,

$$n_{C,f} = \frac{1}{M_C}\frac{x_{fc}}{x_{fc}+x_a}\left[\rho_c \int_{r_{maxe}}^{r_{max}} \frac{\varepsilon_{c,f}(z)P_{c,f}(r,z)}{r}\Re_f(r)dr \right.$$

$$\left. + \frac{F_2}{A_f}\int_{r_{min}}^{r_{max}} \frac{P_2(r)}{r\left[u_0 - u_t(r)\right]}\Re_f(r)dr\right] \tag{3.153}$$

3.6 Energy Conservation Equations

3.6.1 Dense Zone

3.6.1.1 Energy Balance for Char Particles

The char particle temperature is calculated by solving an energy balance around the particle. The particle is assumed to have uniform temperature. This assumption implies that the rate of heat transfer within a char particle is fast relative to that between the particle surface and the surrounding gas and therefore temperature gradient occurs across the gas film surrounding the particle. Weimer and Clough [149] has shown that this assumption is valid for char particles of diameter less than 7 mm in a gasifier operating with superficial velocies of up to 3.5 m/s and temperature of 1235 K. These operating conditions are similar to those found in circulating FBCs. With this approach the heat transfer effects are lumped at the particle surface, and the accumulation of thermal energy within the particle is related to the rate of heat transfer between the particle and the surrounding gas and to the rate of heat generation by chemical reaction. Following this, the char particle energy balance takes the following verbal form,

$$\left\{\begin{array}{c} energy \\ accumulated \\ in\ the\ particle \end{array}\right\} = \left\{\begin{array}{c} energy\ generated \\ by\ chemical \\ reaction \end{array}\right\} - \left\{\begin{array}{c} energy \\ loss\ by \\ convection \end{array}\right\} - \left\{\begin{array}{c} energy \\ loss\ by \\ radiation \end{array}\right\} \tag{3.154}$$

or in symbols,

$$\frac{4}{3}\pi r^3 \rho_c c_{p,c} \frac{dT_c}{dt} = \frac{4\pi r^2 \rho_c}{M_C} \frac{x_{fc}}{x_{fc}+x_a} \Delta H^o_{R14} \Re(r) - 4\pi r^2 \Big[h_p (T_c - T_d) + \sigma \epsilon (T_c^4 - T_d^4) \Big] \tag{3.155}$$

Dividing both sides of Equation (3.155) by $4\pi r^2$ and rearranging results in the working form of the char particles energy balance:

$$\frac{dT_c}{dt} = \frac{3 x_{fc} \Delta H^o_{R14}}{r\, M_C\, c_{p,c}\, (x_{fc}+x_a)} \Re(r) - \frac{3}{r \rho_c\, c_{p,c}} \Big[h_p (T_c - T_d) + \sigma \epsilon (T_c^4 - T_d^4) \Big] \tag{3.156}$$

where ΔH^o_{R14} is the heat released from combustion of carbon, given by

$$\Delta H^o_{R14} = \left(2 - \frac{2}{\zeta}\right) \Delta H^o_{R10} + \left(\frac{2}{\zeta} - 1\right) \Delta H^o_{R11} \tag{3.157}$$

and h_p is the convective heat transfer coefficient between gas and char particle calculated by using the expression of Wakao *et al.* [158],

$$h_p = \frac{k_g}{d_p} \Big[2.0 + 1.1 Re_p^{0.6} Pr^{0.33} \Big] \tag{3.158}$$

where particle Reynolds number, Re_p, and Prandtl number, Pr, are defined as,

$$Re_p = \frac{d_p u_0 \rho_c}{\mu_g} \tag{3.159}$$

$$Pr = \frac{c_{p,c} \mu_g}{k_g} \tag{3.160}$$

3.6.1.2 Energy Balance for Dense Zone Walls

The refractory walls of a CFB act as a damper to temperature fluctuations in the bed. As the bed temperature increases or decreases due to changes in operating conditions, walls slow down the response of the bed through its thermal

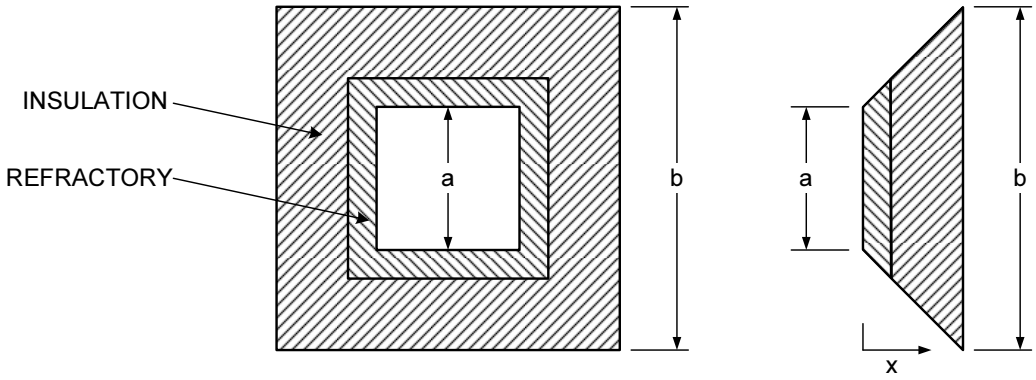

Figure 3.13: Layout of the combustor walls.

inertia by acting either as a heat source or as a heat sink. The combustor wall surrounding the bed have a mass sufficient to make its dynamic effect an important consideration in the temperature dynamics of the bed. Therefore, thermal inertia of the wall is taken into consideration by making an one-dimensional heat transfer analysis.

The combustor has a square cross-section and the walls are refractory lined. In order to minimize the heat loss, walls are insulated with an insulating material. Figure 3.13 illustrates the layout of the walls.

In order to obtain the temperature profile through the dense zone walls the following assumptions are made:

- Heat transfer is one dimensional. Therefore, energy balance is performed on a quarter of the wall.
- Contact resistance between the refractory and insulation material is negligible.
- Properties of both refractory and insulation material are temperature independent.
- Outer surface temperature of the combustor is known.

Following these assumptions, wall energy balance takes the following verbal form,

$$\left\{ \begin{array}{c} energy \\ accumulated \\ in\ the\ wall \end{array} \right\} = \left\{ \begin{array}{c} energy\ in\ by \\ conduction \\ at\ x \end{array} \right\} - \left\{ \begin{array}{c} energy\ out\ by \\ conduction \\ at\ x + \Delta x \end{array} \right\} \tag{3.161}$$

or in symbols,

$$A_x\,\Delta x\,\rho_w\,c_{p,w}\,(T_{dw}|_{t+\Delta t} - T_{dw}|t) = q_x A_x|_x - q_x A_x|_{x+\Delta x} \tag{3.162}$$

Dividing both sides of Equation (3.162) by $\Delta x \Delta t$ and taking $lim_{\Delta x,\Delta t \to 0}$ gives

$$\rho_w\,c_{p,w}\,A_x \frac{\partial T_{dw}}{\partial t} = -\frac{\partial}{\partial x}\left(A_x\,q_x\right) \tag{3.163}$$

Inserting Fourier's law of heat conduction to Equation (3.163) results in

$$\rho_w\,c_{p,w}\,A_x \frac{\partial T_{dw}}{\partial t} = k_w \frac{\partial}{\partial x}\left(A_x \frac{\partial T_{dw}}{\partial x}\right) \tag{3.164}$$

A_x term appearing in Equations (3.162)-(3.164) is the cross-sectional area perpendicular to heat flow and varies with the distance x. Variation of heat transfer area, A_x, with the distance can be expressed as below,

$$A_x = 8H_d\left(x + \frac{A_d^{0.5}}{2}\right) \tag{3.165}$$

Combining Equations (3.164) and (3.165) and rearranging results in the working form of the energy balance in the wall:

$$\frac{\partial T_{dw}}{\partial t} = \frac{k_w}{\rho_w\,c_{p,w}\left(x + \frac{A_d^{0.5}}{2}\right)}\left[\frac{\partial T_{dw}}{\partial x} + \left(x + \frac{A_d^{0.5}}{2}\right)\frac{\partial^2 T_{dw}}{\partial x^2}\right] \tag{3.166}$$

Equation (3.166) is subject to the following boundary conditions:

$$\text{at } x = 0 \qquad h_{dw}(T_d - T_{dw}) = -k_w \frac{\partial T_{dw}}{\partial x} \tag{3.167}$$

$$\text{at } x = L_{bw} \qquad T_{dw} = T_{dw,o} \tag{3.168}$$

In order to predict the heat transfer between bed and the walls, semi empirical correlation developed by Kunii and Levenspiel [159] is adopted for the heat transfer coefficient, h_{dw},

$$h_{dw} = h_r + (1 - \delta_w)\left[\frac{2k_{ew}}{d_p} + 0.05\, c_{p,g}\, \rho_g\, u_0\right] \tag{3.169}$$

where h_r is the radiant heat transfer coefficient between particle surface to wall surface calculated by

$$h_r = \frac{\sigma}{\dfrac{1}{\epsilon_p} + \dfrac{1}{\epsilon_w} + 1}\left[\frac{T_d^4 - T_{dw}^4}{T_d - T_{dw}}\right] \tag{3.170}$$

and k_{ew} is the effective thermal conductivity with stagnant gas in the vicinity of wall surface given by the following correlation:

$$k_{ew} = \varepsilon_w k_g + \frac{(1 - \varepsilon_w)k_p}{0.115\left(\dfrac{k_p}{k_g}\right) + \dfrac{2}{3}} \tag{3.171}$$

In Equations (3.169)-(3.171) δ_w, ε_w, ϵ_p and ϵ_w represent the bubble fraction in the vicinity of the wall, void fraction near the wall, emissivity of particle and emissivity of wall surface. In the model it is assumed that $\delta_w = \delta$ and $\varepsilon_w = \varepsilon_{mf}$ for simplicity.

3.6.1.3 Energy Balance for Dense Zone

In the model no distinction is made in terms of temperature between bubble and emulsion phases. The dense zone is assumed to be represented by a single temperature, T_d. Energy balance on the dense zone is formulated by assuming that the gas and the inert particles are at the same temperature and that the mass of combustion gases and char particles are negligible compared to the mass of inerts. The combined gas/solid phase energy balance includes the following terms:

$$\left\{\begin{array}{c}Energy\\ accumulated\\ in\ dense\ zone\end{array}\right\} = \underbrace{\left\{\begin{array}{c}Energy\\ brought\\ by\ air\end{array}\right\}}_{Q_{air}} + \underbrace{\left\{\begin{array}{c}Energy\\ generated\ by\\ chemical\ reactions\end{array}\right\}}_{Q_{rxn}}$$
$$+ \underbrace{\left\{\begin{array}{c}Energy\\ transferred\ from\\ char\ particles\end{array}\right\}}_{Q_{char}} + \underbrace{\left\{\begin{array}{c}Energy\\ transferred\ from\\ recycled\ particles\end{array}\right\}}_{Q_{rec}}$$
$$- \underbrace{\left\{\begin{array}{c}Energy\\ required\ to\ vaporize\\ moisture\ in\ coal\end{array}\right\}}_{Q_{vap}} - \underbrace{\left\{\begin{array}{c}Energy\\ lost\ with\\ combustion\ gases\end{array}\right\}}_{Q_{gas}} - \underbrace{\left\{\begin{array}{c}Energy\\ lost\ from\\ bed\ walls\end{array}\right\}}_{Q_{wall}}$$
$$- \underbrace{\left\{\begin{array}{c}Energy\\ lost\ with\\ elutriated\ particles\end{array}\right\}}_{Q_{co}} - \underbrace{\left\{\begin{array}{c}Energy\\ lost\ with\\ bed\ drain\ stream\end{array}\right\}}_{Q_{bd}} \quad (3.172)$$

The items appearing in Equation (3.172), can be expressed in symbols as:

$$Q_{air} = n_a \int_{T_{ref}}^{T_a} c_{p,a} dT \quad (3.173)$$

$$Q_{rxn} = A_d\, \Delta H^o_{R13} \left[\varepsilon_{mf}(1-\delta) \int_0^{H_d} r_{CO,e}\, dz + \delta \int_0^{H_d} r_{CO,b}\, dz\right]$$
$$+ F_{vm}\, x_{vl} \left[\frac{x_{C,vm}}{M_C}\Delta H^o_{R4} + \frac{x_{H,vm}}{M_{H_2}}\Delta H^o_{R5} + \frac{x_{S,vm}}{M_S}\Delta H^o_{R6}\right] \quad (3.174)$$

$$Q_{char} = \frac{3M_{c,d}}{\rho_c} \int_{r_{min}}^{r_{max}} \left[h_p(T_c - T_d) + \sigma\epsilon(T_c^4 - T_d^4)\right] \frac{dr}{r} \quad (3.175)$$

$$Q_{rec} = G_s\, A_f\, c_{p,i}(T_{rec} - T_{ref}) \quad (3.176)$$

$$Q_{vap} = F_{coal}\, x_{H_2O}\, \lambda^o_{H_2O} \quad (3.177)$$

$$Q_{gas} = (n_e + n_b) \sum_{j=1}^{6} y_j \int_{T_{ref}}^{T_d} c_{p,g,j} dT \quad (3.178)$$

$$Q_{wall} = A_{dw}\, h_{dw}\, (T_d - T_{dw,s}) \quad (3.179)$$

$$Q_{co} = \frac{G_s\, A_f}{(1-\eta_{cyc})} c_{p,i}(T_d - T_{ref}) \tag{3.180}$$

$$Q_{bd} = F_{bd}\, c_{p,i}(T_d - T_{ref}) \tag{3.181}$$

where overall cyclone efficiency, η_{cyc}, is given by the following equation.

$$\eta_{cyc} = \int_{r_{min}}^{r_{max}} \eta_{cyc}(r)\, P_{i,f}(r, H_f) dr \tag{3.182}$$

When all of the above terms are assembled, the resulting equation yields the dense zone energy balance,

$$\frac{dT_d}{dt} = \frac{1}{M_i c_{p,i}} \left[Q_a + Q_{rxn} + Q_p + Q_{rec} - Q_{vap} - Q_g - Q_{dw} - Q_{co} - Q_{bd} \right] \tag{3.183}$$

3.6.2 Dilute Zone

3.6.2.1 Surface Energy Balance for Dilute Zone Walls

A surface energy balance is formulated to solve for the temperature of the dilute zone wall at any height through the dilute zone by noting that rate of energy transferred from dilute zone to wall must equal to rate of energy transferred through the wall, *i.e.*,

$$\left\{ \begin{array}{c} energy\ transferred \\ from\ dilute\ zone \\ to\ wall \end{array} \right\} = \left\{ \begin{array}{c} rate\ of\ energy \\ tranferred \\ through\ wall \end{array} \right\} \tag{3.184}$$

or in symbols,

$$h_f(z)\,[T_f(z) - T_{fw}(z)] - \frac{[T_{fw}(z) - T_\infty]}{R_{fw}(z)} = 0 \tag{3.185}$$

where h_f and R_{fw} are the gas side total heat transfer coefficient and thermal resistance across the wall, respectively. Gas side total heat transfer coefficient is calculated by using empirical equation of Basu and Nag [160],

$$h_f(z) = 40\,\rho_{sus}(z)^{0.5} \tag{3.186}$$

where suspension density, ρ_{sus}, is calculated from,

$$\rho_{sus}(z) = \varepsilon_{c,f}(z)\,\rho_c + \varepsilon_{i,f}(z)\,\rho_i \tag{3.187}$$

3.6.2.2 Energy Balance for Dilute Zone

The gas temperature profile in the dilute zone is obtained by solving an energy balance which considers convective transport and, generation and loss of energy. On a differential volume element of thickness Δz in the dilute zone, the energy balance takes the following verbal form,

$$\left\{\begin{array}{c} energy \\ accumulated \\ in\ the\ control \\ volume \end{array}\right\} = \left\{\begin{array}{c} energy\ in \\ by\ convection \\ at\ z \end{array}\right\} - \left\{\begin{array}{c} energy\ out \\ by\ convection \\ at\ z+\Delta z \end{array}\right\} + \left\{\begin{array}{c} energy\ generation \\ and\ loss\ rate\ within \\ the\ control\ volume \end{array}\right\} \tag{3.188}$$

or in symbols,

$$\frac{\partial}{\partial t}(A_f \Delta z(1-\varepsilon_{s,f})\rho_g c_{p,g}(T_f - T_r)) = M_g n_f c_{p,g}(T_f - T_r)|_z - M_g n_f c_{p,g}(T_f - T_r)|_{z+\Delta z} + A_f \Delta z(1-\varepsilon_{s,f})\boldsymbol{R} \tag{3.189}$$

Dividing both sides of Equation (3.189) by $A_f \Delta z(1-\varepsilon_{s,f})$ and taking $lim_{\Delta z \to 0}$ results in,

$$\frac{\partial}{\partial t}(\rho_g(T_f - T_r)) = -\frac{M_g}{A_f(1-\varepsilon_{s,f})}\frac{\partial}{\partial z}(n_f(T_f - T_r)) + \frac{\boldsymbol{R}}{c_{p,g}} \tag{3.190}$$

Let,

$$\Delta T = (T_f - T_r) \tag{3.191}$$

$$\rho_g = \frac{PM_g}{RT_f} \tag{3.192}$$

and combine Equations (3.190)-(3.192) to obtain,

$$\frac{PM_g}{R}\frac{\partial}{\partial t}\left(\frac{\Delta T}{T_f}\right) = -\frac{M_g}{A_f(1-\varepsilon_{s,f})}\frac{\partial}{\partial z}(n_f \Delta T) + \frac{\boldsymbol{R}}{c_{p,g}} \tag{3.193}$$

Expanding derivatives in Equation (3.193) by summation rule and rearranging results in the working form of the energy balance in the dilute zone,

$$\begin{aligned}\frac{\partial T_f}{\partial t} = &-\frac{RT_f^2 n_f}{A_f(1-\varepsilon_{s,f})PT_r}\frac{\partial T_f}{\partial z} + \frac{RT_f^2}{PM_g T_r c_{p,g}}\boldsymbol{R} \\ &- \frac{RT_f^2(T_f - T_r)}{A_f(1-\varepsilon_{s,f})PT_r}\frac{\partial n_f}{\partial z}\end{aligned} \tag{3.194}$$

Equation (3.194) has the following boundary condition,

$$\text{at } z_f = 0 \qquad T_f = T_d \tag{3.195}$$

In above equations $\boldsymbol{R}$ is the combined energy generation and loss rate per unit volume of the dilute zone. It is the sum of energy generated by chemical reactions, $\boldsymbol{R}_{rxn}$, energy loss from the dilute zone walls, $\boldsymbol{R}_{fw}$, and energy transferred from/to char and ash particles present in the dilute zone, $\boldsymbol{R}_p$. These terms can be expressed as follows,

$$\begin{aligned}\boldsymbol{R}_{rxn} = &\Delta H^o_{R13} r_{CO,f} + \frac{F_{vm}(1-x_{vl})}{V_f(1-\varepsilon_{s,f})}\left[\frac{x_{C,vm}}{M_C}\Delta H^o_{R4}\right. \\ &\left. + \frac{x_{H,vm}}{M_{H_2}}\Delta H^o_{R5} + \frac{x_{S,vm}}{M_S}\Delta H^o_{R6}\right]\end{aligned} \tag{3.196}$$

$$\boldsymbol{R}_{fw} = -\frac{4D_f}{A_f(1-\varepsilon_{s,f})}h_{fw}(T_f - T_{fw}) \tag{3.197}$$

$$\boldsymbol{R}_p = \frac{3F_2}{A_f \rho_c} \int_{rmin}^{r_{maxe}} \frac{P_3(r)}{r(u_0 - u_t(r))} \left[h_p(T_c - T_f) + \sigma\epsilon(T_c^4 - T_f^4)\right] dr$$

$$+ 3\varepsilon_{c,f}(z) \int_{r_{maxe}}^{r_{max}} \frac{P_{c,f}(r,z)}{r} \left[h_p(T_c - T_f) + \sigma\epsilon(T_c^4 - T_f^4)\right] dr$$

$$+ 3\varepsilon_{i,f}(z) \int_{r_{maxe}}^{r_{max}} \frac{P_{i,f}(r,z)}{r} \left[h_p(T_i - T_f) + \sigma\epsilon(T_i^4 - T_f^4)\right] dr \qquad (3.198)$$

3.7 Steady State Forms of Model Equations

Initial conditions assigned to dynamic model should be physically correct and accurate. In addition, since several sub-models are solved simultaneously, initial conditions assigned to a sub-model should be consistent with those of other models. This can be achieved by providing the initial conditions of the dynamic model from the simultaneous solution of governing equations with all temporal derivatives set to zero.

As initial conditions, char particles temperatures, size distribution, hold-up and flow rates, inert hold-up, species concentration profiles in bubble and emulsion phases, dense zone wall temperature profile and dense zone temperature are prescribed in the dense zone model. For the dilute zone, initial conditions are prescribed for species concentration profiles, gas and wall temperature profiles, and char and inert hold-up profiles and size distributions.

Following are the steady-state equations solved for the initial conditions required.

3.7.1 Dense Zone

Char Particles Temperatures

$$\frac{\rho_c}{M_C} \frac{x_{fc}}{(x_{fc} + x_a)} \Delta H^o_{R14}\, \Re(r) - \left[h_p(T_c - T_d) + \sigma\epsilon_d(T_c^4 - T_d^4)\right] = 0 \qquad (3.199)$$

Char Particles Size Distribution

$$\frac{dW(r)}{dr} = F_0 P_0(r) - W(r) \left[\frac{F_1}{M_d\, \Re(r)} + [1 - \eta_{cyc}(r)] \frac{\kappa(r)}{\Re(r)} - \frac{3}{r}\right] \qquad (3.200)$$

where,

$$W(r) = M_d P_d(r) \Re(r) \tag{3.201}$$

Equation (3.200) is solved with following boundary condition,

$$\text{at } r = r_{max} \qquad W(r) = 0 \tag{3.202}$$

Once the solution for $W(r)$ becomes available, dense zone char hold-up, M_d, dense zone char size distribution, $P_d(r)$, riser exit char flow rate, F_2, riser exit char size distribution, $P_2(r)$, recycle char flow rate, F_3, recycle char size distribution, $P_3(r)$, fly ash char flow rate, F_4 and flys ash char size distribution, $P_4(r)$ are obtained from the following equations:

$$M_d = \int_{r_{min}}^{r_{max}} W(r) dr \tag{3.203}$$

$$P_d(r) = \frac{W(r)}{M_d} \tag{3.204}$$

$$F_2 = \int_{r_{min}}^{r_{max}} \kappa(r) W(r) dr \tag{3.205}$$

$$P_2(r) = \frac{\kappa(r) W(r)}{F_2} \tag{3.206}$$

$$F_3 = \int_{r_{min}}^{r_{max}} \eta_{cyc}(r) F_2 P_2(r) dr \tag{3.207}$$

$$P_3(r) = \frac{\eta_{cyc}(r) F_2 P_2(r)}{F_3} \tag{3.208}$$

$$F_4 = \int_{r_{min}}^{r_{max}} \left[1 - \eta_{cyc}(r)\right] F_2 P_2(r) dr \tag{3.209}$$

$$P_4(r) = \frac{\left[1 - \eta_{cyc}(r)\right] F_2 P_2(r)}{F_4} \tag{3.210}$$

Species Concentration Profiles in Bubble Phase

$$\frac{dn_{j,b}}{dz} = A_d\delta\left[\Re_{j,b} + K_{be}(C_{j,e} - C_{j,b})\right] \tag{3.211}$$

Equation (3.211) is solved with following boundary condition,

$$\text{at } z = 0 \qquad n_{j,b} = y_{j,b}\frac{n_{a,pri}}{1 + \dfrac{u_e}{u_b}\dfrac{1-\delta}{\delta}\varepsilon_{mf}} \tag{3.212}$$

Species Concentration Profiles in Emulsion Phase

$$\frac{dn_{j,e}}{dz} = A_{bed}\delta\left[\frac{(1-\delta)}{\delta}\varepsilon_{mf}\Re_{j,e} + K_{be}(C_{j,b} - C_{j,e})\right] \tag{3.213}$$

Equation (3.213) is solved with following boundary condition,

$$\text{at } z = 0 \qquad n_{j,e} = y_{j,e}\frac{n_{a,pri}}{1 + \dfrac{u_b}{u_{mf}}\dfrac{\delta}{(1-\delta)\varepsilon_{mf}}} \tag{3.214}$$

Dense Zone Wall Temperature Profile

$$\frac{d^2T_{dw}}{dx^2}(x + A_d^{0.5}/2) + \frac{dT_{dw}}{dx} = 0 \tag{3.215}$$

Equation (3.215) is a two–point boundary value problem. It is converted to an initial value problem by defining a new variable ψ as,

$$\psi = \frac{dT_{dw}}{dx} \tag{3.216}$$

and combining with the original equation,

$$\frac{d\psi}{dx}(x + A_d^{0.5}/2) + \psi = 0 \tag{3.217}$$

The appropriate boundary conditions for Equations (3.216) and (3.217) are, then, obtained from Equations (3.167) and (3.168) and represented by the following equations respectively,

$$\text{at } x = 0 \qquad \psi = -\frac{1}{k_{dw}} h_{dw}(T_d - T_{dw}) \tag{3.218}$$

$$\text{at } x = L_{dw} \qquad T_{dw} = T_{dw,o} \tag{3.219}$$

Dense Zone Temperature

$$Q_a + Q_{rxn} + Q_p + Q_{rec} - Q_{vap} - Q_g - Q_{dw} - Q_{co} - Q_{bd} = 0 \tag{3.220}$$

3.7.2 Dilute Zone

Species Concentration Profiles in Dilute Zone

$$\frac{dn_{j,f}}{dz} = A_f(1 - \varepsilon_{s,f})\Re_{j,f} \tag{3.221}$$

Boundary condition for Equation (3.221) can be expressed as,

$$\text{at } z_f = 0 \qquad n_{j,f} = n_{j,e} + n_{j,b} + n_{a,sec}\, y_{j,a} \tag{3.222}$$

Dilute Zone Temperature

$$\frac{dT_f}{dz} = \frac{A_f(1 - \varepsilon_{s,f})}{n_f c_{p,g}} \boldsymbol{R} \tag{3.223}$$

Equation (3.223) has the following boundary condition,

$$\text{at } z_f = 0 \qquad T_f = T_d \tag{3.224}$$

CHAPTER 4

NUMERICAL SOLUTION METHOD AND PROCEDURE

4.1 General

Numerical analysis of large-scale scientific and engineering problems has gained significant interest in the last two decades due to advancements in the processing and storage capabilities of modern computers. Several numerical techniques and computational schemes have been proposed for the solution of partial differential equations (PDEs) governing the transport processes in these systems. Among these techniques method of lines (MOL), which is a semi-discrete method, has proven to be a very accurate and efficient approach for a diverse range of applications including unsteady isothermal/non-isothermal, laminar/turbulent flows and radiative heat transfer. MOL enables explicit/implicit solutions with higher-order approximations in temporal discretization and provides the flexibility in utilization of well established difference schemes for spatial discretization without additional effort in formulation. Hence, in the present study, the governing equations are solved using the MOL technique.

4.2 Steady State Solution

The steady state model equations are comprised of 17 non-linear first order and 1 non-linear second order ordinary differential equations (ODEs) to solve simultaneously for the unknowns $n_{j,b}$, $n_{j,e}$, $n_{j,f}$ with $j = 1, 2, \ldots, 5$, T_f, $W(r)$, T_{dw} and 3 non-linear algebraic equations to solve for T_c, T_d and T_{fw}. The model has been implemented in a computer code written in FORTRAN 90. The numerical solution of the differential equations has been carried out by using the backward differentiation formula (BDF) method embedded in

the ODE solver, namely, LSODES of the LSODE family [161]. The source code of LSODES and its dependencies can be obtained from the website, *http://www.netlib.org/odepack/*. Solution of the non-linear algebraic equations has been performed by using a code in which bisection and the secant rule are fused to produce an efficient computational scheme for finding roots of nonlinear equations of the form $f(x) = 0$ when $f(x)$ is a continuous real function of a single variable x. The code is named ZERO and can be found in the website *ftp://ftp.wiley.com/public/college/math/sapcodes/*. Detailed description of ZERO can be found elsewhere [162]. Numerical integrals appearing in the model equations have been carried out by the code INTLG2 which utilizes 2nd order Lagrange polynomial on odd numbered grid for numerical integration.

4.2.1 Structure of the Code

The structure of the code for the solution of steady state model equations is given in Figures 4.1-4.5. The code has been arranged as much as possible in a modular fashion, with different programs with different tasks. Hence the number of subprograms is fairly large. However, this feature aids in both understanding and, if necessary, modifying the code.

Subroutines of steady state prediction program can be categorized as

- main driver routine which exerts the overall control of the code: CFBCSIM,
- auxiliary routines for creation of log files, reading of input data, checking the coal analysis, calculation of char properties, calculation of composition of volatiles, allocation of arrays, generation of grid points, assumptions and initial estimates and preliminary calculations and stoichiometric combustion calculation: LOGFILES, READINPUT, CHECKANALYSES, CHARPROP, VMCOMP, CREATEARRAYS, GRIDGEN, ASSUMPTIONS, ESTIMATES, PRECALC and STOICHCOMB,
- routines for initialization of boundary conditions of ODEs: PSD_INITIAL, DENSE_INITIAL, DILUTE_INITIAL and WALL_DENSE_INITIAL,

- driver routines for solution of ODEs and non-linear algebraic equations: PSD_SOLVE, DENSE_SOLVE, DILUTE_SOLVE, ENERGY_DENSE, WALL_DENSE_SOLVE, ENERGY_CHAR, ENERGY_DENSE_WALL and ENERGY_DILUTE_WALL,
- routines for calculation of derivatives: PSD_DERV, DENSE_DERV, DILUTE_DERV and WALL_DENSE_DERV,
- functions for assemblage of non-linear algebraic equations: FCN_CHAR, FCN_DENSE, FCN_DENSE_WALL and FCN_DILUTE_WALL,
- function routines for computation of species generation/depletion terms in emulsion and bubble phases, and in dilute zone: F_ERATE, F_BRATE and F_DRATE,
- functions for calculation heat and mass transfer coefficients: F_KM, F_HBW, F_HP and F_HDW,
- functions for property evaluation: F_AIRDEN, F_AIRVIS, F_AIRTC, F_AIRH, F_D and F_AIRCP,
- routines for printing results of ODE solver: PSD_PRINT, DENSE_PRINT, DILUTE_PRINT and WALL_DENSE_PRINT,
- routines for hydrodynamics: HYDRODENSE and HYDRODILUTE,
- routines for numerical integration, ODE solution and root finding: INTLG2, LSODES and ZERO,
- functions for char combustion kinetics: F_RKC, F_KM and F_DRDT,
- routines for transferring dependent variables and their derivatives to 1D array to be used by LSODE: PSD_TRANSFER, DENSE_TRANSFER, DILUTE_TRANSFER and WALL_DENSE_TRANSFER,
- routines for transferring dependent variables and their derivatives back to real variables: PSD_BACKTRANSFER, DENSE_BACKTRANSFER, DILUTE_BACKTRANSFER and WALL_DENSE_BACKTRANSFER.

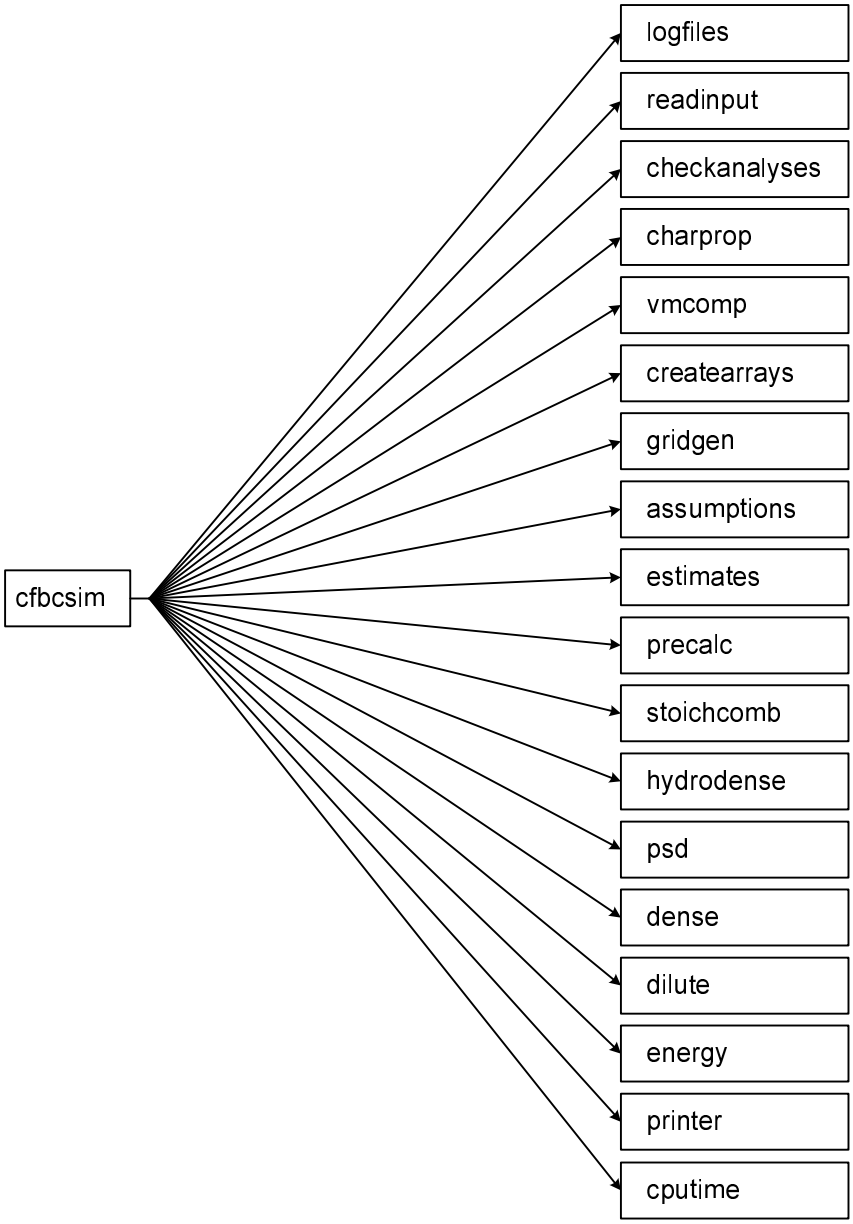

Figure 4.1: Organization of steady state model main routine CFBCSIM.

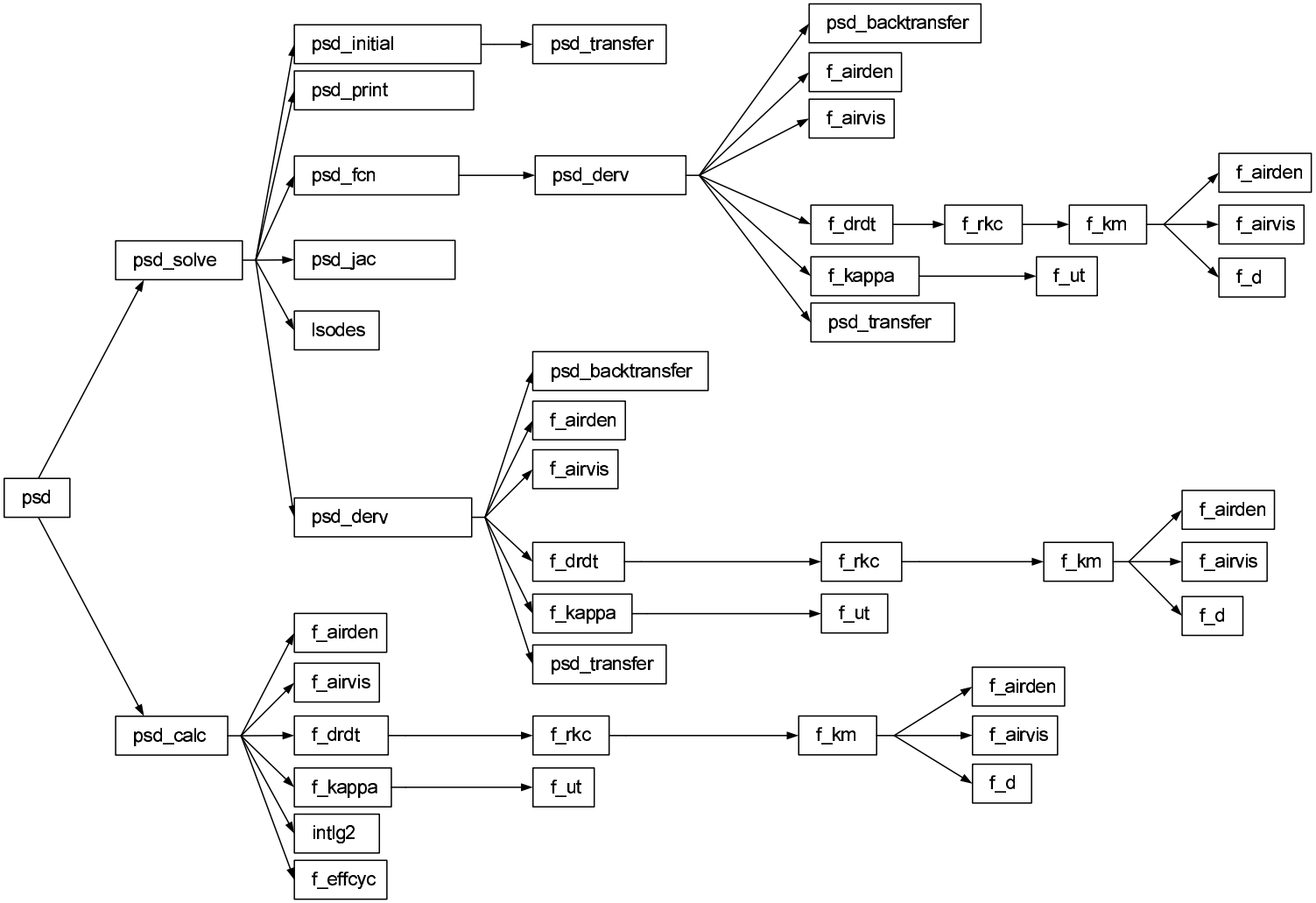

Figure 4.2: Organization of steady state model subroutine PSD.

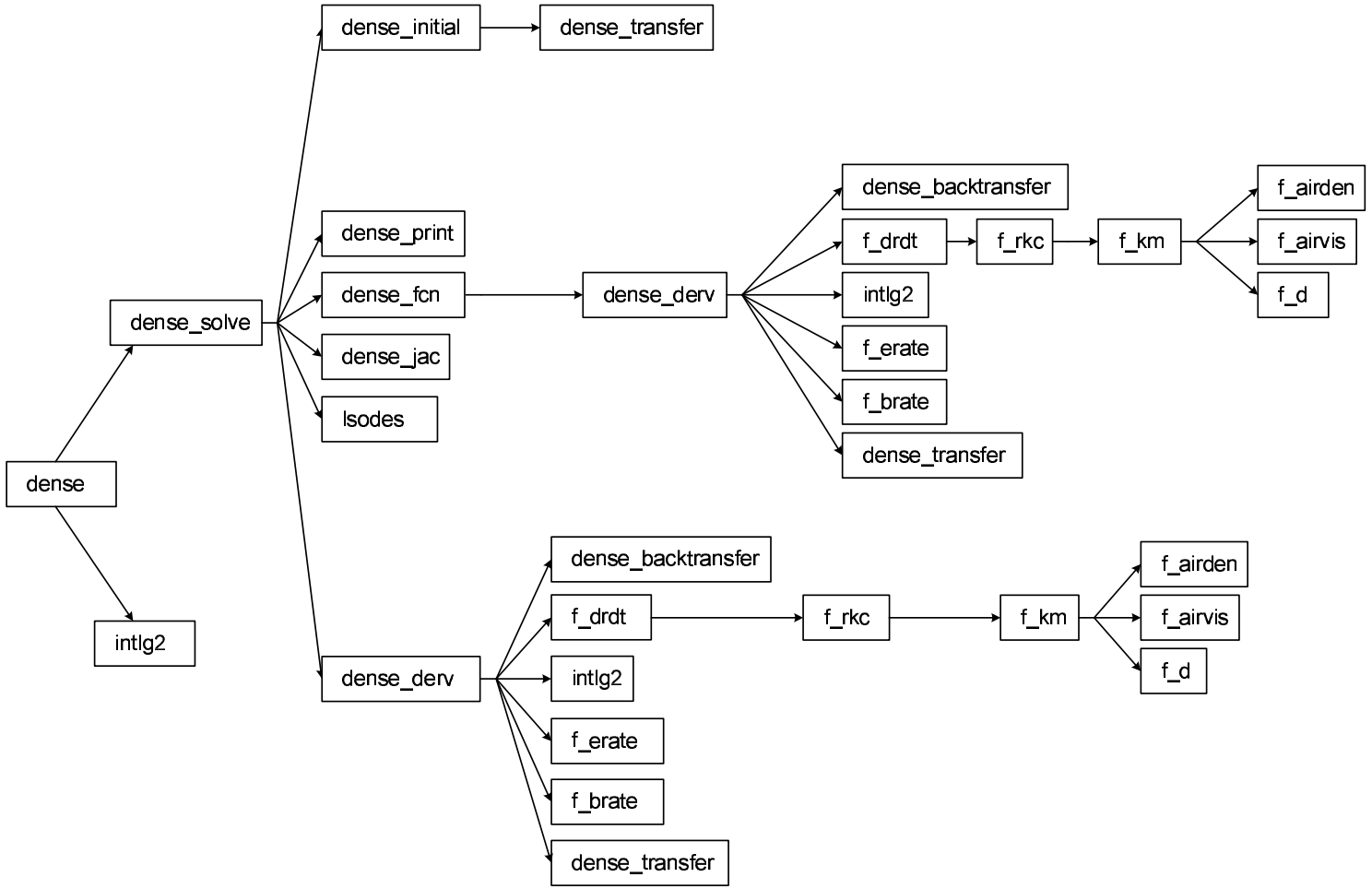

Figure 4.3: Organization of steady state model subroutine DENSE.

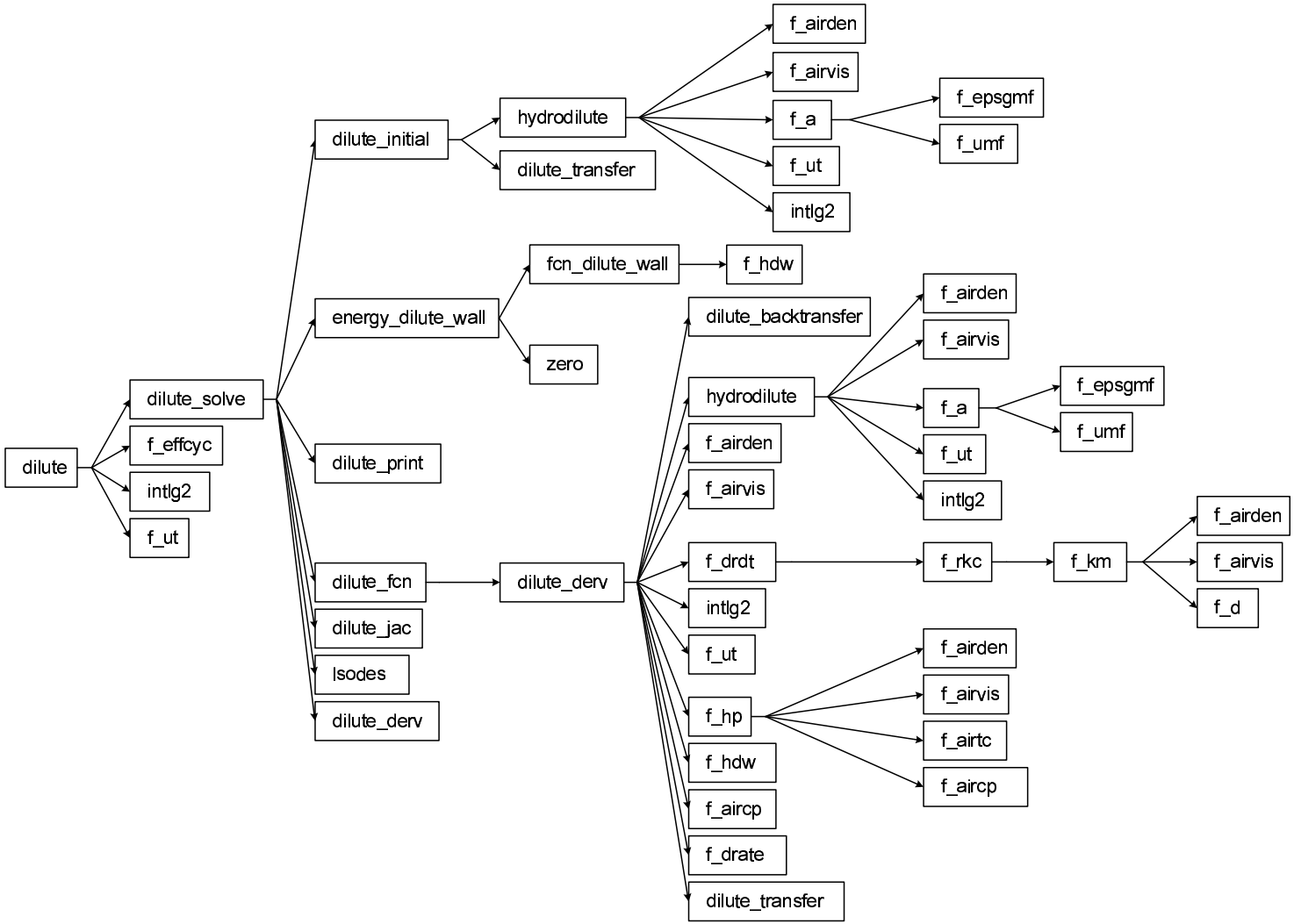

Figure 4.4: Organization of steady state model subroutine DILUTE.

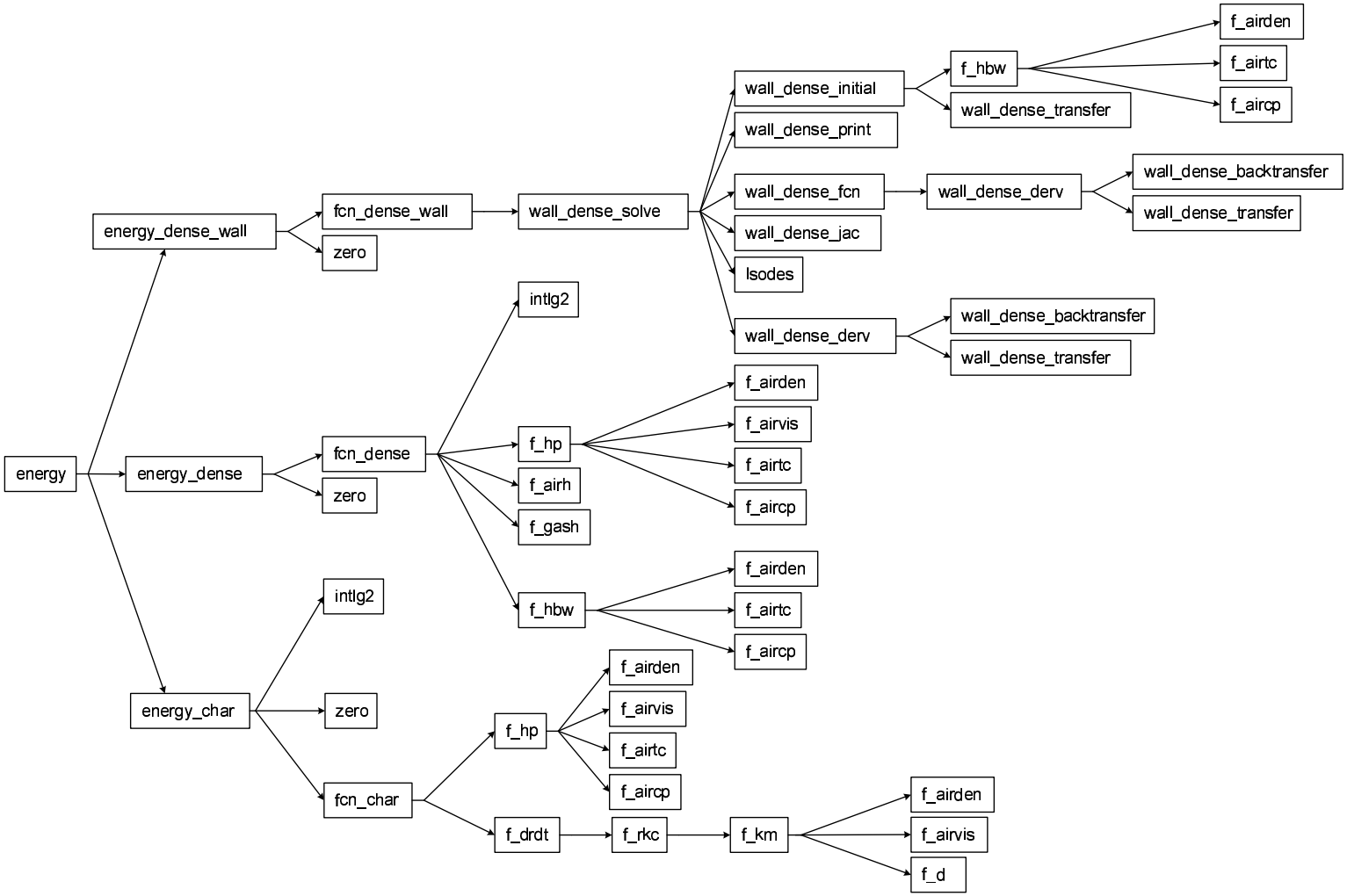

Figure 4.5: Organization of steady state model subroutine ENERGY.

4.2.2 Mode of Operation

The general algorithm of the solution of governing equations of steady state model are depicted in Figures 4.6-4.13. The solution procedure starts with making initial guesses for dense zone temperature, T_d, average emulsion phase O_2 mole fraction, $\overline{y}_{O_2,e}$, dense zone char hold-up, $M_{c,d}$ and dilute zone wall resistance, R_{fw}. This is followed by computation of char particles temperatures, $T_c(r)$, by using estimated parameters. There are five loops of iterations to be converged for T_d, $\overline{y}_{O_2,e}$, $M_{c,d}$, $\overline{T}_c$ and R_{fw}. For each loop, a convergence criterion is set as the absolute difference between calculated and estimated values of the parameters,

$$|\Gamma_{calc} - \Gamma_{est}| < \epsilon \tag{4.1}$$

The predictions reported in this study were obtained with ϵ values of 1.0×10^{-3} kg, 1.0×10^{-4}, 1.0 K, 1.0 K and 5.0×10^{-1} $J/m^2 \cdot s \cdot K$ for iterations on $M_{c,d}$, $\overline{y}_{O_2,e}$, $\overline{T}_c$, T_{bed} and R_{fw}, respectively.

Spatial domains of dense zone, dilute zone, char particles radius, bed wall thickness were divided into $(N_d - 1)$, $(N_f - 1)$, $(N_p - 1)$ and $(N_{dw} - 1)$ intervals, respectively, for regular printing of results and for numerical integration. The predictions reported in this study were obtained with N_d, N_f, N_p and N_{bw} values of 31, 51, 101 and 21, respectively.

4.3 Transient Solution

4.3.1 Numerical Solution by the Method of Lines

The method of lines, consists of converting the system of PDEs into an ODE initial value problem by discretizing all the equations in all but one independent variable and integrating the resulting ODEs by using an ODE integrator. The advantage of MOL is that sophisticated packages exist for the numerical solution of ordinary differential equations [163] and these packages when used for the integration of resulting ODEs take the burden of time discretization and choose the time steps in such a way that maintain the accuracy and stability of

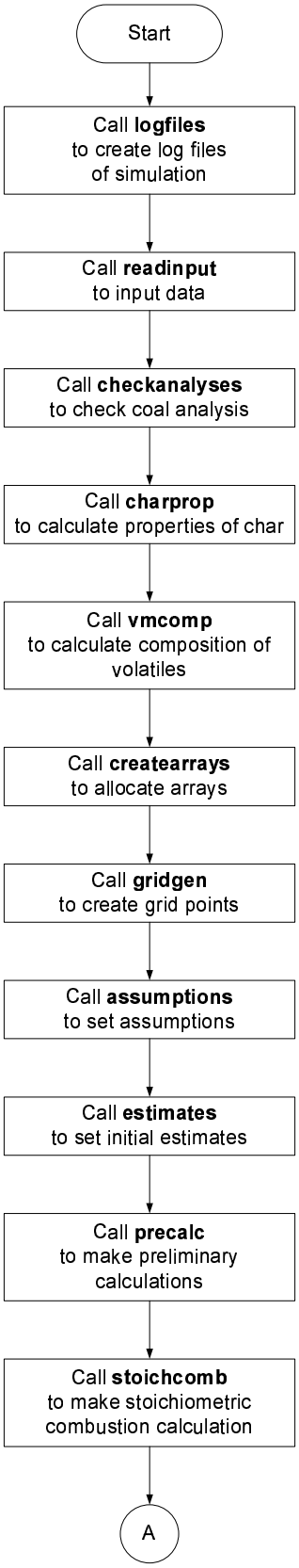

Figure 4.6: Algorithm of the steady state code (Part I).

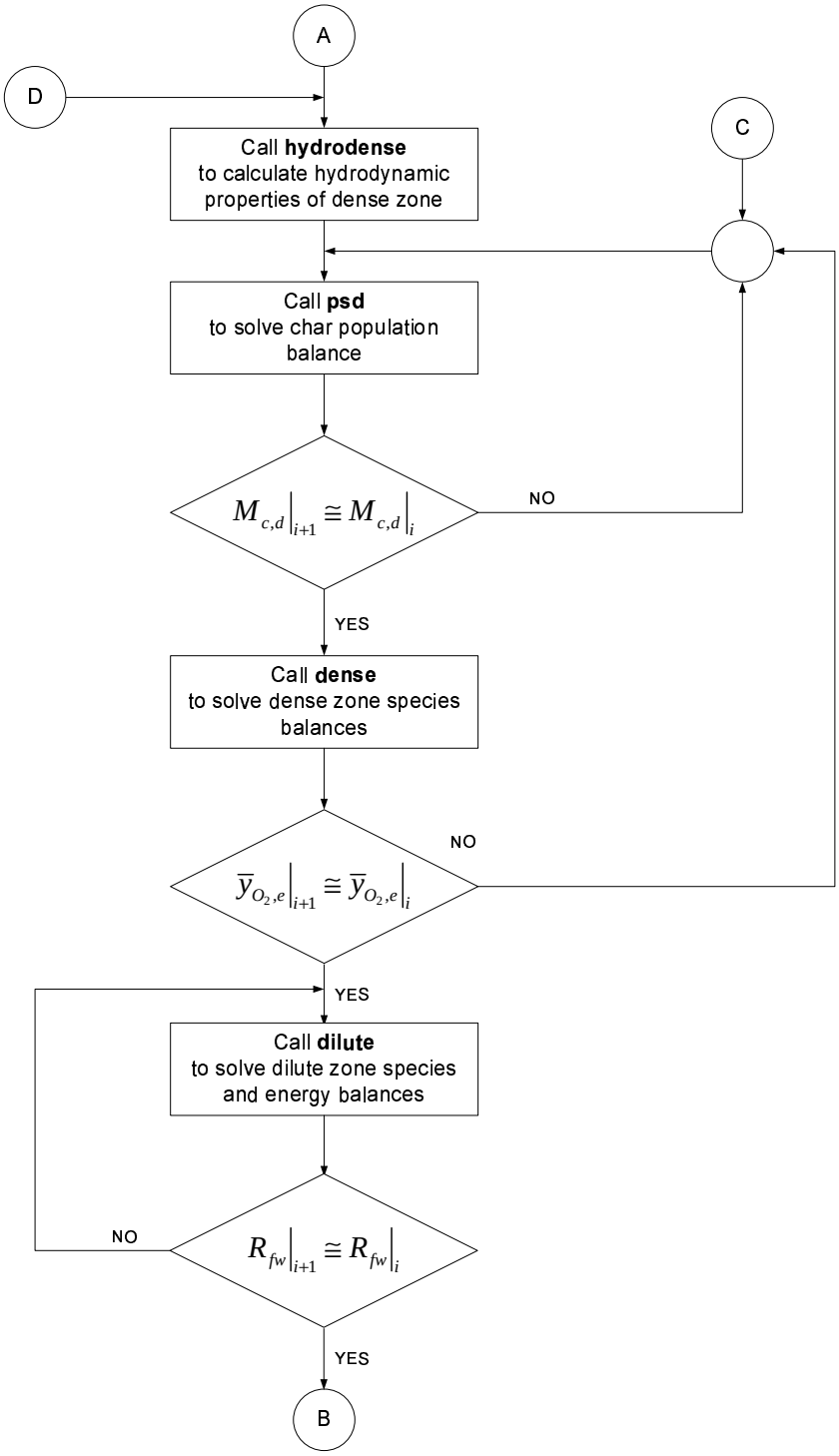

Figure 4.7: Algorithm of the steady state code (Part II).

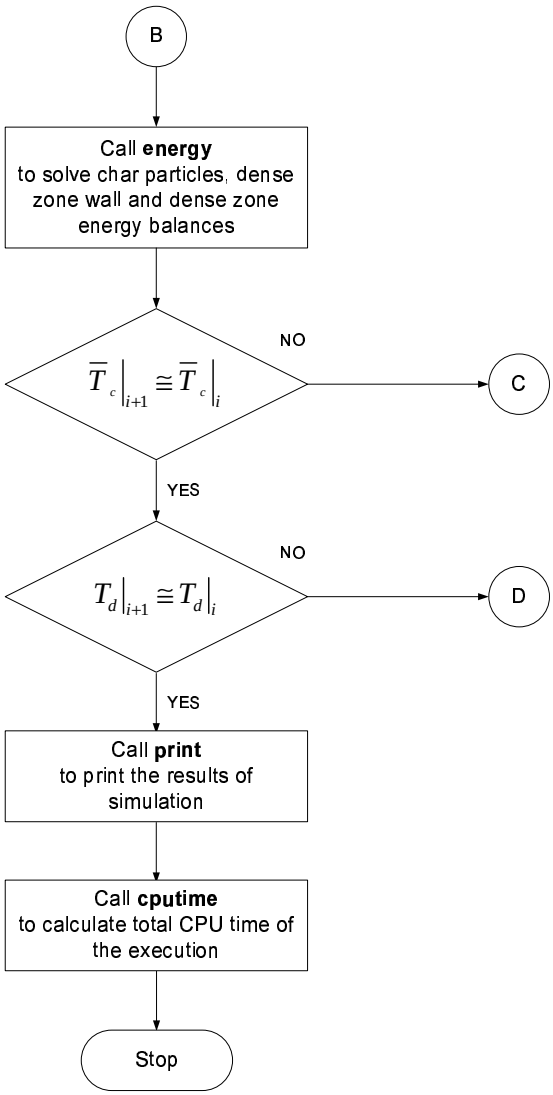

Figure 4.8: Algorithm of the steady state code (Part III).

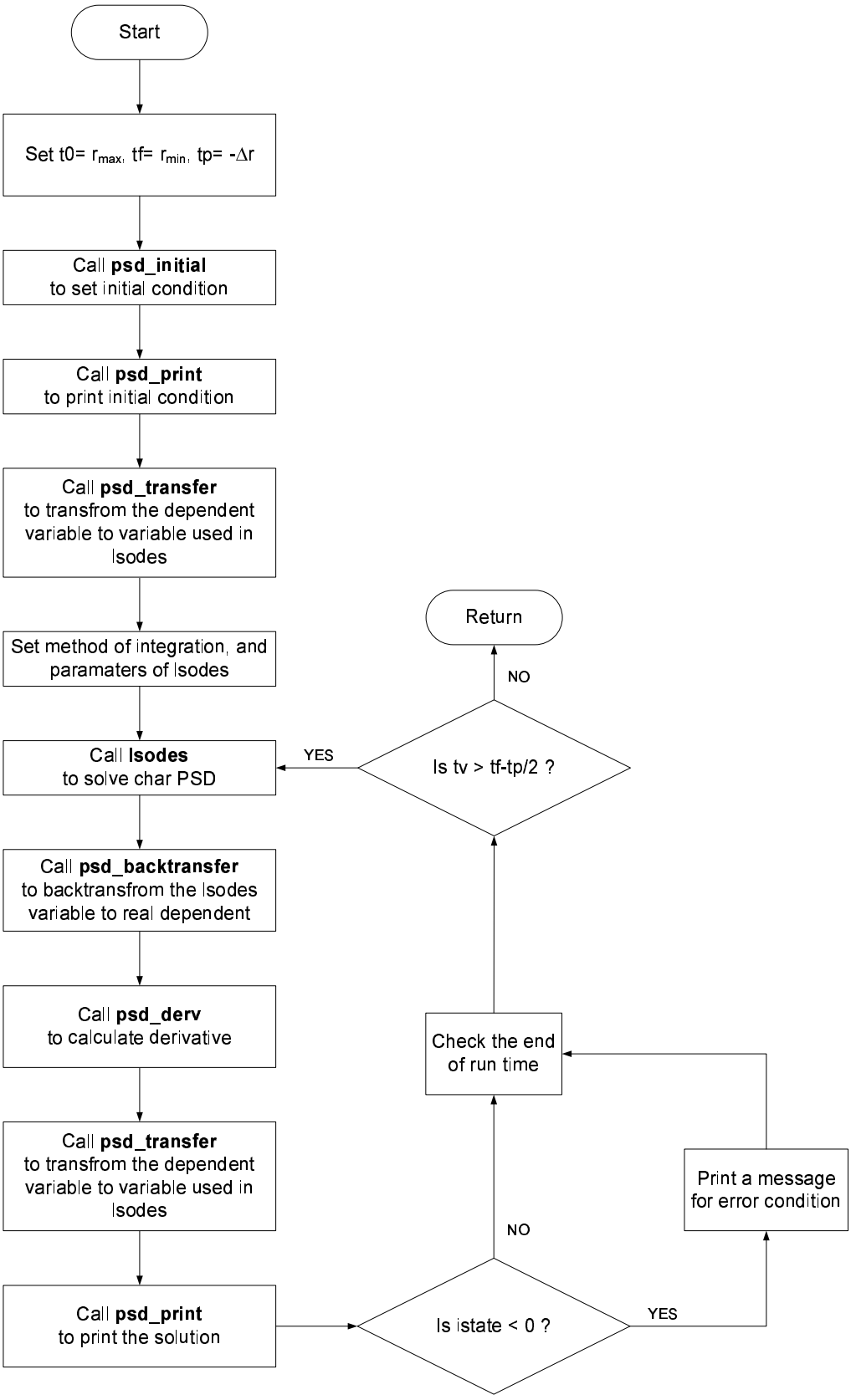

Figure 4.9: Algorithm of the subroutine PSD_SOLVE.

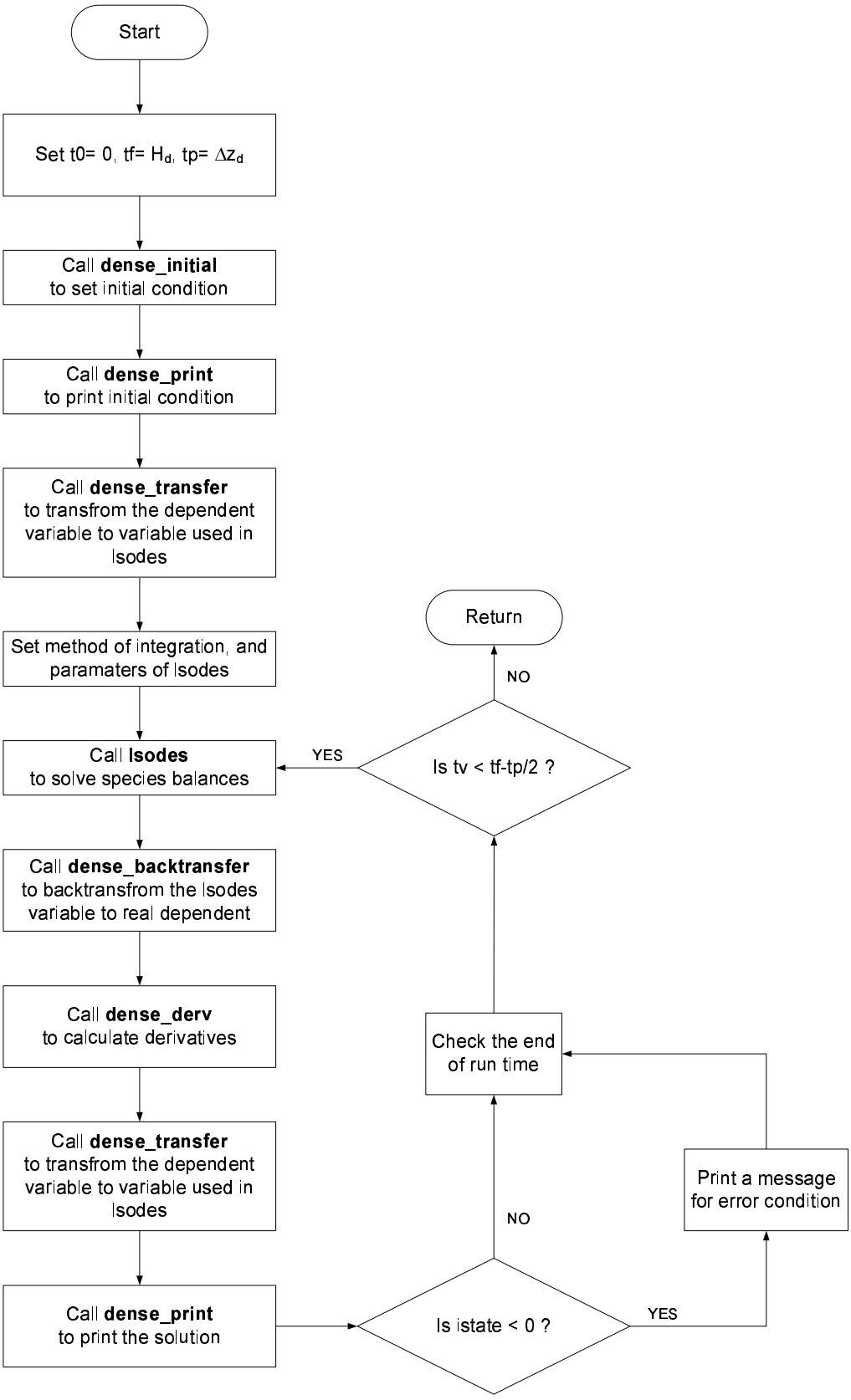

Figure 4.10: Algorithm of the subroutine DENSE_SOLVE.

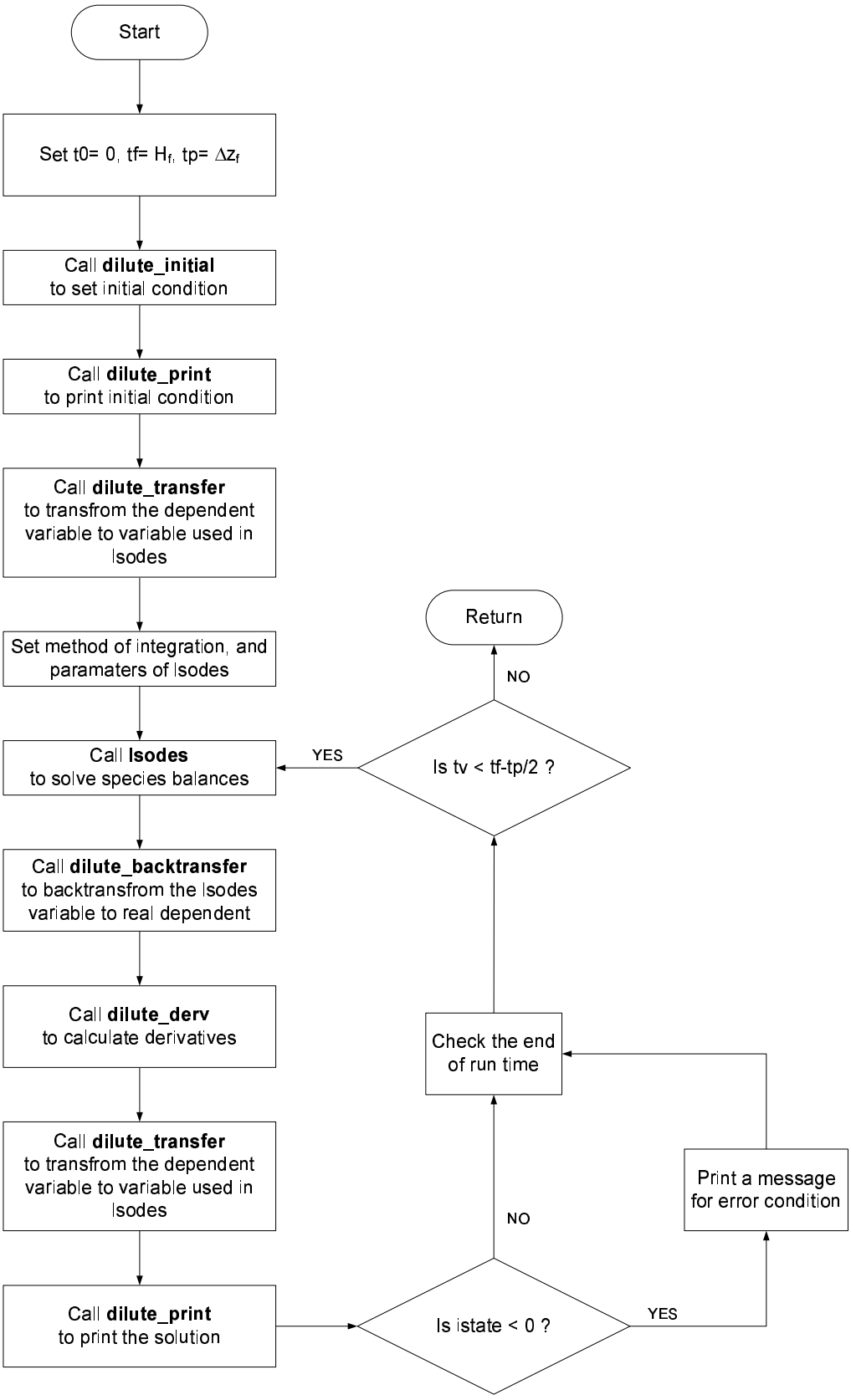

Figure 4.11: Algorithm of the subroutine DILUTE_SOLVE.

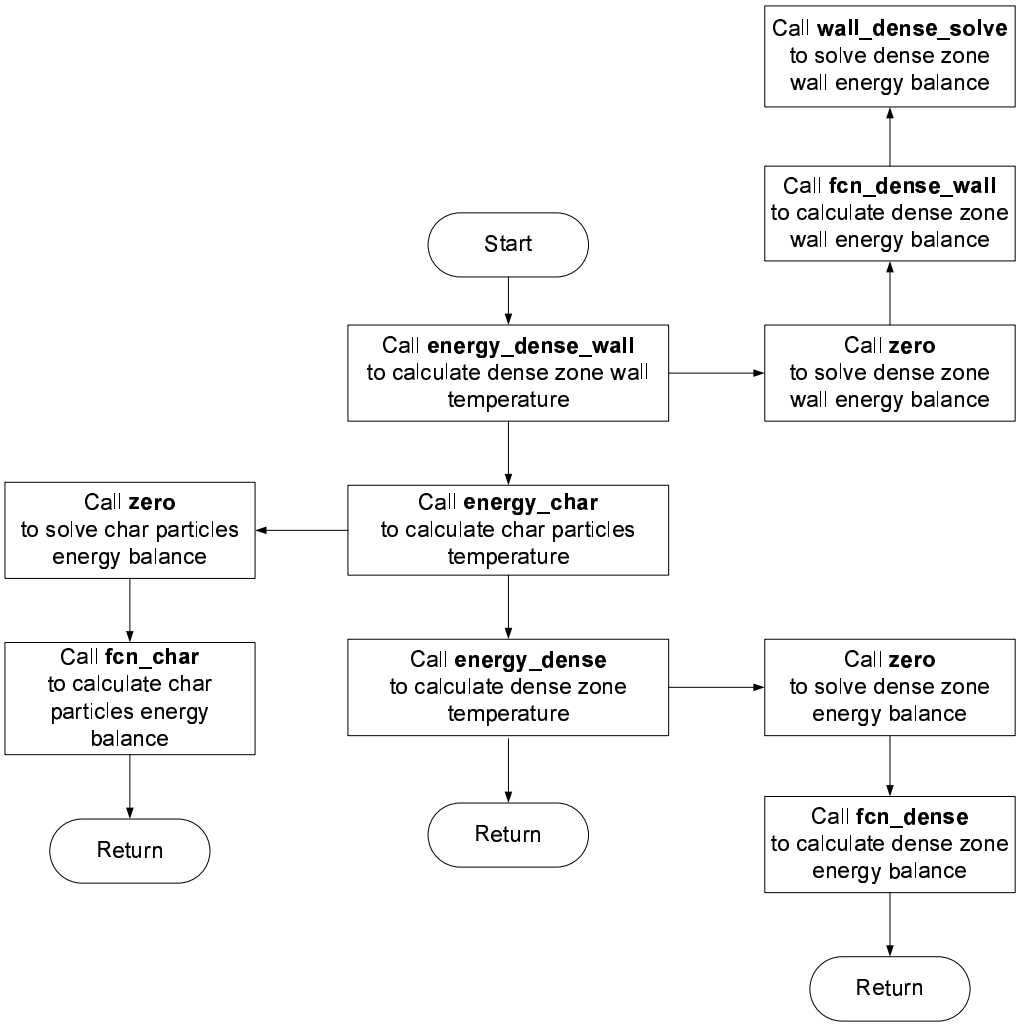

Figure 4.12: Algorithm of the subroutine ENERGY.

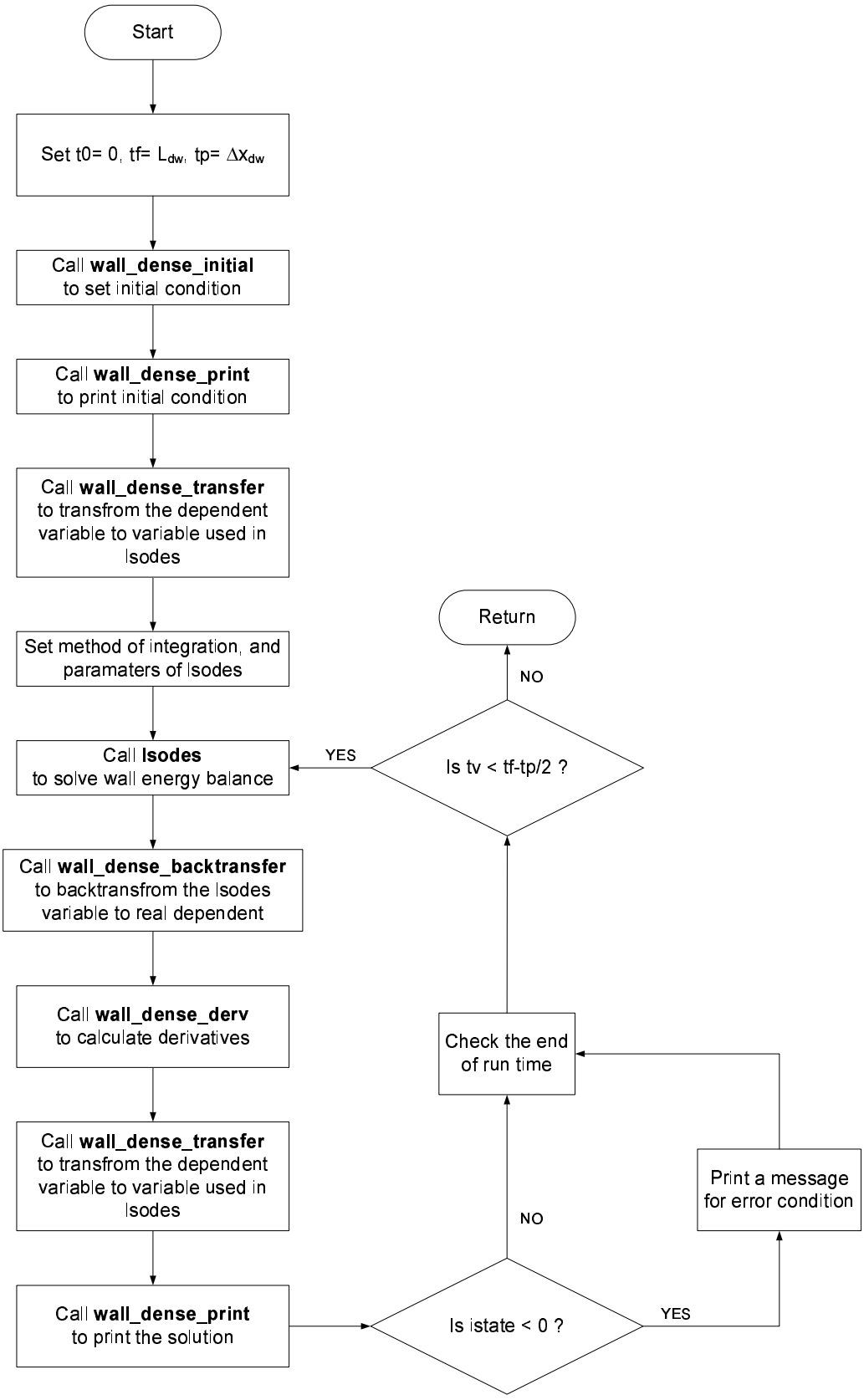

Figure 4.13: Algorithm of the subroutine WALL_DENSE_SOLVE.

the evolving solution. The most important advantage of the MOL approach is that it has not only the simplicity of the explicit methods but also the superiority (stability advantage) of the implicit ones unless a poor numerical method for the solution of ODEs is employed. By using the MOL approach, it is possible to achieve higher-order approximations in the discretization of spatial derivatives without significant increases in computational complexity and additional difficulties with boundary conditions, and comparable orders of accuracy in the time integration without using extremely small time steps due to the use of highly efficient and reliable initial value ODE solvers.

4.3.2 Spatial Discretization

In general, the large-scale scientific and engineering problems like the one under consideration frequently end up with non-linear PDEs or system of ODEs and PDEs. Thus, the application of the MOL approach to the numerical solution of PDEs results in nonlinear ODE problem as well. Unfortunately, a general stability analysis of a system of nonlinear ODEs is not possible. Therefore, the ideas for linear ODEs are applied to non-linear ones for investigating the stability properties.

A system of linear ODEs can be written conveniently in the general matrix form as

$$d\bar{y}/dt = \bar{A}\bar{y} \tag{4.2}$$

where $\bar{A}$ is a constant square matrix, $\bar{y}$ is the vector of dependents. The general solution to Equation (4.2) is obtained as [164]

$$\begin{aligned} y_1 &= C_{11}e^{\lambda_1 t} + C_{12}e^{\lambda_2 t} + \cdots + C_{1n}e^{\lambda_n t} \\ y_2 &= C_{21}e^{\lambda_1 t} + C_{22}e^{\lambda_2 t} + \cdots + C_{2n}e^{\lambda_n t} \\ &\vdots \\ y_n &= C_{n1}e^{\lambda_1 t} + C_{n2}e^{\lambda_2 t} + \cdots + C_{nn}e^{\lambda_n t} \end{aligned} \tag{4.3}$$

where C_{11} to C_{nn} are eigenvectors and λ_1 to λ_n are the eigenvalues. In order that the solution of Equation (4.2) to be stable, all eigenvalues must have negative real parts. More generally, for a system of n linear, constant coefficient ODEs to be stable, the n eigenvalues must be in the left half of the complex plane. This is the stability of the ODE problem. If this condition is not met for all of the eigenvalues, the associated exponentials will then grow with time making the system unstable.

The ODE problem stability can be satisfied by choosing the appropriate direction of discretization of the convective term in accordance with the sign of the characteristic speed. The characteristic speeds for the equations derived in this model are the speeds of different systems. It was shown that [164], in order to produce stable ODE systems, the convective term in a PDE must be discretized by using upwind or downwind differencing schemes when characteristic speed is positive or negative, respectively. Therefore in this thesis study, the convective term in a particular PDE is discretized using upwind differencing scheme if the characteristic speed for this equation is positive, *i.e.* for Equations (3.122), (3.133), (3.166), (3.146), (3.194) and the differencing scheme used for the convective term is downwind if the characteristic speed is negative, *i.e.* for Equation (3.105). Diffusive term in Equation (3.166) is discretized by using central differences.

In this study the point collocation finite element method which is a member of the class of methods of weighted residuals in which the solution can be represented by approximating functions, is used. The accuracy of the solution is ensured by using a high (fourth) order discretization scheme which is based on the general definition of five–point Lagrange interpolation polynomial

$$y = \sum_{i=1}^{5} \prod_{\substack{j=1 \\ i \neq j}}^{5} \frac{x - x_j}{x_i - x_j} y_i \tag{4.4}$$

The details of the discretization scheme used can be found in Oymak [165] and Schiesser [166]. Numerical derivative of a dependent variable is then computed on one of the five–point grids illustrated in Table 4.1.

Table 4.1: Types of discretization schemes.

Type	Discretization scheme	Grid points to be used				
1	Downwind	i	$i+1$	$i+2$	$i+3$	$i+4$
2	Biased-downwind	$i-1$	i	$i+1$	$i+2$	$i+3$
3	Centered	$i-2$	$i-1$	i	$i+1$	$i+2$
4	Biased-upwind	$i-3$	$i-2$	$i-1$	i	$i+1$
5	Upwind	$i-4$	$i-3$	$i-2$	$i-1$	i

For type 1, the spatial derivative of a dependent variable at point i is obtained by interpolating a five-point Lagrange interpolation polynomial that passes through the values of the concerned dependent variable at the four nodes to the right of the point i. For type 2, one node to the left and three nodes to the right of the point i, where the spatial derivative is computed, are used. Type 3 considers two nodes to the left and two nodes to the right of point i. Types 4 and 5 can be handled similarly. Thus type 3 is a five-point centered approximation, types 2 and 4 are five-point biased-downwind and biased-upwind approximations respectively, and types 1 and 5 are five-point downwind and upwind approximations respectively. In this study, types 1 and 5 are used for boundary edges of spatial domains concerned and types 2 and 4 are used for interior nodes as recommended by Silebi and Schiesser [167].

4.3.3 Time Integration

The second principal step in the MOL approach is the integration of the system of the initial value ODEs. Two points should be concerned in this step; the accuracy and stability of the integration. The accuracy requirement is handled more or less automatically by any quality ODE integrator (*e.g.* LSODES [161], VODE [168], RADAU [163], ROWMAP [169]), which will adjust the integration step size to meet the user specified error tolerance. Also, quality ODE integrators employ higher–order integration formulas to achieve the required accuracy. Therefore, it can be assumed that the accuracy requirement is met, and one can concentrate on the stability requirement.

The ODE systems obtained by using MOL approach usually have wide spectrum

of eigenvalues, and hence, are typically stiff. If this spectrum can be made to fit inside the stable region of an ODE integrator's stability diagram, then the whole MOL approach becomes stable. There are basically two methods for ODE integration; explicit and implicit methods. Explicit methods have poor stability characteristics which make them impractical for the integration of stiff ODE systems [164]. Hence, implicit methods which have larger stability regions are used in quality ODE solvers for the integration of stiff ODE systems. These methods have high–orders to overcome the limitation put over the step size by the accuracy requested. Therefore, in this thesis study the ODE system evolved is solved by using a high–order (fourth), semi-implicit Runge-Kutta algorithm embedded in the ODE solver ROWMAP [169] which can be obtained from the website *http://www.mathematik.uni-halle.de/institute/numerik/software/*.

4.3.4 Structure of the Code

The structure of the code for the solution of transient model equations is given in Figure 4.14-4.15. The transient code is also arranged in a modular fashion as steady state code for ease of understanding and, if necessary, modification.

Subroutines of the code can be categorized as

- main driver routine for overall control of the code: CFBCDYNSIM,
- reading of input data, calculation of char properties and composition of volatiles, allocation of arrays, generation of grid points, assumptions, initial conditions and preliminary calculations : READINPUT, CHARPROP, VMCOMP, CREATEARRAYS, GRIDGEN, ASSUMPTIONS, READER and PRECALC,
- routines for assemblage of differential equations: DERV,
- routine for printing results: PRINTER,
- routines for hydrodynamics: HYDRODENSE and HYDRODILUTE,

- routines for root finding, numerical integration and ODE solution: ZERO, INTLG2 and ROWMAP,
- function for char combustion kinetics: F_RKC, F_KM and F_DRDT,
- routines for transferring dependent variables and their derivatives to 1D array to be used by ROWMAP: TRANSFER,
- routines for transferring 1D array of dependent variables and derivatives back to real variables to be used by derivative routine: BACKTRANSFER,
- routines for spatial discretization: DLG4,
- function for computation of species generation/depletion terms in emulsion and bubble phases, and in dilute zone: F_ERATE, F_BRATE and F_DRATE,
- function for calculation heat and mass transfer coefficients: F_HP, F_HBW, F_HDW and F_KM,
- function for property evaluation: F_AIRDEN, F_AIRVIS, F_AIRCP, F_AIRTC, F_AIRH and F_D.

4.3.5 Mode of Operation

The general algorithm of the code for the solution of transient model equations is depicted in Figures 4.16-4.18. The overall control of the solution is exerted by the main driver routine, CFBCDYNSIM which calls READINPUT, CHARPROP, VMCOMP, CREATEARRAYS, GRIDGEN, ASSUMPTIONS, READER and PRECALC to specify experiment pertinent data, to calculate char properties, to calculate composition of volatiles, to allocate arrays, to set assumptions, to read and set initial conditions and to make preliminary calculations, respectively. The driver routine for ODE solution, SOLVE_ROWMAP, calls DERV to assemble the ODE system, ROWMAP to integrate the set of ODEs and PRINT to print the solution at specified time intervals. Spatial domains of dense zone, dilute zone,

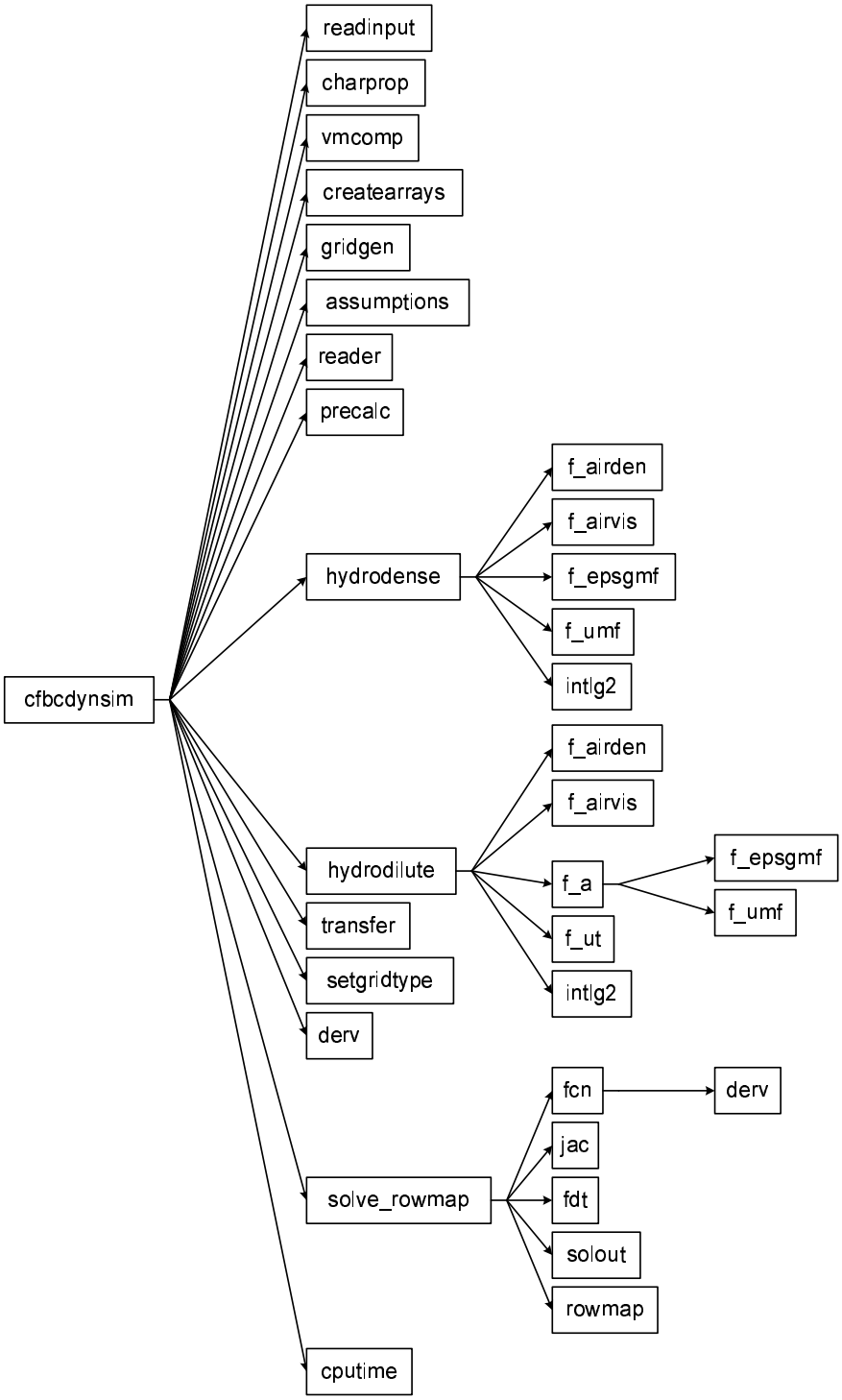

Figure 4.14: Organization of unsteady state model main routine CFBCDYNSIM.

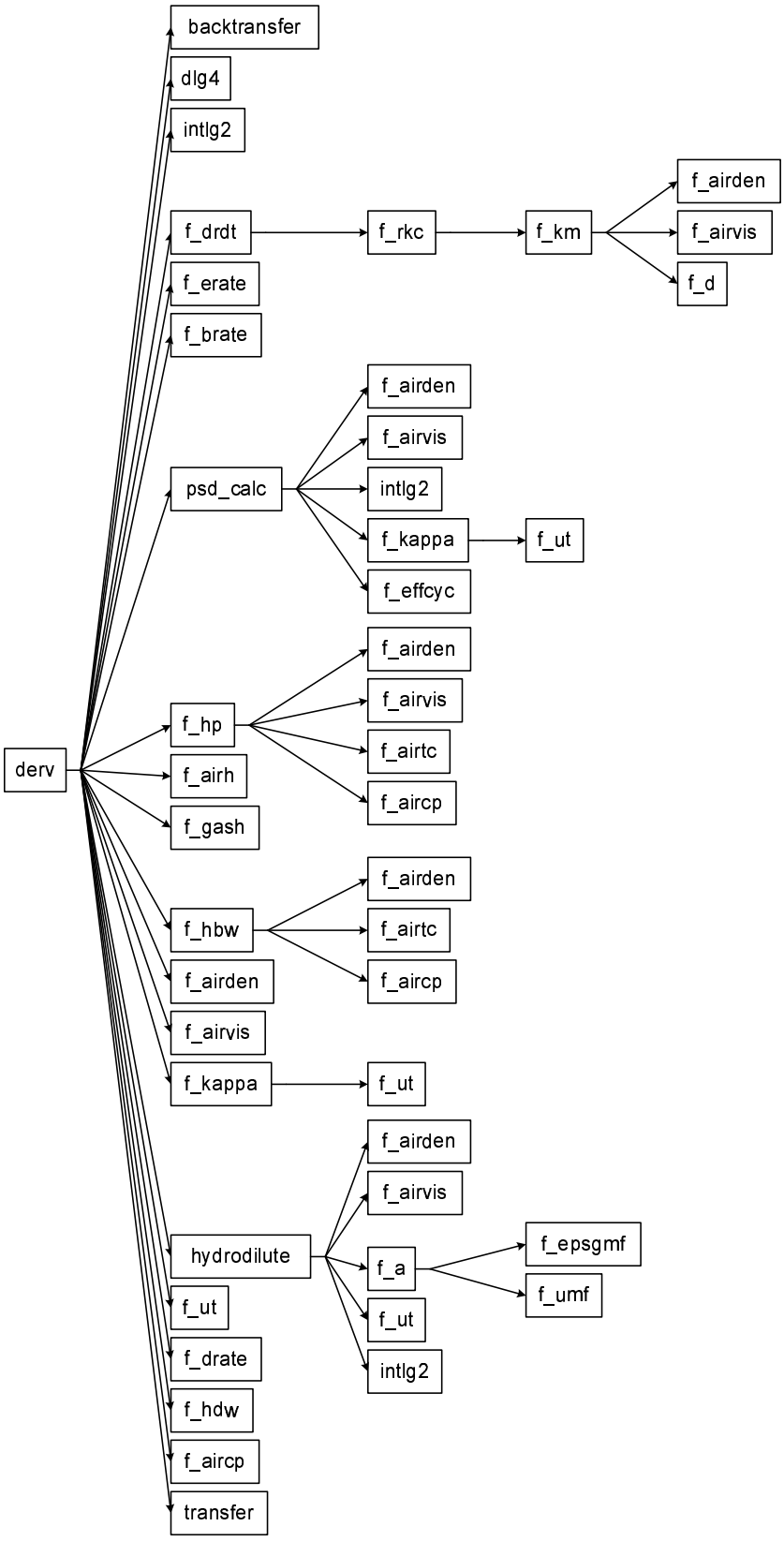

Figure 4.15: Organization of unsteady state model subroutine DERV.

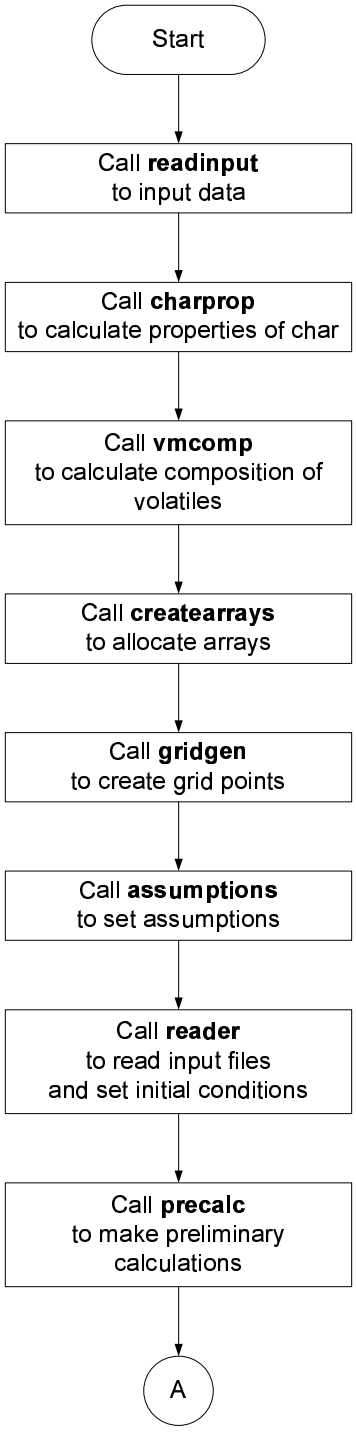

Figure 4.16: Algorithm of the unsteady state code (Part I).

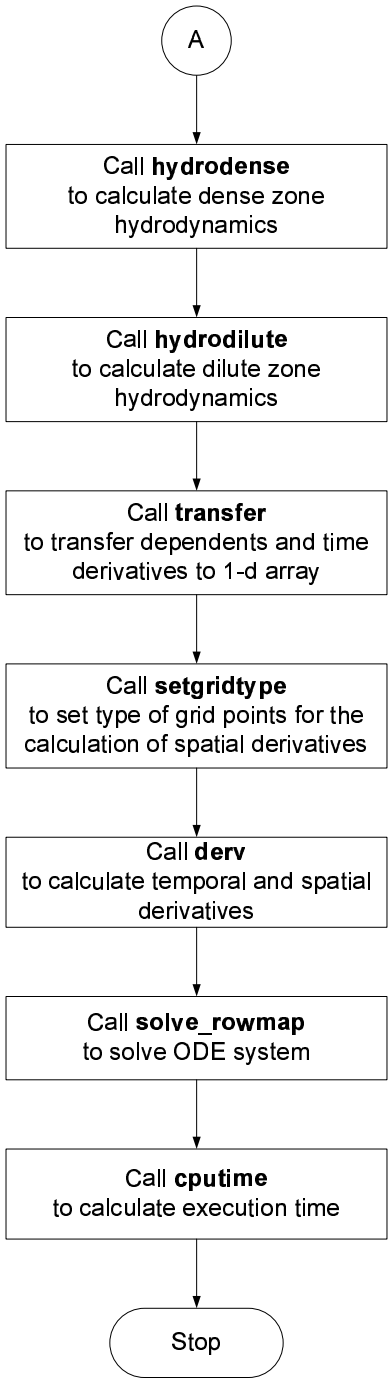

Figure 4.17: Algorithm of the unsteady state code (Part II).

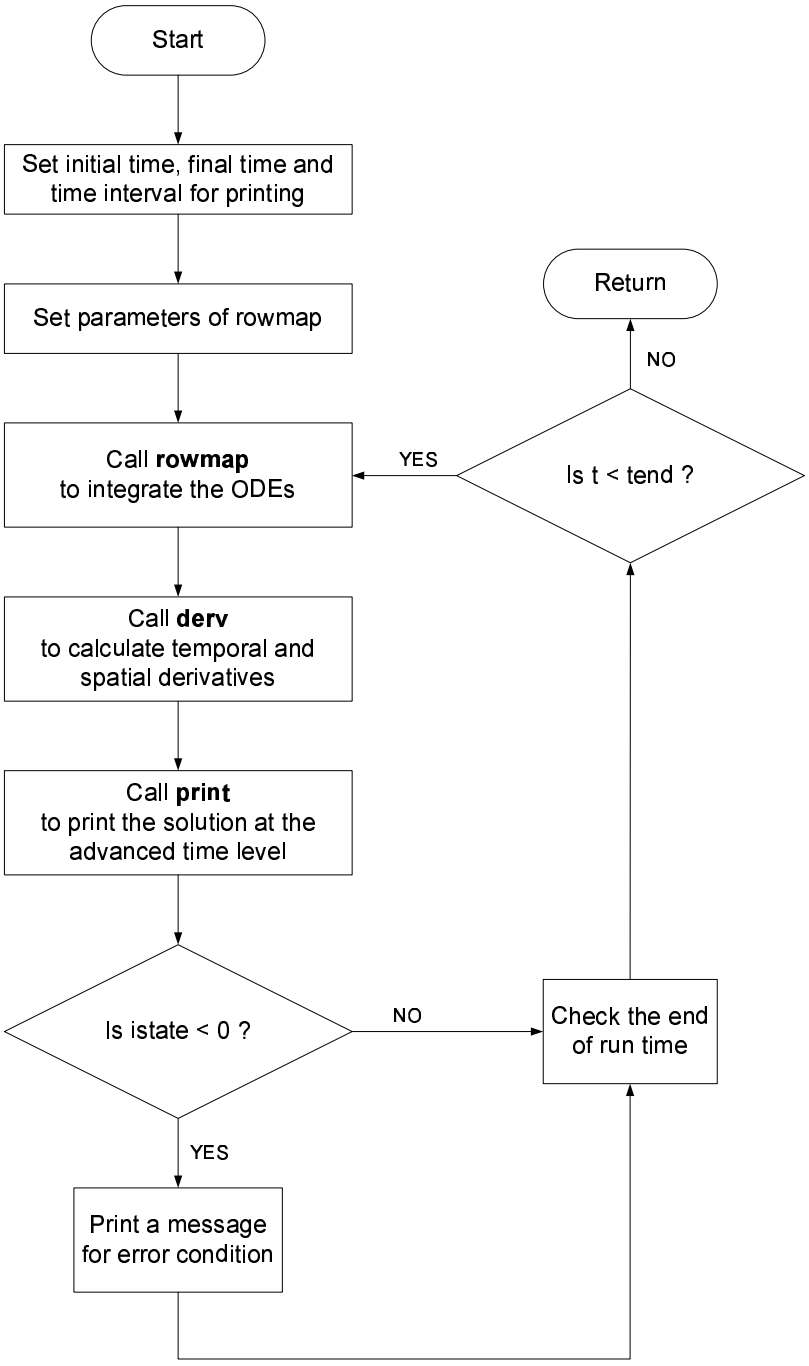

Figure 4.18: Algorithm of the subroutine SOLVE_ROWMAP.

char particles radius and dense zone wall thickness were divided into $(N_d - 1)$, $(N_f - 1)$,$(N_p - 1)$ and $(N_{dw} - 1)$ intervals, respectively, for regular printing of results, numerical integration and spatial discretization. The predictions reported in this study were obtained with N_d, N_f, N_p and N_{dw} values of 31, 51, 101 and 21, respectively. The solution of governing equations by using the MOL approach is based on the evaluation of the derivative vector by which the solution is advanced from one time step to the next. The evaluation of the derivative vector can be summarized as follows.

All dependent variables are known a priori at the beginning of each cycle, either as a result of the previous cycle or from the prescribed initial conditions as computed by the steady state code. Once the spatial derivatives appearing in the governing equations have been evaluated using the values of the present cycle, the ODE system has been assembled and sent to the ODE solver in the form of a 1D array to compute the dependent variables at the advanced time level. This completes the progression of the solution to the end of the new cycle having the new values of the dependents. This cyclic procedure continues until the end of the run is reached.

CHAPTER 5

RESULTS AND DISCUSSION

5.1 General

The assessment of the validity and predictive accuracy of the developed CFBC model was carried out by applying it to the prediction of steady state behavior of Technical University of Nova Scotia (TUNS) 0.3 MWt Atmospheric Circulating Fluidized Bed Combustor (CFBC) Test Rig under two different operating conditions.

5.2 Test Case 1

The predictive performance of CFBC model under steady state conditions was first tested by comparing its predictions with the experimental data reported by Wu [170]. Details of the combustor, operating conditions and results of the model validation are given below.

5.2.1 Description of Combustor

The experiment reported by Wu [170] was carried out in the 0.3 MWt TUNS CFBC Test Rig. A schematic drawing of the combustor is given in Figure 5.1. The combustor is 6.3 m tall with a square cross section of 0.2 m by 0.2 m. Combustor consists of riser, primary cyclone, impact separator, secondary cyclone, standpipe and L-valve. Primary air enters the riser through a stainless steel distributor plate located at the base of the riser. Secondary air enters the riser through the secondary air port at a height of 1.5 m above the distributor plate. The primary and secondary air are supplied by a 6 psi blower. Aeration air enters the L-valve through a horizontal pipe with orifices along its length located in the horizontal leg of the L-valve. Separation of entrained solids begins in the

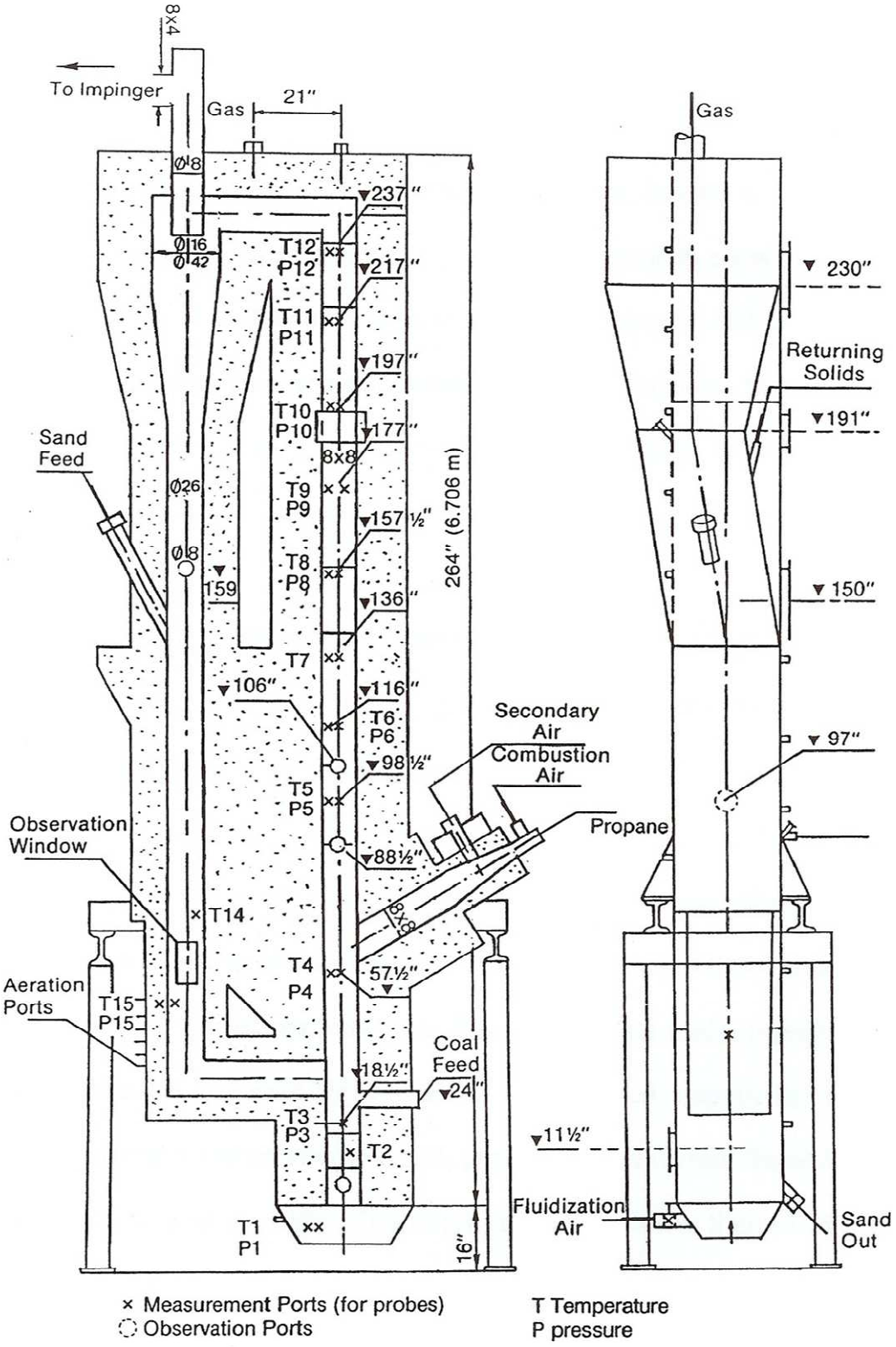

Figure 5.1: Schematic diagram of 0.3 MWt TUNS CFBC Test Rig.

primary cyclone. After the primary cyclone, the remaining gas/solid mixture enters the impact separator and then the secondary cyclone. Solids captured in the primary cyclone are returned to the bed by the standpipe and L-valve. The solid circulation rate is controlled by adjusting the aeration air in the L-valve.

Flue gas and fines escaping from the cyclones and impact separator enter the baghouse containing a heat exchanger to cool the gases and thereby protect the bag material. The bag filters capture the remaining fine particles in the gas, leaving the clean flue gas to exhaust through the stack into the atmosphere. Solids removed in the baghouse are collected in a hopper for disposal. The coal is fed to the combustor by means of a screw feeder with a digital meter. Bed material can be removed through a solids drain located at the bottom of the riser to maintain bed inventory.

Pressure drop and temperature in the riser are measured at 15 pressure and 15 temperature locations. The pressure taps are connected to U-tube manometers to allow measurement of pressure distribution throughout the riser. Nine Chromel-Alumel thermocouples, introduced into the riser section through temperature measuring taps, are connected to an computer using a Keithley Metrabyte DAS 1800 data acquisition system.

5.2.2 Operating Conditions

Analysis of the coal used in the experiment reported by Wu is given in Table 5.1. As can be seen from the table, it is a high calorific value bituminous coal with low ash and moisture contents. The particle size distribution of the coal used in the experiments is shown in Table 5.2. Coal has a wide size distribution typical for fluidized bed combustion and it has a d_{32} of 269 μm and d_{50} of 832 μm. Operation conditions of the experiment are presented in Table 5.3. Due to low ash content of the coal burned, experiment was carried out using sand with a mean diameter of 350 μm as bed material.

Table 5.1: Characteristics of coal used in Test Case 1.

Proximate Analysis (as-fired)		Ultimate Analysis (dry)	
Component	Weight (%)	Component	Weight (%)
Moisture	3.60	C	71.99
Ash	13.15	H	5.00
VM	30.30	O	4.43
FC	52.95	N	1.24
		S	3.70
HHV: 30.6 MJ/kg		Ash	13.64

Table 5.2: PSD of coal used in Test Case 1.

Size (μm)	Weight Percent
0 - 53	5.12
53 - 106	3.87
106 - 212	6.46
212 - 500	13.50
500 - 1000	16.40
1000 - 1400	15.00
1400 - 2375	17.78
2375 - 3025	20.80
3025 - 5425	1.07

Table 5.3: Operating conditions of Test Case 1.

Parameter	Value
Coal flow rate, kg/s	7.77×10^{-3}
Primary air flow rate, Nm^3/s	49×10^{-3}
Secondary air flow rate, Nm^3/s	29×10^{-3}
PA/SA ratio, %	63/37
Excess air,%	35
Superficial gas velocity, m/s	8
Net solid circulation rate, $kg/m^2.s$	20
Air temperature, K	308.15

5.2.3 Validation of Steady-State Model

In order to assess the validity and predictive accuracy of model, it was applied to the prediction of the behavior of TUNS 0.3 MWt CFBC Test Rig while operating under steady state conditions and predictions were compared with measurements.

Figure 5.2 compares the predicted and measured concentrations of O_2 and CO, and predicted CO_2 concentration along the combustor. As can be seen from the figure, O_2 concentrations decrease until the secondary air port whereas CO_2 concentrations display an opposite trend in the same region. As for the dilute zone, the decrease in O_2 and increase in CO_2 concentrations keep on but with a lower slope. CO measurements, on the other hand, show maxima in the dense zone and decrease gradually along the combustor with a lower slope. As depicted in the Figure 5.2, favorable comparisons are obtained between the predicted and measured profiles of O_2 and CO. Predicted CO_2 concentration profile, on the other hand, shows the physically expected trend.

Figure 5.3 illustrates the comparison between the measured and predicted temperatures along the combustor for the experiment under consideration. As can be seen from the figure, agreement between measurements and predictions is reasonably good.

Figure 5.4 shows the comparison between the measured and predicted carbon content. As can be seen from the figure, measurements and predictions are in favorable agreement. The discrepancy between measurements and predictions in the dilute zone may be attributed to the difficulty in representative solid sampling in highly non-homogeneous riser.

Figure 5.5 depicts the comparison between the measured and predicted dense zone and recycle size distributions. As can be seen from the figure, predictions show the physically expected trend, i.e., finer recycle and coarser dense zone. Furthermore, they are in good agreement with measured size distributions.

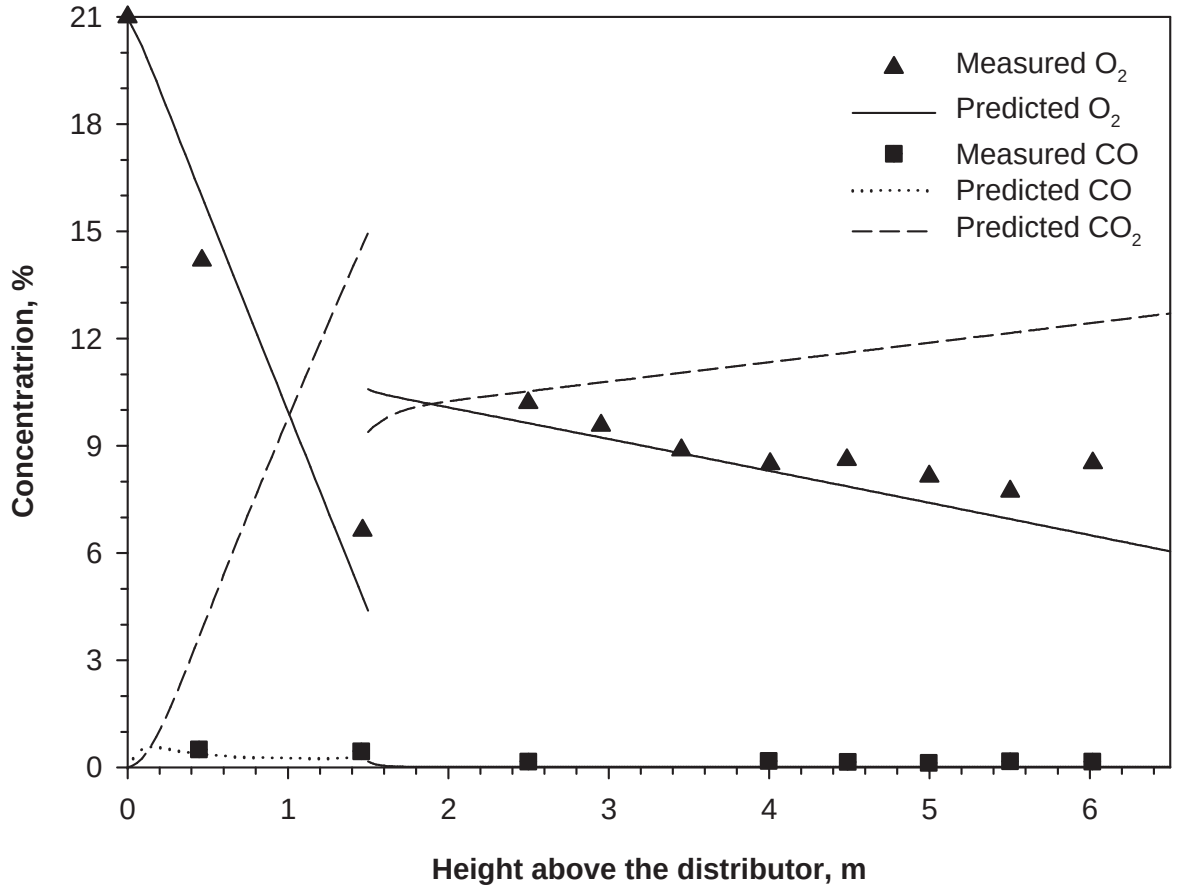

Figure 5.2: Measured and predicted concentration profiles for Test Case 1.

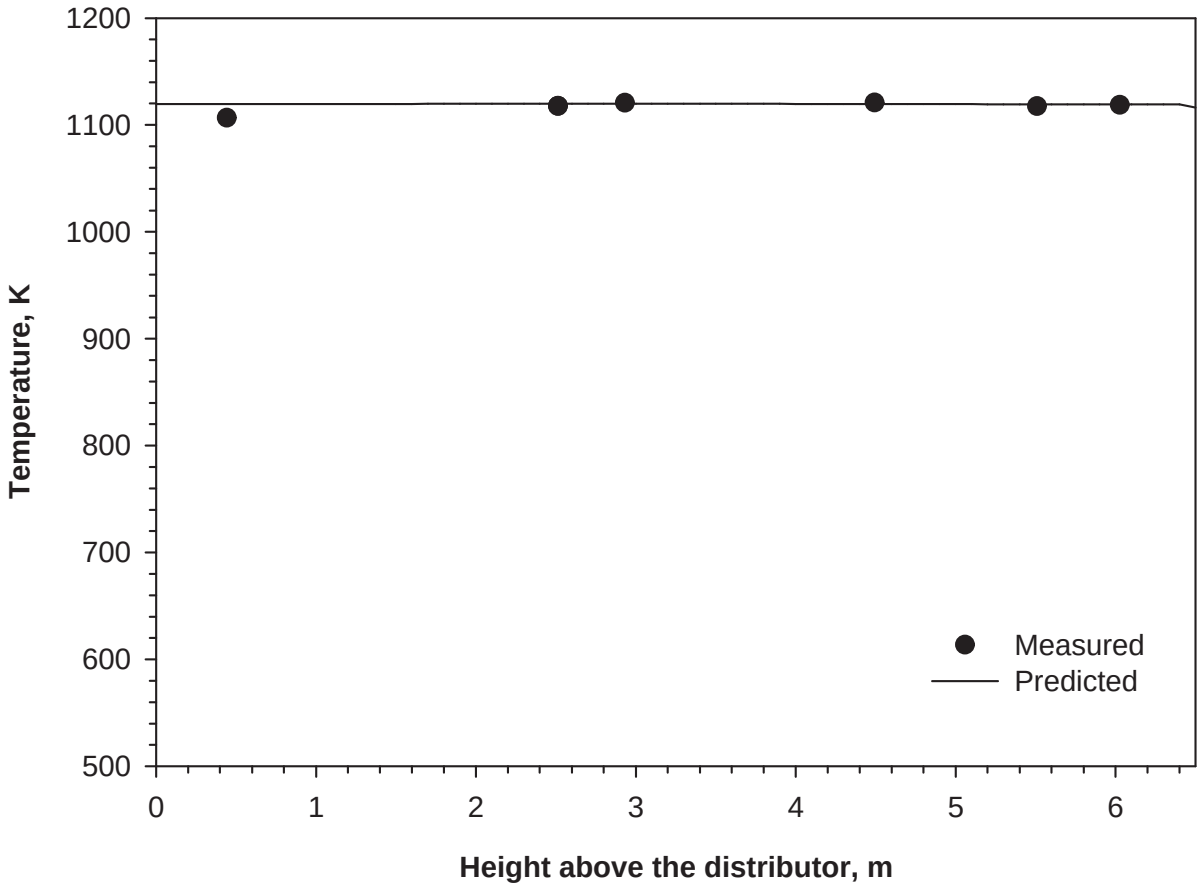

Figure 5.3: Measured and predicted temperature profiles for Test Case 1.

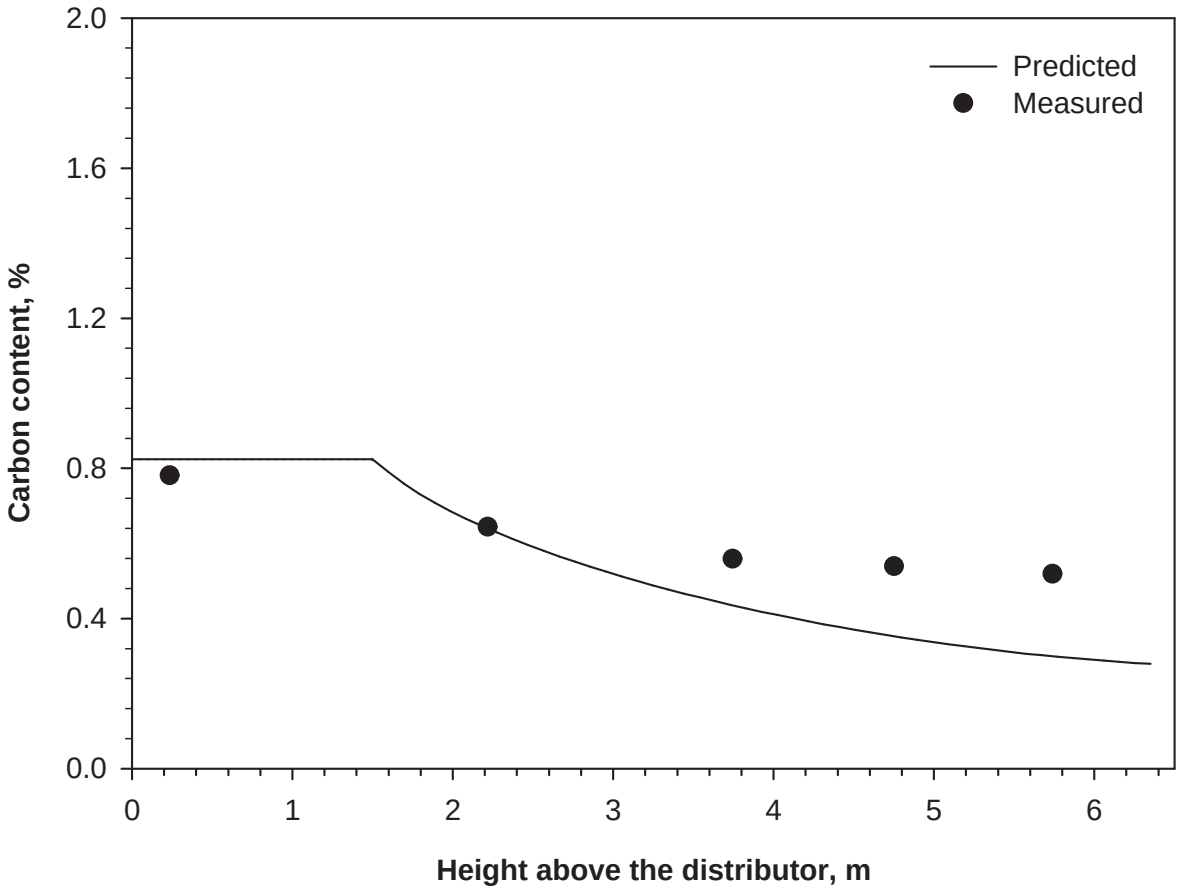

Figure 5.4: Measured and predicted C content profiles for Test Case 1.

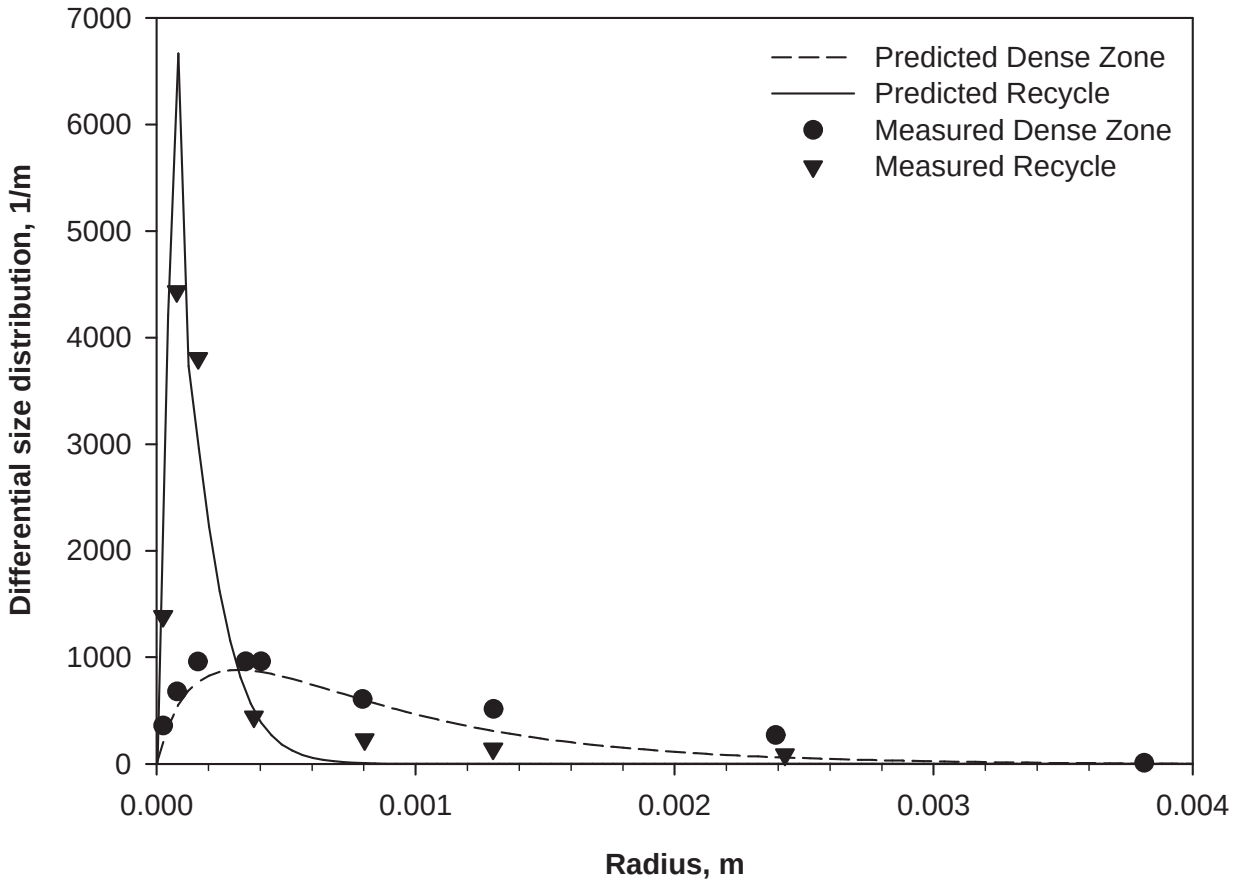

Figure 5.5: Measured and predicted particle size distribution for Test Case 1.

5.3 Test Case 2

The predictive performance CFBC model was also tested by comparing its predictions with the experimental data reported by Park [171] under steady state conditions.

5.3.1 Description of Combustor

The experiment reported by Park [171] was also carried out in the 0.3 MWt TUNS CFBC Test Rig. However, the test rig was modified to enlarge its cross-section and also to add water walls. A schematic drawing of the combustor is given in Figure 5.6. Details of the modifications can be found in [18].

A blower supplies air to the combustor in two streams called primary air and secondary air. Some of the primary air may be diverted to a by-pass. When the flow of PA and SA is too high, the by-pass releases the extra air to the atmosphere relieving the pressure on the blower. The primary air first enters a wind box and then enters the bottom of the riser through a distributor plate. The secondary air enters the riser at a height of 1.5 m. Valves control the flow of primary, secondary and by-pass air. The primary air and by-pass air flow are measured together using an orifice plate. By-pass air is measured by another orifice plate. Primary air flow is then determined by the difference between these two readings. The secondary air is also measured by a separate orifice plate.

The riser is 6.35 m tall with a square cross section of 0.23 m by 0.23 m. The riser is made of two types of refractory as shown in Figure 5.7. The front side is made of refractory casting and other three sides (back, left and right sides) are made of refractory brick. The distributor plate and the wind box are installed at the bottom of the riser. Thermocouple, pressure probe and gas and solid sampling probe are installed in different locations in the front wall. The bed drain port is at the bottom section of the riser and a ball valve is used to control the bed drain. A water wall section of height 3.127 m is installed at the two sides (front and rear sides) of the riser starting at a height of 4.826 m . The water wall section serves two purposes: it can control the temperature of the furnace by absorbing

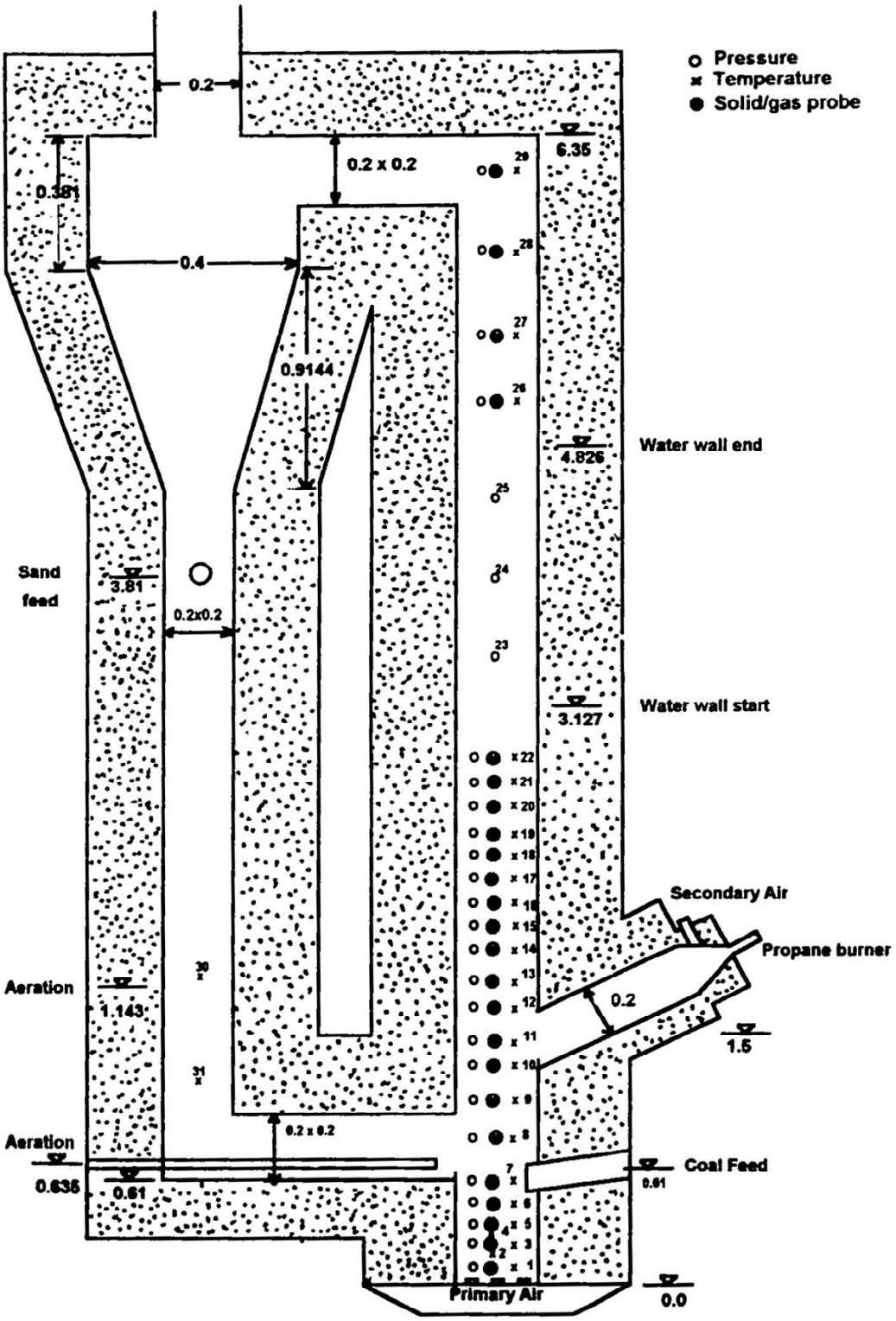

Figure 5.6: Schematic diagram of modified 0.3 MWt TUNS CFBC Test Rig.

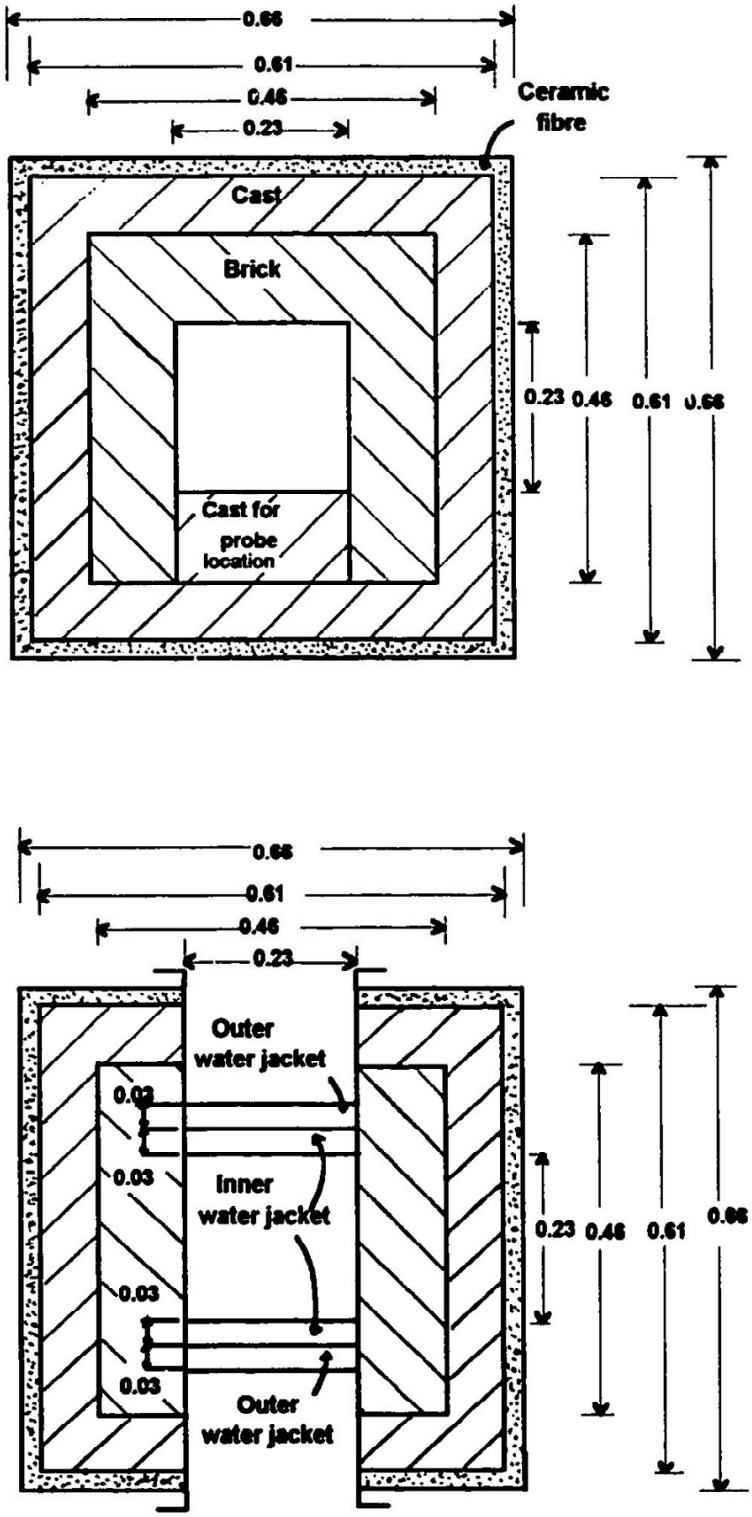

Figure 5.7: Cross-sectional view of 0.3 MWt TUNS CFBC Test Rig walls.

heat; and it can be used for heat transfer tests. Feed stock enters the riser at a height of 0.61 m.

Solid from the return leg enters the riser at a height of 0.81 m. The solid circulation system includes a primary cyclone, a down comer (return leg), an L-valve, an impact separator and a secondary cyclone. All of them are refractory-lined. The sand feeder in the return leg consists of a hopper and a ball valve and serve two purposes. It is used for feeding sand to the system before start up and is used in the measurement of solid circulation rate. Thermocouples and pressure probes are installed in the return leg. Aeration is provided in two locations of the L-valve in the vertical section at a height of 1.143 m and in the horizontal section at a height of 0.635 m. Aeration in the horizontal section is done by a purge (perforated) tube inserted from the return leg side. Aeration air supply to the L-valve is measured by a rotameter and comes from the university air line at a pressure of 80 psi.

Coal is fed to the furnace from a hopper by a screw feeder which is a pneumatic-assisted gravimetric system. The hopper, along with the screw feeder and motor, sits on top of a platform. A load cell senses the weight and sends the signal to a digital display unit. The hopper is kept at the same pressure throughout the test time by connecting an air line from the university air supply at 80 psi. The hopper is divided into two parts that can be isolated from each other by a ball valve for loading even during the operation of the furnace.

For start-up of the furnace, a propane burner is installed at a height of 1.5 m in the riser. The propane burner and the secondary air entry are coaxial. The burner has a propane flow control device with an automatic safety shut-off device. The flow of propane can be controlled by a flow control valve.

The flue gas produced in the risers enters the primary cyclone where the solids are partially separated. The flue gas then enters an impact separator and then the secondary cyclone. A large portion of solids remaining with the flue gas is separated in the impact separator and the secondary cyclone and then enter the

return kg. The flue gas with the remaining fly ash enters the bag house which is divided into two sections. The first section contains a water-cooled heat exchanger that extracts heat from the flue gas which then enters the second section of the bag house which contains filter bags. Here the flue gas is separated from the fly ash, and then exits to the atmosphere. The fly ash can be drained from the bag house periodically.

Sampling and measuring devices include gas and solid sampling probes, temperature measuring devices (thermocouples) and pressure measurement devices (manometers). The gas coming out of the sampling probe first enters a filter to separate out the solids and then enters a condenser to remove the moisture in the gas, which passes through a water trap and then a desiccator. A suction pump is used to draw the gas from the riser and then pass it through a gas analyzer. The clean and dried gas splits into different streams according to the arrangement of analyzers. Solid samples are collected in a water-cooled container after its exit from the probe. Solids leave the riser naturally, due to the higher pressure inside the riser. Temperatures of the furnace at different elevations are measured continuously using thermocouples using a data acquisition system (DAS). Differential pressures at different locations were measured using manometers.

5.3.2 Operating Conditions

Analysis of the coal used in the experiment reported by Park is given in Table 5.4. As can be seen from the table, it is a high calorific value bituminous coal with low ash and moisture contents. The particle size distribution of the coal used in the experiments is shown in Table 5.5. Coal has a wide size distribution typical for fluidized bed combustion and it has a d_{32} of 245 μm and d_{50} of 773 μm. Operation conditions of the experiment is presented in Table 5.6. Due to low ash content of the coal burned, experiment was carried out using sand with a mean diameter of 337 μm as bed material.

Table 5.4: Characteristics of coal used in Test Case 2.

Proximate Analysis (as-fired)		Ultimate Analysis (dry)	
Component	Weight (%)	Component	Weight (%)
Moisture	1.23	C	72.44
Ash	11.01	H	4.89
VM	33.70	O	5.49
FC	54.06	N	1.41
		S	4.62
HHV: 30.6 MJ/kg		Ash	11.15

Table 5.5: PSD of coal used in Test Case 2.

Size (μm)	Weight Percent
0 - 75	7.66
75 - 106	4.17
106 - 212	8.88
212 - 417	13.07
417 - 500	4.18
500 - 710	9.95
710 - 1000	9.65
1000 - 2000	27.17
2000 - 4000	15.27

Table 5.6: Operating conditions of Test Case 2.

Parameter	Value
Coal flow rate, kg/s	11.55×10^{-3}
Primary air flow rate, Nm^3/s	62.6×10^{-3}
Secondary air flow rate, Nm^3/s	35.3×10^{-3}
PA/SA ratio, %	67/33
Excess air,%	22.6
Superficial gas velocity, m/s	8.2
Net solid circulation rate, $kg/m^2.s$	32.5
Air temperature, K	298.15

5.3.3 Validation of Steady-State Model

In order to further assess the validity and predictive accuracy of model, it was applied to the prediction of the behavior of TUNS 0.3 MWt CFBC Test Rig reported by Park [171] and predictions were compared with available measurements, *i.e.*, temperature and voidage profile.

Figure 5.8 shows the predicted concentrations of O_2, CO and CO_2 concentration along the combustor. As can be seen from the figure, O_2 concentrations decrease until the secondary air port whereas CO_2 concentrations display an opposite trend in the same region. As for the dilute zone, the decrease in O_2 and increase in CO_2 concentrations keep on but with a lower slope. CO measurements, on the other hand, show maxima in the dense zone and decrease gradually along the combustor with a lower slope. Higher amounts of CO in the dense zone is the result of air staging leading to strong reducing conditions in the dense zone. As depicted in the Figure 5.2, predicted O_2, CO and CO_2 concentration profiles shows physically expected trend.

Figure 5.9 illustrates the comparison between the measured and predicted temperatures along the combustor for the experiment under consideration. As can be seen from the figure, temperature profile along the combustor is highly uniform and agreement between measurements and predictions is reasonably good. The slight decrease in temperature in the dilute zone between 3.127 m and 4.826 m is due to the presence of water walls.

Figure 5.10 shows the comparison between the measured and predicted voidage along the combustor for the experiment under consideration. As can be seen from the figure, measurements and predictions are in favorable agreement. The discrepancy between measurements and predictions in the dense zone is considered to be due to error in pressure measurement in the dense zone as such low voidage (~ 0.6) is practically impossible when operating at such a high gas velocity.

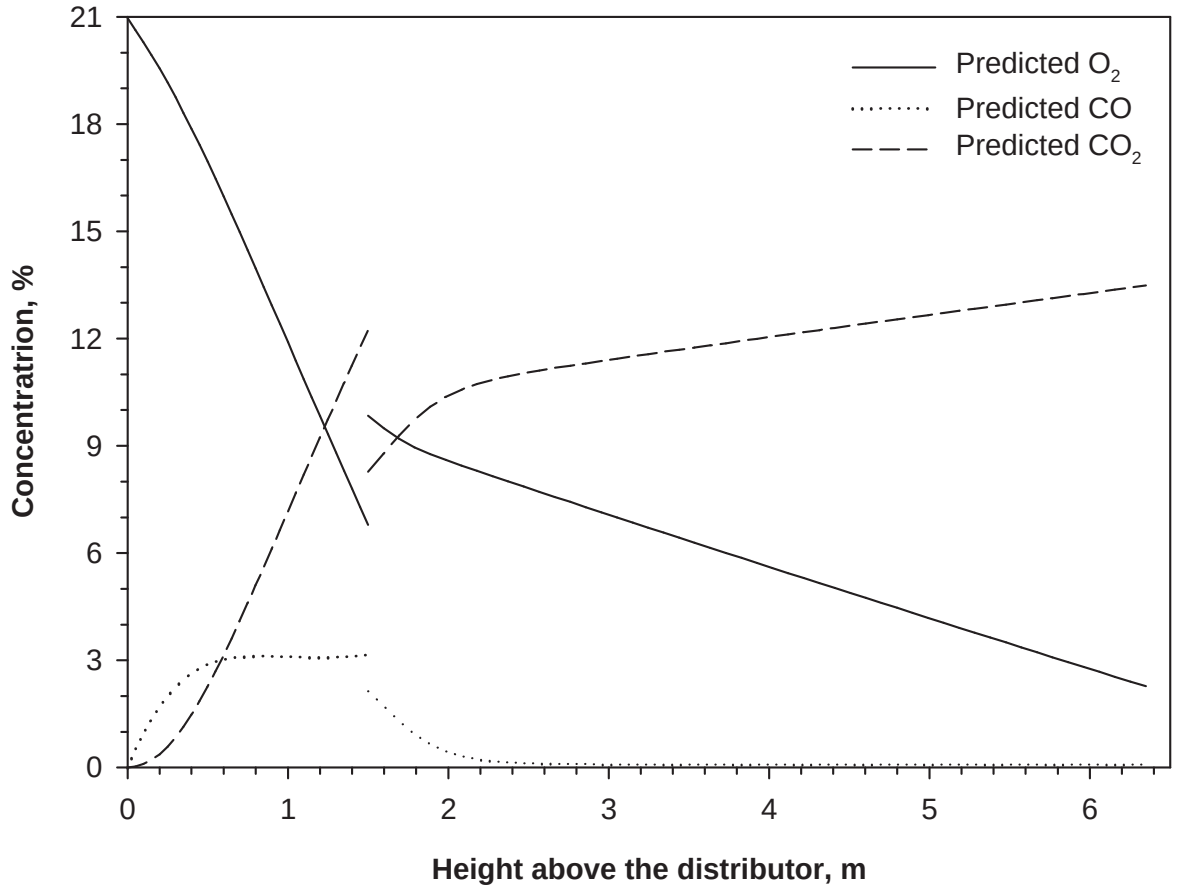

Figure 5.8: Predicted concentration profiles for Test Case 2.

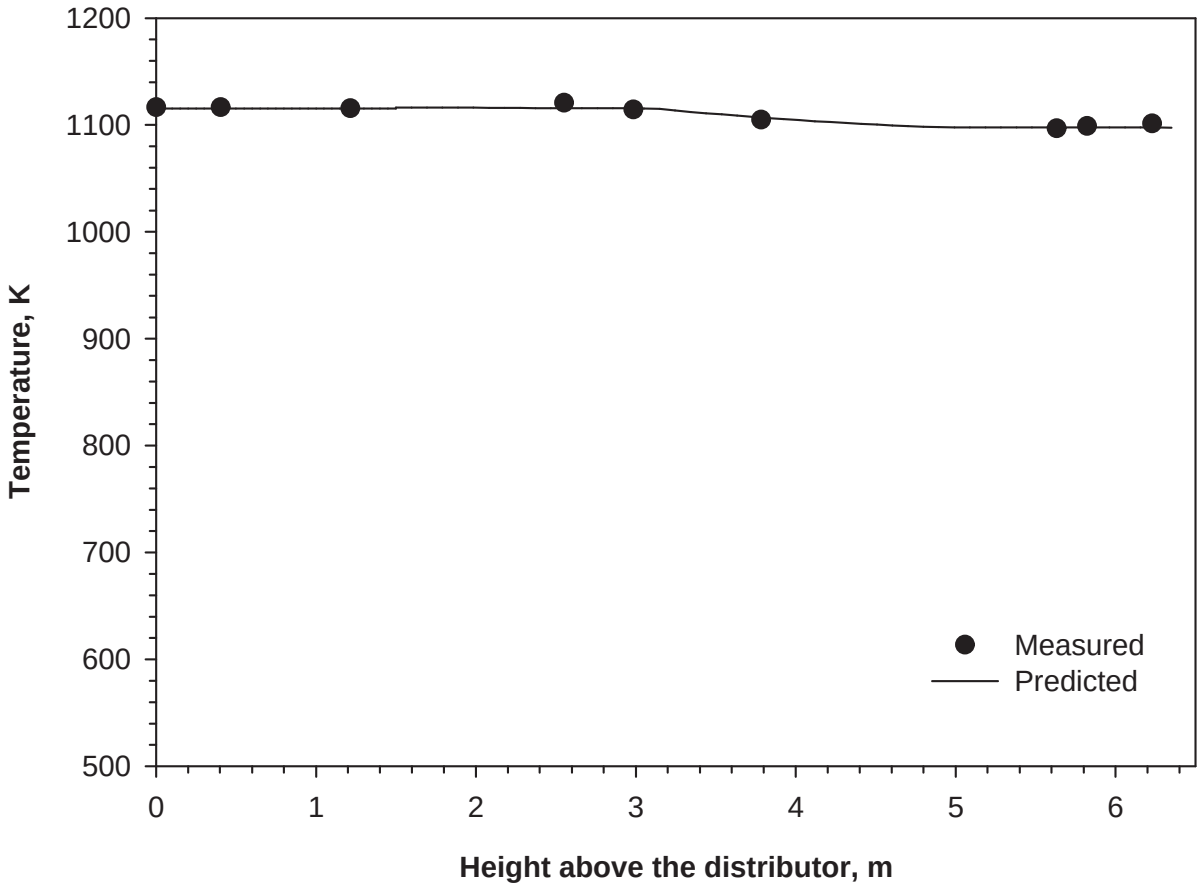

Figure 5.9: Measured and predicted temperature profiles for Test Case 2.

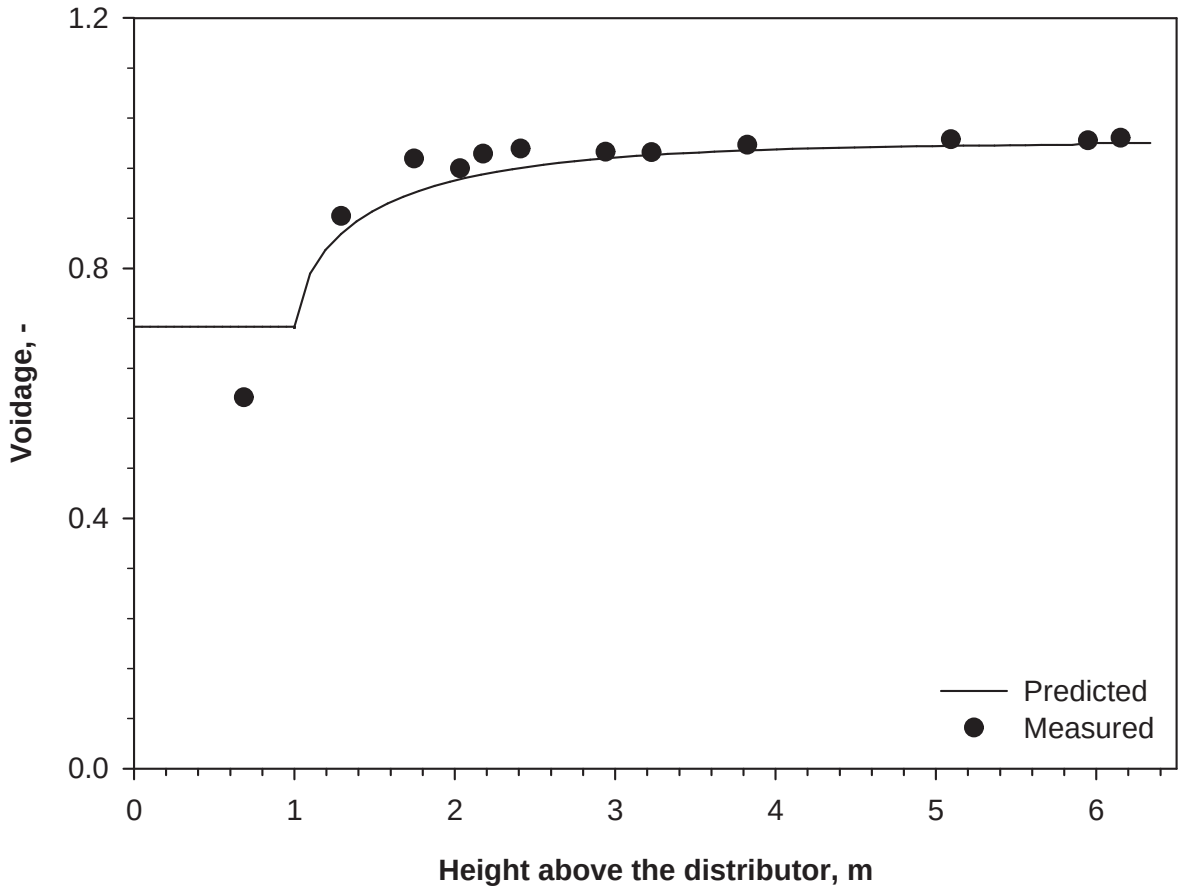

Figure 5.10: Measured and predicted voidage profiles for Test Case 2.

CHAPTER 6

CONCLUSIONS

6.1 General

A dynamic mathematical model of a continuous atmospheric circulating fluidized bed combustor has been developed on the basis of first principles and empirical correlations. The model accounts for dense and dilute zone hydrodynamics, volatiles release and combustion, char particles combustion and their size distribution, and heat transfer from/to gas, particles, waterwalls and refractory.

Inputs to the model include configuration and dimensions of the combustor and its internals, air and coal flows, coal analysis, all solid and gas properties, inlet temperatures of air, cooling water, and feed solids, size distribution of feed solids; outputs include transient values of combustor temperatures, gas concentrations, char and inert hold-ups and their size distributions.

The solution procedure employs method of lines approach for the governing non-linear partial differential equations and combined bisection and secant rule for non-linear algebraic equations. The solution procedure needs the several sub-models to be solved simultaneously. The initial conditions required for each sub-model are provided from the simultaneous solution of governing equations of dynamic model with all temporal derivatives set to zero.

Assessment of predictive accuracy of the model was carried out by applying it to the prediction of the steady state behavior of Technical University of Nova Scotia 0.3 MWt CFBC Test Rig by setting all temporal derivatives to zero in the dynamic model and comparing its predictions with measurements available on the same rig.

On the basis of comparisons between steady-state predictions of the model and measurements, the following conclusions have been reached:

- Model can predict concentration profiles of O_2, CO and CO_2 reasonably good.
- Temperature profiles predicted by the model are in good agreement with the measurements.
- Model can reproduce char size distribution at the exit of combustor fairly well.
- Voidage profile predicted by model are in favorable agreement with measurements.

The model presented in this study proves to be a useful tool in predicting steady state performance of atmospheric circulating fluidized bed combustors.

6.2 Suggestions for Future Work

For the improvement of the model the following recommendations for future extension of the work are suggested:

- Validation of the transient model by comparing its predictions with unsteady state measurements obtained from a CFB combustor.
- The fragmentation and attrition modelling of coal particles are required for better representation of char particles size evolution and heterogeneous reactions.
- The pollutant formation and reduction modelling to predict NO_x and SO_2 emissions are required considering the increased public sensitivity on environment.

- Elutriation and entrainment are modelled by using empirical correlations and considering the axial direction only. In order to see the effect of radial variation, a dilute zone hydrodynamic model based on core-annulus flow structure should be employed.

- A radiation model should be coupled to dilute zone heat transfer model to better simulate the actual physical phenomena in the dilute zone.

REFERENCES

[1] International Energy Agency, "Energy Information Centre", *http://www.iea.org*, 2006.

[2] Basu P. and Fraser S. A., "Circulating Fluidized Bed Boilers: Design and Operations". *Butterworth-Heinemann*, 1991.

[3] Hiltunen M. and Tang J. T., "NOx Abatement in Ahlstrom Pyropower Circulating Fluidized Bed Boilers", in *Proceedings of the 2nd International Conference on CFB* (Basu P. and Large J. F., Eds.), Pergamon Press, 429–436, Compiegne, France, May 14-18, 1988.

[4] Basu P. Sett A. Gbordzoe E. A. M., "A Simplified Model for Combustion of Carbon in a Circulating Fluidized Bed Combustor", in *Proceedings of the 9th International Conference on FBC* (Mustonen J. P., Ed.), ASME, Vol. 2, 738–742, Boston, USA, May 3-7, 1987.

[5] Weiss V., Scholer J., and Fett F. N., "Mathematical Modeling of Coal Combustion in a CFB Reactor", in *Proceedings of the 2nd International Conference on CFB* (Basu P. and Large J. F., Eds.), Pergamon Press, 289–298, Compiegne, France, May 14-18, 1988.

[6] Das A. and Bhattacharya S. C., "Circulating Fluidized Bed Combustion", *Applied Energy*, Vol. 69, 227–246, 1990.

[7] Sengupta S. P. and Basu P., "A Generalized Mathematical Model fo Circulating Fluidized Bed Boiler Furnace", in *Proceedings of the 11th International Conference on FBC* (E. J. Anthony, Ed.), ASME, Vol. 3, 1295–1301, Montreal, Canada, April 21-24, 1991.

[8] Hyppänen T., Lee Y. Y., and Rainio A., "A Three-Dimensional Model for Circulating Fluidized Bed Boilers", in *Proceedings of the 11th International Conference on FBC* (E. J. Anthony, Ed.), ASME, Vol. 1, 439–448, Montreal, Canada, April 21-24, 1991.

[9] Saraica P. C., Azevedo J. L. T., and Carvalho M. G., "Modelling Combustion, NOx Emissions and SO2 Retention in a Circulating Fluidized Bed",

in *Proceedings of the 12th International Conference on FBC* (Rubow N. L., Ed.), ASME, Vol. 1, 375–380, San Diego, California, USA, May 9-13, 1993.

[10] Saraiva P. C., Azevedo J. L. T., and Carvalho M. G., "Mathematical Simulation of a Circulating Fluidized Bed Combustor", *Combustion Science and Technology*, Vol. 93, 223–243, 1993.

[11] Basu P., Talukdar J., and Wu S., "Experimental Validation of One and Half Dimensional Model of Char Combustion in a Circulating Fluidized Bed", *AIChE Symposium Series*, Vol. 90, No. 301, 114–123, 1994.

[12] Haider M and Linzer W., "A One-Dimensional Sationary Simulation Model for Ciculating Fluidized Bed Boilers", in *Proceedings of the 4th International Conference on CFB* (Avidan A. A., Ed.), American Institute of Chemical Engineers, 685–697, Somerset, Pennsylvania, USA, August 1-5, 1994.

[13] Wang X. S., Gibbs B. M., and Rhodes M. J., "Modelling of Circulating Fluidized Bed Combustion of Coal", *Fuel*, Vol. 73, No. 7, 1120–1127, 1994.

[14] Adanez J., De Diego L. F., Gayan F., Armesto L., and Cabanillas A., "A Model for Prediction of Carbon Combustion Efficiency in Circulating Fluidized Bed Combustors", *Fuel*, Vol. 74, No. 7, 1049–1056, 1995.

[15] Adanez J., De Diego L. F., Gayan F., Armesto L., and Cabanillas A., "Modeling of Coal Combustion in Circulating Fluidized Bed Combustors", in *Proceedings of the 13th International Conference on FBC* (Heinschel K. J., Ed.), ASME, Vol. 1, 305–315, Orlando, Florida, USA, May 7-10, 1995.

[16] Hannes J., Renz U., and Van den Bleek C. M., "The IEA Model for Circulating Fluidized Bed Combustion", in *Proceedings of the 13th International Conference on FBC* (Heinschel K. J., Ed.), ASME, Vol. 1, 287–296, Orlando, Florida, USA, May 7-10, 1995.

[17] Legros R., Gharebaagh R. S., Paris J., Chaouki J., and Preto F., "Process Simulation of a Circulating Fluidized Bed Coal Combustor", in *Proceedings of the 13th International Conference on FBC* (Heinschel K. J., Ed.), ASME, Vol. 1, 317–324, Orlando, Florida, USA, May 7-10, 1995.

[18] Talukdar J., "Coal Combustion in a Circulating Fluidized Bed", *PhD Thesis*, Technical University of Nova Scotia, Halifax, Nova Scotia, Canada, 1995.

[19] Hannes J., "Mathematical Modeling of Circulating Fluidized Bed Combus-

tion", *PhD Thesis*, Rheinisch Westfälische Technische Hochschule Aachen, Aachen, Germany, 1996.

[20] Montat D., Fauquet P., Lafanechere L., and Bursi J. M., "SILVA: EDF Two-Phase 1D Annular Model of a CFB Boiler Furnace", in *Proceedings of the 14th International Conference on FBC* (Preto F. D. S., Ed.), ASME, Vol. 2, 1023–1032, Vancouver, Canada, May 11-14, 1997.

[21] Remberg C. G., Nemet A., and Fett F. N., "Towards a More General Process Model for Power Plants with Atmospheric or Pressurized Fluidized Bed Combustion", in *Proceedings of the 14th International Conference on FBC* (Preto F. D. S., Ed.), ASME, Vol. 2, 1139–1149, Vancouver, Canada, May 11-14, 1997.

[22] Hannes J., Renz U., and Van den Bleek C. M., "Mathematical Modelling of CFBC in Industrial Scale Power Plants", in *Proceedings of the 14th International Conference on FBC* (Preto F. D. S., Ed.), ASME, Vol. 2, 1151–1161, Vancouver, Canada, May 11-14, 1997.

[23] Gharebaagh R. S., Legros R., Chaouki J., and Paris J., "Simulation of Circulating Fluidized Bed Reactors Using ASPEN PLUS", *Fuel*, Vol. 77, No. 4, 327–337, 1998.

[24] Ducarne E. D., Dolignier J. C., Marty E., Martin G., and Delfosse L., "Modeling of Gaseous Pollutants Emissions in Circulating Fluidized Bed Combustion of Municipal Refuse", *Fuel*, Vol. 77, No. 13, 1399–1410, 1998.

[25] Huilin L., Rushan B., Lidan Y., Guangbo Z., and Xiu T., "Numerical Computation of a Circulating Fluidized Bed Combustor", *International Journal of Energy Research*, Vol. 22, 1351–1364, 1998.

[26] Adanez J., Gayan P., Grasa G., De Diego L. F., Armesto L., and Cabanillas A., "Circulating Fluidized Bed Combustion in the Turbulent Regime: Modelling of Carbon Combustion Efficiency and Sulphur Retention", in *Proceedings of the 15th International Conference on FBC* (R. B. Reuther, Ed.), ASME, No. 115, Savannah, Georgia, USA, May 16-19, 1999.

[27] Huilin L., Lidan Y., Rushnan B., and Guangbo Z., "Dynamic Simulation of a Circulating Fluidized Bed Boiler of Low Circulating Ratio with Wide Particle Size Distributions", in *Proceedings of the 15th International Conference on FBC* (R. B. Reuther, Ed.), ASME, No. 43, Savannah, Georgia, USA, May 16-19, 1999.

[28] Wang Q., Luo Z., Li X., Fang M., Ni M., and Cen K., "A Mathematical Model for a Circulating Fluidized Bed (CFB) Boiler", *Energy*, Vol. 24, 633–653, 1999.

[29] Knoebig T., Luecke K., and Werther J., "Mixing and Reaction in the Circulating Fluidized Bed : A Three-Dimensional Combustor Model", *Chemical Engineering Science*, Vol. 54, 2151–2160, 1999.

[30] Huilin L., Guangbo Z., Rushan B., Yongjin C., and Gidaspow D., "A Coal Combustion Model for Circulating Fluidized Bed Boilers", *Fuel*, Vol. 79, 165–172, 2000.

[31] Adanez J., Gayan P., Grasa G., De Diego L. F., Armesto L., and Cabanillas A., "Circulating Fluidized Bed Combustion in the Turbulent Regime: Modeling of Carbon Combustion Efficiency and Sulphur Retention", *Fuel*, Vol. 80, 1405–1414, 2001.

[32] Myohanen K., Hyppanen T., Miettinen J., and Parkkonen R., "Three-Dimensional Modeling and Model Validation of Circulating Fluidized Bed Combustion", in *Proceedings of the 17th International Conference on FBC* (Pisupati S., Ed.), ASME, No. 48, Jacksonville, Florida, USA, May 18-21, 2003.

[33] Zhang L., Li T. D., Zheng Q. Y., and Lu C. D., "A General Dynamic Model for Circulating Fluidized Bed Combustion Systems with Wide Particle Size Distribution", in *Proceedings of the 11th International Conference on FBC* (E. J. Anthony, Ed.), ASME, Vol. 3, 1289–1294, Montreal, Canada, April 21-24, 1991.

[34] Mori S., Narukawa K., Yamada I., Takebayashi T., Tanii H., Tomoyasu Y., and T. Mii, "Dynamic Model of a Circulating Fluidized Bed Coal Fired Boiler", in *Proceedings of the 11th International Conference on FBC* (E. J. Anthony, Ed.), ASME, Vol. 3, 1261–1265, Montreal, Canada, April 21-24, 1991.

[35] Hyppänen T., Lee Y. Y., Kettunen A., and Riiali J., "Dynamic Simulation of a CFB Based Utility Power Plant", in *Proceedings of the 12th International Conference on FBC* (Rubow N. L., Ed.), ASME, Vol. 2, 1121–1127, San Diego, California, USA, May 9-13, 1993.

[36] Park C. K. and Basu P., "A Model for Prediction of Transient Response to the Change of Fuel Feed Rate to a Circulating Fluidized Bed Boiler Furnace", *Chemical Engineering Science*, Vol. 52, No. 20, 3499–3509, 1997.

[37] Muir J. R., Brereton C., Grace J. R., and Lim C. J., "Dynamic Modeling for Simulation and Control of a Circulating Fluidized Bed Combustor", *AIChE Journal*, Vol. 43, No. 5, 1141–1152, 1997.

[38] Remberg C. G. and Fett F. N., "A Dynamic Simulation Model for Power Plants with Atmospheric and Pressurized Circulating Fluidized Bed Combustion: Interactions of Plant Components and Design Studies", in *Proceedings of the 15th International Conference on FBC* (R. B. Reuther, Ed.), ASME, No. 146, Savannah, Georgia, USA, May 16-19, 1999.

[39] Li Z., Ni W., Yue G., and Wang Z., "A Real Time Dynamic Mathematical Model of CFBC", in *Proceedings of the 15th International Conference on FBC* (R. B. Reuther, Ed.), ASME, No. 60, Savannah, Georgia, USA, May 16-19, 1999.

[40] Costa B., Faille D., Lamquet O., Marchiondelli C., and Spelta S., "Dynamic Modeling of a 250 MWe CFB Boiler", in *Proceedings of the 16th International Conference on FBC* (D. W. Geiling, Ed.), ASME, No. 36, Reno, Nevada, USA, May 13-16, 2001.

[41] Chen Y., Zuwei H., and Mingdao X., "Dynamic Modeling for Simulation of 410 t/h Pyroflow CFB Boiler", in *Proceedings of the 16th International Conference on FBC* (D. W. Geiling, Ed.), ASME, No. 56, Reno, Nevada, USA, May 13-16, 2001.

[42] Kettunen A., Hyppanen T., Kirkinen A., and Maikkola E., "Model-Based Analysis of Transient Behavior of Large Scale CFB Boilers", in *Proceedings of the 17th International Conference on FBC* (Pisupati S., Ed.), ASME, No. 130, Jacksonville, Florida, USA, May 18-21, 2003.

[43] Hongwei C., Jianqiang G., Yonghua L., and Zhi Z., "Real-Time Simulation Model on Combustion System of 450 t/h Circulating Fluidized Bed Boiler", in *Proceedings of the 17th International Conference on FBC* (Pisupati S., Ed.), ASME, No. 96, Jacksonville, Florida, USA, May 18-21, 2003.

[44] Yerushalmi J. and Avidam A., *High Velocity Fluidization*, 225–291. New York , *Academic Press*, 1985.

[45] Rhodes M. J. and Geldart D., "A Model for the Circulating Bed", *Powder Technology*, Vol. 53, 155–162, 1987.

[46] Svensson A., Johnsson F., and Leckner B., "Fluid Dynamics of the Bottom Bed of CFB Boilers", in *Proceedings of the 12th International Conference*

on FBC (Rubow N. L., Ed.), ASME, Vol. 1, 887–897, San Diego, California, USA, May 9-13, 1993.

[47] Adanez J., Gayan P., Garcia-Labiano F., and De Diego L. F., "Axial Voidage Profiles in Fast Fluidized Beds", *Powder Technology*, Vol. 81, 259–268, 1994.

[48] Johnsson F. and Leckner B., "Vertical Distribution of Solids in a CFB Furnace", in *Proceedings of the 13th International Conference on FBC* (Heinschel K. J., Ed.), ASME, Vol. 1, 671–679, Orlando, Florida, USA, May 7-10, 1995.

[49] Andersson S., Johnsson F., and Leckner B., "Fluidization Regimes in Non-Slugging Fluidized Beds", in *Proceedings of the 10th International Conference on FBC* (Manaker A. M., Ed.), ASME, Vol. 1, 239–247, San Francisco, USA, 30 April - 3 May, 1989.

[50] Svensson A., Johnsson F., and Leckner B., "Fluidization Regimes in Circulating Fluidized Bed Boilers", in *Proceedings of the Fluidization VII: International Symposium of the Engineering Foundation* (Potter O. E. and Nicklin D. J., Eds.), AIChE, Brisbane, Australia, May 3-8, 1992.

[51] Werther J. and Wein J., "Expansion Behavior of Gas Fluidized Beds in the Turbulent Regime", *AIChE Symposium Series: Fluid Particle Technology*, Vol. 90, No. 301, 31–44, 1994.

[52] Svensson A., Johnsson F., and Leckner B., "Bottom Bed Regimes in a Circulating Fluidized Bed Boiler", *International Journal of Multiphase Flow*, Vol. 22, No. 6, 1187–1204, 1996.

[53] Zijerveld R. C, Johnsson F., Marzocchella A., Schouten J. C, and Van den Bleek C. M., "Fluidization Regimes and Transitions from Fixed Bed to Dilute Transport Flow", *Powder Technology*, Vol. 95, 185–204, 1998.

[54] Schnitzlein M. and Weinstein H., "Flow Characterization in High Velocity Fluidized Beds Using Pressure Fluctuations", *Chemical Engineering Science*, Vol. 43, 2605–2614, 1988.

[55] Bolton L. W. and Davidson J. F., "Recirculation of Particles in Fast Fluidized Risers", in *Proceedings of the 2nd International Conference on CFB* (Basu P. and Large J. F., Eds.), Pergamon Press, 139–146, Compiegne, France, May 14-18, 1988.

[56] Brereton C. M. H. and Grace J. R., "Microstructural Aspects of the

Behaviour of Circulating Fluidized Beds", *Chemical Engineering Science*, Vol. 48, 2564–2572, 1993.

[57] Bai D., Shibuya E., Masuda Y., Nakagawa N., and Kato K., "Flow Structure in a Fast Fluidized Bed", *Chemical Engineering Science*, Vol. 51, 957–966, 1996.

[58] Bi H. T., Ellis N., I. A. Abba, and Grace J. R., "A State of the Art Review of Gas-Solid Turbulent Fluidization", *Chemical Engineering Science*, Vol. 55, 4789–4825, 2000.

[59] Lee G. S. and Kim S. D., "Pressure Fluctuations in Turbulent Fluidized Beds", *Journal of Chemical Engineering Japan*, Vol. 21, 515–521, 1988.

[60] Leu L. P., Huang J. W., and Gua B. B., "Axial Pressure Distribution in Turbulent Fluidized Beds", in *Proceedings of the 2nd Asian Conference on Fluidized Bed and Three Phase Reactors* (Lu W. M. and Leu L. P., Eds.), 71–79, Kenting, Taiwan, 1990.

[61] Horio M., "Hydrodynamics of Circulating Fluidization: Present Status and Research Needs", in *Proceedings of the 3rd International Conference on CFB* (Basu P., Horio M., and Hasatani M., Eds.), Pergamon Press, 3–14, Nagoya, Japan, October 14-18, 1990.

[62] Najajima M., Harada M., Asai M., Yamazaki R., and Jimbo G., "Bubble Fraction and Voidage in an Emulsion Phase in the Transition to a Turbulent Fluidized Bed", in *Proceedings of the 3rd International Conference on CFB* (Basu P., Horio M., and Hasatani M., Eds.), Pergamon Press, 79–84, Nagoya, Japan, October 14-18, 1991.

[63] Bi H. T. and Grace J. R., "Effects of Measurement Method on Velocities Used to Demarcate the Transition to Turbulent Fluidization", *Chemical Engineering Journal*, Vol. 57, 261–267, 1995.

[64] F. Johnsson, Andersson S., and Leckner B., "Expansion of a Freely Bubbling Fluidized Bed", *Powder Technology*, Vol. 68, 117–123, 1991.

[65] Davidson J. F. and Harrison D., "Fluidized Particles". New York , *Cambridge University Press*, 1963.

[66] Darton R. C., La Nauze R. D., Davidson J. F., and Harrison D., "Bubble Growth due to Coalesence in Fluidized Beds", *Transactions of the American Institute of Chemical Engineers*, Vol. 55, 274–283, 1977.

[67] Broadhurst T. E. and Becker H. A, "Onset of Fluidization and Slugging in Beds of Uniform Particles", *AIChE Journal*, Vol. 21, No. 2, 238–247, 1975.

[68] Ergun S., "Fluid Flow Through Packed Columns", *Chemical Engineering Progress*, Vol. 48, 89–94, 1952.

[69] Koenigsdorff R. and Werther J., "Gas-Solid Mixing and Flow Structure Modeling of the Upper Dilute Zone of a Circulating Fluidized Bed", *Powder Technology*, Vol. 82, 317–329, 1995.

[70] Hartge E. U., Rensner D., and Werther J., "Solid Concentration and Velocity Patterns in Circulating Fluidized Beds", in *Proceedings of the 2nd International Conference on CFB* (Basu P. and Large J. F., Eds.), Pergamon Press, 165–180, Compiegne, France, May 14-18, 1988.

[71] Werther J., Hartge E. U., and Kruse M., "Radial Gas Mixing in the Upper Dilute Core of a Circulating Fluidized Bed", *Powder Technology*, Vol. 70, No. 3, 293–301, 1992.

[72] Horio M., Morishita K., Tachibana O., and Murata M., "Solids Distribution and Movement in Circulating Fluidized Beds", in *Proceedings of the 2nd International Conference on CFB* (Basu P. and Large J. F., Eds.), Pergamon Press, 147–154, Compiegne, France, May 14-18, 1988.

[73] Li H., Xia Y., Tung Y., and Kwauk M., "Micro-Visualization of Two-Phase Structure in a Fast Fluidized Bed", in *Proceedings of the 3rd International Conference on CFB* (Basu P., Horio M., and Hasatani M., Eds.), Pergamon Press, 183–188, Nagoya, Japan, October 14-18, 1991.

[74] Harris B J. and Davidson F., "Modelling Options for Ciculating Fluidized Beds: A Core/Annulus Depositions Model", in *Proceedings of the 4th International Conference on CFB* (Avidan A. A., Ed.), American Institute of Chemical Engineers, 32–39, Somerset, Pennsylvania, USA, August 1-5, 1994.

[75] Li Y. and Kwauk M., "The Dynamics of Fast Fluidization", in *Proceedings of the Fluidization III: International Symposium of the Engineering Foundation* (Grace J. R. and Matsen J. M., Eds.), Plenum Press, 537–544, Henniker, New Hampshire, USA, August 3-8, 1980.

[76] Wen C. Y. and Chen L. H:, "Fluidized Bed Freeboard Phenomena: Entrainment and Elutriation", *AIChE Journal*, Vol. 28, No. 1, 117–128, 1982.

[77] Arena U., Massimilla L., and Pirozzi D., "Hydrodynamic Behavior of Two Circulating fluidized Bed Units of Different Sizes", in *Proceedings of the 2nd International Conference on CFB* (Basu P. and Large J. F., Eds.), Pergamon Press, 223–230, Compiegne, France, May 14-18, 1988.

[78] Kunii D. and Levenspiel O., "Flow Modeling of Fas Fluidized Beds", in *Proceedings of the 3rd International Conference on CFB* (Basu P., Horio M., and Hasatani M., Eds.), Pergamon Press, 91–98, Nagoya, Japan, October 14-18, 1991.

[79] Berrui F. and Kalogerakis N., "Modelling of Internal Flow Structure of Circulating Fluidized Beds", *Canadian Journal of Chemical Engineering*, Vol. 67, 1010–1014, 1989.

[80] Rhodes M. J., "Modeling the Flow Structure of Upward-Flowing Gas-Solid Suspensions", *Powder Technology*, Vol. 60, 27–38, 1990.

[81] Senior R. C. and Brereton C. M. H., "Modelling of Circulating Fluidized Bed Solid Flow and Distribution", *Chemical Engineering Science*, Vol. 47, 281–296, 1992.

[82] Harris B. J., "The Hydrodynamics of Circulating Fluidized Beds", *PhD Thesis*, Cambridge University, Cambridge, England, 1992.

[83] De Diego L. F., Gayan P., and Adanez J., "Modeling of the Flow Structure in Circulating Fluidized Beds", *Powder Technology*, Vol. 85, 19–27, 1995.

[84] Davidson J. F., "Circulating Fluidized Bed Hydrodynamics", *Powder Technology*, Vol. 113, 249–260, 2000.

[85] Sinclair J. L. and Jackson R., "Gas-Particle Flow in a Vertical Pipe with Particle-Particle Interactions", *AIChE Journal*, Vol. 35, 1473–1486, 1989.

[86] Tsuo Y. P. and Gidaspow D., "Computation of Flow Patterns in Circulating Fluidized Beds", *AIChE Journal*, Vol. 36, 885–896, 1991.

[87] Pita J. P. and Sundaresan S., "Developing Flow of a Gas-Particle Mixture in a Vertical Riser", *AIChE Journal*, Vol. 39, No. 4, 541–552, 1993.

[88] Sinclair J. L., "Hydrodynamic Modeling", in *Circulating Fluidized Beds* (Grace J. R, Knowlton T. M., and Avidan A. A., Eds.), Springer, London, UK, 149–177, 1997.

[89] Pugsley T. S and Berruti F., "A Predictive Hydrodynamic Model for Circulating Fluidized Bed Risers", *Powder Technology*, Vol. 89, 57–69, 1996.

[90] Grace J. R. and Taghipour F., "Verification and Validation of CFD Models and Dynamic Similarity for Fluidized Beds", *Powder Technology*, Vol. 139, 99–110, 2004.

[91] Van Wachem B. G. M., Schouten J. C, Van den Bleek C. M, Krishna R., and Sinclair J. L., "Comparative Analysis of CFD Models of Dense Gas-Solid Systems", *AIChE Journal*, Vol. 47, No. 5, 1035–1051, 2001.

[92] Berruti F., Chaouki J., Godfroy L., Pugsley T. S., and Patience G. S., "Hydrodynamics of Circulating Fluidized Bed Risers: A Review", *The Canadian Journal of Chemical Engineering*, Vol. 73, 579–602, 1995.

[93] Cruz E., Steward F. R., and Pugsley T., "Modeling of CFB Riser Hydrodynamics Using Fluent", in *Proceedings of the 7th International Conference on CFB* (Grace J. R., Zhu J., and De Lasa H., Eds.), Canadian Society for Chemical Engineering, 310–316, Niagara Falls, Ontario, Canada, May 5-8, 2002.

[94] Patience G. S. and Chaouki J., "Gas Phase Hydrodynamics in the Riser of a Circulating Fluidized Bed", *Chemical Engineering Science*, Vol. 48, 3195–3205, 1993.

[95] Werther J., "Fluid Mechanics of Large Scale CFB Units", in *Proceedings of the 5th International Conference on CFB* (Kwauk M. and Li J., Eds.), Science Press, 1–14, Beijing, China, August 1-5, 1994.

[96] Zhang W., Johnsson F., and Leckner B., "Fluid-Dynamic Boundary Layers in CFB Boilers", *Chemical Engineering Science*, Vol. 50, No. 2, 201–210, 1995.

[97] Bai D., Shibuya E., Masuda Y .and Nishio K., Nakagawa N., and Kato K., "Distinction Between Upward and Downward Flows in Circulating Fluidized Beds", *Powder Technology*, Vol. 84, 75–81, 1995.

[98] Bi H. T., Zhou J., qin S. Z., and Grace J. R., "Annular Wall Layer Thickness in Circulating Fluidized Bed Risers", *Canadian Journal of Chemical Engineering*, Vol. 74, 811–814, 1996.

[99] Tian Z., Fu H., and Dong X., "Microcirculation Movement with Vortex of Fine Particulate Solids in a Circulating Fluidized Bed and Its Great Influ-

ence on Furnace Processes of CFB", in *Proceedings of the 6th International Conference on CFB* (Werther J., Ed.), DECHEMA, 95–100, Wurzburg, Germany, August 22-27, 1999.

[100] Harris A. T., Thorpe R. B., and Davidson J. F., "Characterisation of the annular Film Thickness in Circulating Fluid-Bed Risers", *Chemical Engineering Science*, Vol. 57, 2579–2587, 2002.

[101] Kunii D. and Levenspiel O., "Entrainment of Solids from Fluidized Beds I. Hold-up of Solids in the Freeboard II. Operation of Fast Fluidized Beds", *Powder Tehnology*, Vol. 61, 193–206, 1990.

[102] Wirth K. E., "Steady State Diagram for Circulating Fluidized Beds", in *Proceedings of the 3rd International Conference on CFB* (Basu P., Horio M., and Hasatani M., Eds.), Pergamon Press, 99–104, Nagoya, Japan, October 14-18, 1990.

[103] Kunii D. Levenspiel O., "Fluidized Reactor Models: 1. For Bubbling Beds of Fine, Intermediate and Large Particles. 2. For the Lean Phase: Freeboard and Fast Fluidization", *Industrial and Engineering Chemistry and Research*, Vol. 29, 1226–1234, 1990.

[104] Hazlett J. D. and Bergougnou M. A., "Influence of Bubble Size Distribution at the Bed Surface on Entrainment Profile", *Powder Technology*, Vol. 70, 99–107, 1992.

[105] Choi J. H., Ryu H. J., Shun D. W., Son J. E., and Kim S. D., "Temperature Effect on the Particle Entrainment Rate in a Gas Fluidized Bed", *Industrial and Engineering Chemistry and Research*, Vol. 37, 1130–1135, 1998.

[106] Choi J. H., Chang I. Y, Shun D. W., Yi C. K, Son J. E., and Kim S. D., "Correlation on the Particle Entrainment Rate in Gas Fluidized Beds", *Industrial and Engineering Chemistry and Research*, Vol. 38, 2491–2496, 1999.

[107] Rhodes M. and Geldart D., "The Upward Flow of Gas/Solid Suspensions, Part 1: A Model for the Circulating Fluidized Bed Incorporating Dual Level Gas Entry into the Riser", *Chemical Engineering Research and Design*, Vol. 67, 20–29, 1989.

[108] Kunii D. and Levenspiel O., "Fluidization Engineering". *Wiley, New York, USA*, 1st Ed., 1969.

[109] Schnelle K. B. Jr. and Brown C. A., "Air Pollution Control Technology Handbook". *CRC Press, Florida, USA*, 1st Ed., 2002.

[110] De Nevers N., "Air Pollution Control Engineering". *McGraw-Hill, New York, USA*, 2nd Ed., 2000.

[111] Geldart D. and Jones P., "The Behavior of L-Valves with Granular Powders", *Powder Technology*, Vol. 67, 163–174, 1991.

[112] Park D, Levenspiel O., and Fitzgerald T. J., "Plume Model for Large Particle Fluidized Bed Combustors", *Fuel*, Vol. 60, 295–306, 1981.

[113] Brem G., "Overall Modeling of Atmospheric Fluidized Bed Combustion and Experimental Verification", in *Atmospheric Fluidized Bed Combustion: Research, Development and Application* (Valk M., Ed.), Elsevier, Amsterdam, 1995.

[114] Brereton C., "Combustion Performance", in *Circulating Fluidized Beds* (Grace J. R, Knowlton T. M., and Avidan A. A., Eds.), Springer, London, UK, 1996.

[115] Anthony D. B. and Howard J. B., "Coal Devolatilization and Hydrogasification", *AIChE Journal*, Vol. 22, No. 4, 625–656, 1976.

[116] Smoot D. L. and Pratt D. T., "Coal Combustion and Devolatilization". New York, USA , *Plenum Press*, 1985.

[117] Suuberg E. M., Peters W. A., and Howard J. B., "Product Composition and Kinetics of Lignite Pyrolysis", *Industrial and Engineering Process Design and Development*, Vol. 17, No. 1, 37–46, 1978.

[118] Kobayashi H., Howard J. B., and Sarofim A. F., "Coal Devolatilization at High Temperatures", in *Proceedings of 16th International Conference on Combustion*, The Combustion Institute, 411–425, Pittsburgh, USA, 1976.

[119] Smoot L. D., "Pulverized Coal Diffusion Flames: A Perspective Through Modeling", in *Proceedings of the 18th International Conference on Combustion*, The Combustion Institute, 1185–1202, Pittsburgh, USA, 1981.

[120] Contractor R., Dry R. J., White C., Mao Q. M., Konstantinidis S., and Potter O.E., "Circulating Fluidized Beds: Diameter, Solids Hold-up, Axial Gas Mixing and Contact Efficiency", *Powder Technology*, Vol. 111, 132–144, 2000.

[121] Stubington J. F. and Chan S. W., "The Interpretation of Oxygen-Probe Measurments in Fluidized Bed Combustors", *Journal of the Instituta of Energy*, Vol. 63, 139–142, 1990.

[122] Hayhurst A. N. and Tucker R. F., "The Combustion of Carbon Monoxide in a Two-Zone Fluidized Bed", *Combustion and Flame*, Vol. 79, 175–189, 1990.

[123] Hesketh R. P. Davidson J. F., "Combustion of Methane and Propane in an Incipiently Fluidized Bed", *Combustion and Flame*, Vol. 85, 449–467, 1991.

[124] Van der Vaart D. R., "Mathematical Modelling of Methane Combustion in a Fluidized Bed", *Industrial and Engineering Chemistry Research*, Vol. 31, 999–1007, 1992.

[125] Basu P. and Halder P. K., "Combustion of Single Carbon Particles in a Fast Fluidized Bed of Fine Solids", *Fuel*, Vol. 68, No. 8, 1056–1063, 1989.

[126] Basu P., "Combustion of Coal in Circulating Fluidized-Bed Boilers: A Review", *Chemical Engineering Science*, Vol. 54, 5547–5557, 1999.

[127] Field M. A. Gill D. W., Morgan R. B, and Hawksley P. G. W., "Combustion of Pulverized Coal". *British Coal Utilization Research Association*, 1967, Leatherhead, Great Britain.

[128] Caram H. S. and Amundson N. R., "Diffusion and Reaction in a Stagnant Boundary Layer About a Carbon Particle", *Industrial and Engineering Chemistry Fundamentals*, Vol. 16, No. 2, 171–181, 1977.

[129] Ross I. B., Patel M. S., and Davidson J. F., "The Temperature of Burning Carbon Particles in Fluidized Beds", *Transactions of Institution of Chemical Engineers*, Vol. 59, 83–88, 1981.

[130] Mon E. and Amundson N. R., "Diffusion and Reaction in a Stagnant Boundary Layer About a Carbon Particle: 2. An Extension", *Industrial and Engineering Chemistry Fundamentals*, Vol. 17, No. 4, 313–321, 1978.

[131] Linjewile T. M. and Agarwal P. K., "The Influence of Product CO/CO_2 Ratio of the Ignition and Temperature History of Petroleum Coke Particles in Incipiently Gas-Fluidized Beds", *Fuel*, Vol. 74, No. 1, 12–16, 1995.

[132] Fuertes A. B., Marban G., and Pis J. J., "Combustion Kinetics of Coke

Particles in a Fluidized Bed Reactor", *Fuel Processing Technology*, Vol. 38, 193–210, 1994.

[133] Overturf B. W. and Reklaitis G. V., "Fluidized Bed Reactor Model with Generalized Particle Balances Part II: Coal Combustion Application", *AIChE Journal*, Vol. 29, No. 5, 820–829, 1983.

[134] Hoy H. R. and Gill D. W., "The Combustion of Coal in Fluidized Beds", in *Principles of Combustion Engineering for Boilers* (Lawn C. J., Ed.), Academic Press, London, UK, 1987.

[135] Halder S. and Saha R. K., "Combustion Kinetics of Lignite Char in a Fluidized Bed", *Journal of the Institute of Energy*, Vol. 64, 55–61, 1991.

[136] Smith I. W., "The Intrinsic Reactivity of Carbons to Oxygen", *Fuel*, Vol. 57, 409–414, 1978.

[137] Basu P. and Subbarao D., "An Experimental Investigation of Burning Rate and Mass Transfer in a Turbulent Fluidized Bed", *Combustion and Flame*, Vol. 66, No. 3, 261–269, 1986.

[138] Hottel H. C., Williams G. C., Nerheim N. M., and Schneider G. R., "Kinetic Studies on Stirred Reactors, Combustion of Carbon Monoxide and Propane", in *Proceedings of the 10th International Symposium on Combustion*, The Combustion Institute, 111–121, Pittsburgh, USA, 1965.

[139] Howard J. B., Williams G. C., and Fine D. H., "Kinetics of Carbon Monoxide Oxidation in Postflame Gases", in *Proceedings of the 14th International Symposium on Combustion*, The Combustion Institute, 975–986, Pennsylvania, USA, 1973.

[140] Yetter R. A., Dryer F. L., and Rabitz H., "Complications of One-Step Kinetics for Moist CO Oxidation", in *Proceedings of the 21st International Symposium on Combustion*, The Combustion Institute, 749–760, Munich, Germany, 1986.

[141] Levenspiel O., Kunii D., and Fitzgerald T., "The Processing of Solids of Changing Size in Bubbling Fluidized Beds", *Powder Technology*, Vol. 2, 87–96, 1968.

[142] Chen T. P. and Saxena S. C., "Particle Size Distribution in a Fluidized Bed Reactor", *Powder Technology*, Vol. 15, 283–285, 1976.

[143] Overturf B. W. and Reklaitis G. V., "Fluidized Bed Reactor Model with Generalized Particle Balances Part I: Formulation and Solution", *AIChE Journal*, Vol. 29, No. 5, 813–819, 1983.

[144] Wang Q., Luo Z., Ni M., and Cen K., "Particle Population Balance Model for a Circulating Fluidized Bed Boiler", *Chemical Engineering Journal*, Vol. 93, 121–133, 2003.

[145] Chen T. P. and Saxena S. C., "Solids Population Balance for Attrition in Fluidized Beds", *Powder Technology*, Vol. 18, 279–281, 1977.

[146] Ray Y. C., Jiang T. S., and Jiang T. L., "Particle Population Model for a Fluidized Bed with Attrition", *Powder Technology*, Vol. 52, 35–48, 1987.

[147] Milioli F. E. and Foster P. J., "A Model for Particle Size Distribution and Elutriation in Fluidized Beds", *Powder Technology*, Vol. 83, 265–280, 1995.

[148] Weimer A. W. and Clough D. E., "Dynamics of Particle Size Conversion Distributions in Fluidized Beds: Application to Char Gasification", *Powder Technology*, Vol. 26, 11–16, 1980.

[149] Weimer A. W. and Clough D. E., "Modelling of Char Particle Size Conversion Distributions in a Fluidized Bed Gasifier: Non: Isothermal Efects", *Powder Technology*, Vol. 27, 85–103, 1980.

[150] Saastamoinena J. J., Tourunena A., Hämäläinen J., Hyppänen T., Loschkin M., and Kettunen A., "Analytical Solutions for Steady and Unsteady State Particle Size Distributions in FBC and CFBC Boilers for Nonbreaking Char Particles", *Combustion and Flame*, Vol. 132, 395–405, 2003.

[151] Zenz F. F. and Weil N. A., "A Theoretical-Empirical Approach to the Mechanism of Particle Entrainment from Fluidized Beds", *AIChE Journal*, Vol. 4, No. 4, 472–479, 1958.

[152] Tanaka I., Shinohara H., Hirosue H., and Tanaka Y., "Elutriation of Fines from Fluidized Bed", *Journal of Chemical Engineering of Japan*, Vol. 5, No. 1, 51–57, 1972.

[153] Merrick D. and Highley J., "Particle Size Reduction and Elutriation in a Fluidized Bed Process", *AIChE Symposium Series*, Vol. 70, No. 137, 366–378, 1974.

[154] Geldart D., Cullinan J., Georghiades S., Gilvray D, and Pope D. J., "The Effect of Fines on Entrainment from Fluidized Beds", *Transactions of the Institute of Chemical Engineers*, Vol. 57, 269–275, 1979.

[155] George S. E. and Grace J. R., "Entrainment of Particles from Pilot Scale Fluidized Beds", *Canadian Journal of Chemical Engineering*, Vol. 59, 279–284, 1982.

[156] Smolders K. and Baeyens J., "Elutriation of Fines from Gas Fluidized Beds: Mechanism of Elutriation and Effect of Freeboard Geometry", *Powder Technology*, Vol. 92, 35–46, 1997.

[157] Tasirin S. M. and Geldart D., "Entrainment of FCC from Fluidized Beds: A New Correlation for the Elutriation Rate Constants $K_{i\infty}^*$", *Powder Technology*, Vol. 95, 240–247, 1998.

[158] Wakao N., Kaguei S., and Funazkri T., "Effects of Fluid Dispersion Coefficients on Particle to Fluid Heat Transfer Coefficients in Packed Beds", *Chemical Engineering Science*, Vol. 34, No. 3, 325–336, 1979.

[159] Kunii D. and Levenspiel O., "Fluidization Engineering". Boston, USA , *Butterworth-Heinemann*, 2nd Ed., 1991.

[160] Basu P. and Nag P. K., "Heat Transfer to Walls of a Circulating Fluidized Bed Furnace", *Chemical Engineering Science*, Vol. 51, No. 1, 1–26, 1996.

[161] Radhakrishnan K. and Hindmarsh A. C., "Description and Ose of LSODE, the Livermore Solver for Ordinary Differential Equations", in *Lawrance Livermore National Laboratory Report No: UCRL-ID-113855*, California, USA, 1993.

[162] Shampine L. F., Allen Jr. R. C., and Pruess S., "Fundamentals of Numerical Computing". *Wiley, New York, USA*, 1st Ed., 1997.

[163] Hairer E. and Wanner G., "Solving Ordinary Differential Equations II. Stiff and Differential-Algebraic Problems". New York, USA , *Springer Werlag*, 2nd Ed., 1991.

[164] Schiesser W. E., "The Numerical Method of Lines". New York, USA , *Academic Press*, 1st Ed., 1991.

[165] Oymak O., "Method of Lines Solution of Time-Dependent 2D Navier-Stokes

Equations for Incompressible Separated Flows", *PhD Thesis*, Middle East Technical University, Ankara, Turkey, 1997.

[166] Schiesser W. E., "Variable Grid Spatial Differentiator in the Numerical Method of Lines", in *DSS/2 Manual*, Lehigh University, Pittsburgh, USA, 1988.

[167] Silebi C. A. and Schiesser W. E., "Dynamic Modelling of Transport Process Systems". New York, USA , *Academic Press*, 1st Ed., 1992.

[168] Brown P. N., Byrne G. D., and Hindmarsh A. C., "VODE: A Variable Coefficient ODE Solver", *SIAM Journal on Scientific and Statistical Computing*, Vol. 10, No. 5, 1038–1051, 1989.

[169] Weiner R., Schmitt B. A., and Podhaisky H., "ROWMAP - A ROW-code with Krylow Techniques for Large Stiff ODEs", in *Technical Report No. 39*, FB Mathematik und Informatik, Universitäd Halle, Halle an der Saale, Germany, 1996.

[170] Wu S., "Combustion and sulfur Capture in Circulating Fluidized Beds", *PhD Thesis*, Technical University of Nova Scotia, Halifax, Nova Scotia, Canada, 1991.

[171] Park C. K., "Dynamic Behavior of Circulating Fluidized Bed Boiler Furnace", *Master's Thesis*, Technical University of Nova Scotia, Halifax, Nova Scotia, Canada, 1995.

[172] Sandler S. I., "Chemical and Engineering Thermodynamics". New York, USA , *John Wiley and Sons*, 3rd Ed., 1999.

APPENDICES A

DERIVATION OF ROSIN-RAMMLER PSD FUNCTION

In fluidized bed combustion applications, coal particles have a wide size distribution ranging from a microns to centimeters. The size distribution of coal particles is generally determined by use of a set of sieves and then resulting size distribution is represented by mathematical functions, *i.e.*, normal and log-normal distribution, Rosin-Rammler *etc.* Particle size distributions in fluidized bed combustion applications are generally represented by the Rosin-Rammler size distribution function as it is particularly suited to representing particles generated by grinding, milling and crushing operations. Rosin-Rammler size distribution function has the following form:

$$W(d_p) = \exp\left(-b{d_p}^n\right) \tag{A.1}$$

where $W(d_p)$ is the fractional mass of particles with diameter d_p. In terms of radius, r, Rosin-Rammler size distribution function can be expressed as,

$$W(r) = \exp\left(-b\,2^n\,r^n\right) \tag{A.2}$$

In the derivation of char particles size distribution, the fraction of particles with radius between r and $r + \Delta r$ is represented by $P_0(r)\Delta r$. Hence, the fractional mass with radius between r and $r + \Delta r$ is

$$P_0(r)\Delta r = -\frac{dW(r)}{dr}\Delta r \tag{A.3}$$

i.e.,

$$P_0(r) = -\frac{dW(r)}{dr} \tag{A.4}$$

Then, char particles size distribution function $P_0(r)$ can be found by taking the derivative of Rosin-Rammler size distribution function with respect to r as given below:

$$\frac{dW(r)}{dr} = -b\,n\,2^n\,r^{n-1}\,\exp\left(-b\,2^n\,r^n\right) \tag{A.5}$$

Substituting Equation A.5 into Equation A.4 gives the char particles size distribution function utilized for representation of the particle size distribution of feed char particles,

$$P_0(r) = b\,n\,2^n\,r^{n-1}\,\exp\left(-b\,2^n\,r^n\right) \tag{A.6}$$

Parameters required in Equation A.6, b and n, are found by non-linear curve fitting of particle size distribution obtained from sieve analysis.

APPENDICES B

DERIVATION OF CARBON CONSUMPTION RATE

Carbon consumption rate can be expressed in verbal form as follows,

$$\left\{ \begin{array}{c} rate\ of \\ char \\ depletion \end{array} \right\} = \rho_c \left\{ \begin{array}{c} number\ of \\ particles\ in\ the \\ interval\ \Delta r \end{array} \right\} \left\{ \begin{array}{c} decrease\ of \\ particle\ volume \\ due\ to\ combustion \end{array} \right\} \tag{B.1}$$

or in symbols,

$$\left\{ \begin{array}{c} rate\ of \\ char \\ depletion \end{array} \right\} = \rho_c \frac{M_d\, P_d(r)\, dr}{\rho_c \frac{4}{3}\pi r^3} \left(\frac{dV}{dt} \right) \tag{B.2}$$

Replacing dV by $4\pi r^2$ and rearranging gives,

$$\left\{ \begin{array}{c} mass\ of \\ char \\ depleted \end{array} \right\} = \frac{3\, M_d\, P_d(r)\, \Re(r)\, dr}{r} \tag{B.3}$$

Considering the wide size distribution of char particles, the total char depletion rate can be found as follows,

$$\left\{ \begin{array}{c} mass\ of \\ char \\ depleted \end{array} \right\} = \int_{r_{min}}^{r_{max}} \frac{3\, M_d\, P_d(r)\, \Re(r)}{r} dr \tag{B.4}$$

or

$$\left\{ \begin{array}{c} mass\ of \\ char \\ depleted \end{array} \right\} = 3\, M_d \int_{r_{min}}^{r_{max}} \frac{P_d(r)\, \Re(r)}{r} dr \tag{B.5}$$

As can be seen in Equation B.5, the unit of char depletion rate is $kg\ of\ char/s$. To convert it into $mole\ of\ C/s$ basis, it should be multiplied with the ratio of fixed carbon to char content of coal and should be divided into molecular weight of carbon, *i.e.*,

$$\left\{ \begin{array}{c} mass\ of \\ carbon \\ depleted \end{array} \right\} = 3\,M_d \frac{x_{fc}}{x_{fc}+x_{ash}} \frac{1}{M_C} \int_{r_{min}}^{r_{max}} \frac{P_d(r)\,\Re(r)}{r} dr \tag{B.6}$$

Equation B.6 gives the solid carbon consumption rate in the dense zone. As char particles considered to take place only in the emulsion phase, to find out the carbon consumption rate per unit volume of emulsion phase, Equation B.6 should be divided into total volume of emulsion phase, *i.e.*,

$$\left\{ \begin{array}{c} mass\ of \\ carbon \\ depleted \end{array} \right\} = \frac{3\,M_d}{V_d(1-\delta)\varepsilon_{mf}} \frac{x_{fc}}{x_{fc}+x_{ash}} \frac{1}{M_C} \int_{r_{min}}^{r_{max}} \frac{P_d(r)\,\Re(r)}{r} dr \tag{B.7}$$

or as shown in Equation 3.141,

$$n_{C,e} = \frac{3\,M_d}{V_d(1-\delta)\varepsilon_{mf}} \frac{x_{fc}}{x_{fc}+x_{ash}} \frac{1}{M_C} \int_{r_{min}}^{r_{max}} \frac{P_d(r)\,\Re(r)}{r} dr \tag{B.8}$$

APPENDICES C

FORTRAN CODES

C.1 Steady State Simulation Program: CFBCSIM

```
!*******************************************************************************
!
!  Purpose:
!  --------
!  Simulate CFB boilers working at steady-state conditions.
!
!  Main Assumptions:
!  -----------------
!  - Dense Zone  : Bubble and Emulsion (Well-mixed solids, Plug flow of gas)
!  - Dilute Zone : Dilute Upward Flow (Plug flow of gas and solids)
!
!  Record of Revisions:
!  --------------------
!
!  Date      Programmer        Description of Change
!  --------  ----------------  ---------------------------------------------
!  01/01/06  Y. Gogebakan      Original code
!
!*******************************************************************************

      program cfbcsim

      use global
      use constants

!     Type declarations

      implicit none

!     Open simulation history files and write file headers

      call logfiles

!     Read input data file

      call readinput

!     Check coal analyses

      call checkanalyses
```

```
!     Calculate properties of char

      call charprop

!     Calculate composition of volatile matter

      call vmcomp

!     Allocate arrays used in simulation

      call createarrays

!     Generate grid points

      call gridgen

!     Set assumed values

      call assumptions

!     Set initial estimates

      call estimates

!     Perform preliminary calculations

      call precalc

!     Perform stoichiometric combustion calculation

      call stoichcomb

!     Calculate dense zone hydrodynamics

    1 call hydrodense

!     Solve population balance

    2 call psd

!     Check for the convergence of population balance

      diff1 = dabs(mchardense_c-mchardense)
      write(log1,100) iter1,mchardense,mchardense_c,diff1
      mchardense = mchardense_c
      if (diff1.gt.1.0d-3) goto 2

!     Solve dense zone species balances

      call species

!     Check for the convergence of species balances

      diff2 = dabs(avgdense_o2fr_c-avgdense_o2fr)
      write(log2,100) iter2,avgdense_o2fr,avgdense_o2fr_c,diff2
```

```
      avgdense_o2fr = avgdense_o2fr_c
      if (diff2.gt.1.0d-4) goto 2

!     Solve dilute zone species and energy balances

    3 call dilute

!     Solve dense zone energy balances

      call energy_dilute_wall

!     Check for the convergence of energy balances

      diff5 = dabs(avgdilutewalltemp_c-avgdilutewalltemp)
      write(log5,100) iter5,avgdilutewalltemp,avgdilutewalltemp_c,diff5
      avgdilutewalltemp = avgdilutewalltemp_c
      if (diff5.gt.1.0d0) goto 3

!     Solve dense zone energy balances

      call energy

!     Check for the convergence of energy balances

      diff3 = dabs(avgchartemp_c-avgchartemp)
      write(log3,100) iter3,avgchartemp,avgchartemp_c,diff3
      avgchartemp = avgchartemp_c
      if (diff3.gt.1.0d0) goto 2

      diff4 = dabs(densetemp_c-densetemp)
      write(log4,100) iter4,densetemp,densetemp_c,diff4
      densetemp = densetemp_c
      if (diff4.gt.1.0d0) goto 1

!     Print results of simulation

      call printer

!     Calculate and print CPU time

      call cputime

!     Format statements

  100 format(1x,i4,3(4x,1pe14.7))

!     End of the program

      end program cfbcsim

!*******************************************************************************
```

C.2 Dynamic Simulation Program: CFBCDYNSIM

```
!*******************************************************************************
!
!  Purpose:
!  --------
!  Simulate CFB boilers working at dynamic conditions.
!
!  Main Assumptions:
!  -----------------
!  - Dense Zone  : Bubble and Emulsion (Well-mixed solids, Plug flow of gas)
!  - Dilute Zone : Dilute Upward Flow (Plug flow of gas and solids)
!
!  Record of Revisions:
!  --------------------
!
!  Date      Programmer        Description of Change
!  --------  ----------------  ---------------------------------------------
!  01/09/06  Y. Gogebakan      Original code
!
!*******************************************************************************

      program cfbcdynsim

      use global

!     Type declarations

      implicit none

!     Open simulation history files

      open(log0,file='Output\Simulation History - General.txt')

!     Read input data file

      call readinput

!     Calculate properties of char

      call charprop

!     Calculate composition of volatile matter

      call vmcomp

!     Allocate arrays used in simulation

      call createarrays

!     Generate grid points

      call gridgen

!     Set assumed values
```

```
      call assumptions

!     Read initial conditions

      call reader

!     Perform preliminary calculations

      call precalc

!     Calculate hydrodynamics

      call hydrodense
      call hydrodilute(1)

!     Transfer dependents and time derivatives to 1-d array

      call transfer

!     Set type of grid points for the calculation of spatial derivatives

      call setgridtype

!     Compute the initial derivatives

      nc = 1
      call derv
      nc = 2

!     Solve ODEs

      call solve_rowmap

!     Calculate and print CPU time

      call cputime

!     End of the program

      end program cfbcdynsim

!*******************************************************************************
```

APPENDICES D

INPUT DATA FILES

D.1 Input Data File of Test Case 1

```
!*****************************************************************************
!
!  Purpose:
!  --------
!  Input data of CFBCSIM
!
!  Source:
!  -------
!  PhD Thesis of Wu
!
!  Record of Revisions:
!  --------------------
!
!  Date      Programmer        Description of Change
!  --------  ----------------  ---------------------------------------------
!  01/09/06  Y. Gogebakan      Original code
!
!*****************************************************************************

!     Set number of cells and particle grid points

      ndense       = 31         ! Number of points in dense zone
      ndilute      = 51         ! Number of points in dilute zone
      nparticle    = 101        ! Number of points for particle size
      nwall        = 21         ! Number of points in the wall

!     Combustor specific parameters

      norifice     = 162        ! Number of orifices in the distributor plate
      whopper      = 0.200d0    ! Width of hopper section, m
      dhopper      = 0.200d0    ! Depth of hopper section, m
      hhopper      = 1.500d0    ! Heigth of hopper section, m
      wfurnace     = 0.200d0    ! Width of furnace section, m
      dfurnace     = 0.200d0    ! Depth of furnace section, m
      hfurnace     = 5.000d0    ! Heigth of furnace section, m
      dcutcyclone  = 60.0d-6    ! Cut size of cyclone, m

!     Physical properties of combustor walls

      cpwall       =  835.000d0 ! Heat capacity of wall material, j/kg.K
      kwall        =    1.300d0 ! Thermal conductivity of wall material, W/m.K
      denwall      = 1500.000d0 ! Density of wall material, kg/m^3
```

```
      thickwall    =    0.215d0 ! Thickness of wall, m

!     Properties of coal

      xvm          = 30.30d-2   ! Fraction of volatile matter, -
      xfc          = 52.95d-2   ! Fraction of fixed carbon, -
      xash         = 13.15d-2   ! Fraction of ash, -
      xh2o         = 3.60d-2    ! Fraction of moisture, -
      xc           = 71.99d-2   ! Fraction of carbon, -
      xh           = 5.00d-2    ! Fraction of hydrogen, -
      xn           = 1.24d-2    ! Fraction of nitrogen, -
      xo           = 4.43d-2    ! Fraction of oxygen, -
      xscomb       = 3.70d-2    ! Fraction of combustible sulfur, -
      xashd        = 13.64d-2   ! Fraction of ash, -
      dencoal      = 1400.0d0   ! Density of coal, kg/m^3
      rmaxcoal     = 6.000d-3   ! Maximum radius of coal, m
      rmincoal     = 6.000d-6   ! Minimum radius of coal, m
      sphcoal      = 1.0d0      ! Sphericity of coal, -
      rbcoal       = 1.139722d3 ! RR coefficient b of coal, -
      rncoal       = 1.074742d0 ! RR coefficient n of coal, -

!     Properties of inert bed material

      deninert     = 2400.0d0   ! Density of inert bed material, kg/m^3
      avgdpinert   = 0.350d-3   ! Average particle size of inerts, m
      sphinert     = 1.0d0      ! Sphericity of inert bed material, -
      kinert       = 3.1d0      ! Thermal conductivity of inert bed material,
      cpinert      = 800.0d0    ! Heat capacity of inert bed material,

!     Operating parameters

      airrate1     = 49.00d-3   ! Primary air flow rate, Nm^3/s
      airrate2     = 29.00d-3   ! Secondary air flow rate, Nm^3/s
      airtemp      = 308.15d0   ! Fluidizing air temperature, K
      fcoal        = 7.770d-3   ! Coal flow rate, kg/s

!*************************************************************************
```

D.2 Input Data File of Test Case 2

```
!*************************************************************************
!
!  Purpose:
!  --------
!  Input data of CFBCSIM
!
!  Source:
!  -------
!  PhD Thesis of Park
!
!  Record of Revisions:
!  --------------------
!
!  Date      Programmer        Description of Change
!  --------  ----------------  --------------------------------------------
!  01/09/06  Y. Gogebakan      Original code
!
!*************************************************************************

!     Set number of cells and particle grid points

      ndense       = 31         ! Number of points in dense zone
      ndilute      = 51         ! Number of points in dilute zone
      nparticle    = 101        ! Number of points for particle size
      nwall        = 21         ! Number of points in the wall

!     Combustor specific parameters

      norifice     = 162        ! Number of orifices in the distributor plate
      whopper      = 0.230d0    ! Width of hopper section, m
      dhopper      = 0.230d0    ! Depth of hopper section, m
      hhopper      = 1.500d0    ! Heigth of hopper section, m
      wfurnace     = 0.230d0    ! Width of furnace section, m
      dfurnace     = 0.230d0    ! Depth of furnace section, m
      hfurnace     = 4.850d0    ! Heigth of furnace section, m
      dcutcyclone  = 60.0d-6    ! Cut size of cyclone, m

!     Physical properties of combustor walls

      cpwall       =  800.000d0 ! Heat capacity of wall material, j/kg.K
      kwall        =    1.300d0 ! Thermal conductivity of wall material, W/m.K
      denwall      = 1500.000d0 ! Density of wall material, kg/m^3
      thickwall    =    0.215d0 ! Thickness of wall, m

!     Properties of coal

      xvm          = 33.700d-2  ! Fraction of volatile matter, -
      xfc          = 54.060d-2  ! Fraction of fixed carbon, -
      xash         = 11.010d-2  ! Fraction of ash, -
      xh2o         =  1.230d-2  ! Fraction of moisture, -
      xc           = 72.441d-2  ! Fraction of carbon, -
      xh           =  4.890d-2  ! Fraction of hydrogen, -
      xn           =  1.407d-2  ! Fraction of nitrogen, -
      xo           =  5.498d-2  ! Fraction of oxygen, -
```

```
      xscomb       =  4.617d-2  ! Fraction of combustible sulfur, -
      xashd        = 11.147d-2  ! Fraction of ash, -
      dencoal      = 1400.0d0   ! Density of coal, kg/m^3
      rmaxcoal     =  4.000d-3  ! Maximum radius of coal, m
      rmincoal     =  4.000d-6  ! Minimum radius of coal, m
      sphcoal      = 1.0d0      ! Sphericity of coal, -
      rbcoal       = 656.7841d0 ! RR coefficient b of coal, -
      rncoal       =   0.9503d0 ! RR coefficient n of coal, -

!     Properties of inert bed material

      deninert     = 2200.0d0   ! Density of inert bed material, kg/m^3
      avgdpinert   = 0.337d-3   ! Average particle size of inerts, m
      sphinert     = 1.0d0      ! Sphericity of inert bed material, -
      kinert       = 3.0d0      ! Thermal conductivity of inert bed material,
      cpinert      = 750.0d0    ! Heat capacity of inert bed material,

!     Operating parameters

      airrate1     =  62.64d-3  ! Primary air flow rate, Nm^3/s
      airrate2     =  35.32d-3  ! Secondary air flow rate, Nm^3/s
      airtemp      = 298.15d0   ! Fluidizing air temperature, K
      watertemp    = 293.15d0   ! Cooling water temperature, K
      fcoal        =  11.55d-3  ! Coal flow rate, kg/s

!*******************************************************************************
```

APPENDICES E

THERMOPHYSICAL PROPERTIES

E.1 Molecular Weights

Specie	MW (kg/mol)
C	12×10^{-3}
H	1×10^{-3}
O	16×10^{-3}
N	14×10^{-3}
S	32×10^{-3}
H_2	2×10^{-3}
N_2	28×10^{-3}
O_2	32×10^{-3}
CO	28×10^{-3}
CO_2	44×10^{-3}
H_2O	18×10^{-3}
SO_2	64×10^{-3}

E.2 Standard Heats of Combustion and Vaporization

- Latent heat of combustion of C to CO (J/mol) [172]

$$\Delta H_{C \rightarrow CO} = 1.10524 \times 10^5 \tag{E.1}$$

- Latent heat of combustion of CO to CO_2 (J/mol) [172]

$$\Delta H_{CO \rightarrow CO_2} = 2.82989 \times 10^5 \tag{E.2}$$

- Latent heat of combustion of H to H_2O (J/mol) [172]

$$\Delta H_{H \rightarrow H_2O} = 2.41827 \times 10^5 \tag{E.3}$$

- Latent heat of combustion of S to SO_2 (J/mol) [172]

$$\Delta H_{S \rightarrow SO_2} = 2.96813 \times 10^5 \tag{E.4}$$

- Latent heat of vaporization of water (J/kg) [172]

$$\lambda^o = 2.44230 \times 10^6 \tag{E.5}$$

E.3 Physical Constants

- Gravitational acceleration (m/s^2)

$$g = 9.807 \tag{E.6}$$

- Gas constant $(J/mol.K)$

$$R = 8.314 \tag{E.7}$$

- Stefan-Boltzmann constant $(W/m^2.K^4)$

$$\sigma = 5.67 \times 10^{-8} \tag{E.8}$$

E.4 Thermophysical Properties of Gases

- Gas density (kg/m^3)

$$\rho_g = 323.76373 \left(T - 4.6996817\right)^{-0.99007228} \tag{E.9}$$

- Gas viscosity $(kg/m.s)$

$$\mu_g = 2.9901393 \times 10^{-7} \left(T + 10.092613\right)^{0.71630135} \tag{E.10}$$

- Gas thermal conductivity $(J/m.s.K)$

$$k_g = 8.62496 \times 10^{-3} + 5.69351 \times 10^{-5}\,T + 2.70155 \times 10^{-9}\,T^2 \qquad \text{(E.11)}$$

- Specific heat capacities $(J/mol.K)$ [172]

$$c_{p,g} = a + b\,T + c\,T^2 + d\,T^3 \qquad \text{(E.12)}$$

	a	b	c	d
Air	28.088	0.197×10^{-2}	0.480×10^{-5}	-1.965×10^{-9}
N_2	28.883	-0.157×10^{-2}	0.808×10^{-5}	-2.871×10^{-9}
O_2	25.460	1.519×10^{-2}	-0.715×10^{-5}	1.311×10^{-9}
CO_2	22.243	5.977×10^{-2}	-3.499×10^{-5}	7.464×10^{-9}
CO	28.142	0.167×10^{-2}	0.537×10^{-5}	-2.221×10^{-9}
SO_2	25.762	5.791×10^{-2}	-3.809×10^{-5}	8.607×10^{-9}
H_2O	32.218	0.192×10^{-2}	1.055×10^{-5}	-3.593×10^{-9}

CURRICULUM VITAE

Education

1994 - 1998 **B.Sc.**
Modeling of Sulfur Retention in Fluidized Bed Combustors
Middle East Technical University
Department of Chemical Engineering
CGPA: 3.44/4.00 (Ranked 6^{th} out of 137 Graduates)

1998 - 2000 **M.Sc.**
Char Attrition in Fluidized Bed Combustors
Middle East Technical University
Department of Chemical Engineering
CGPA: 3.64/4.00

2000 - 2006 **Ph.D.**
Simulation of Circulating Fluidized Bed Combustors
Middle East Technical University
Department of Chemical Engineering
CGPA: 3.71/4.00

Employment

1998 - 2005 **Teaching Assistant**
Middle East Technical University
Department of Chemical Engineering

2001 - 2005 **Computer Coordinator**
Middle East Technical University
Department of Chemical Engineering

Academic Experience

- Assistantship to some undergraduate courses:
  - Introduction to Chemical Engineering
  - Chemical Engineering Thermodynamics
  - Fluid Mechanics
  - Fundamentals of Heat and Mass Transfer

    - Chemical Engineering Laboratories
    - Introduction to Computers and FORTRAN Programming

- Attended to *Summer Academy 98* organized by University of Erlangen-Nurnberg and İzmir Institute of Technology in İzmir, Turkey in 1998.
- Attended to *Mediterranean Combustion Symposium MCS 99* in Antalya, Turkey in 20-25 June 1999.
- Attended to *Symposium on Coal Policies in Turkey and Clean Coal Technologies* in Ankara, Turkey in 21-22 October 1999.
- Attended to a training course on *"Laser Diagnostics of Combustion Processes* organized by United Nations Industrial Development Organization (UNIDO) and International Centre for Science and High Technology (ICS) in NILES of Cairo University in Cairo, Egypt in 18-22 November 2000.
- Attended to 2^{nd} *Chemical Engineering Conference for Collaborative Research in Eastern Mediterranean* in Ankara, Turkey in 20-24 May 2001.
- Attended to 3^{rd} *International Symposium on Radiative Transfer* in Antalya, Turkey in 17-22 June 2001.
- Attended to 18^{th} *World Energy Congress* in Buenos Aires, Argentina in 21-25 October 2001.
- Attended to *Mediterranean Combustion Symposium MCS 03* in Marrakesh, Morocco in 8-13 June 2003.
- Attended to 18^{th} *International Conference on Fluidized Bed Combustion* in Toronto, Ontario, Canada in 22-25 May 2005.

Areas of Expertise

- Fluidized bed combustion
- Mathematical modeling
- Numerical analysis

Computer Skills

- **Experience:** Deployment and administration of Windows NT4/2000 servers (DNS, WWW, Active Directory), administration of network printing facilities
- **Programming Languages:** Fortran 77/90, Visual Fortran
- **Software Packages:** Microsoft Office (Word, Excel, PowerPoint, FrontPage, Visio), AutoCAD, TecPlot, SigmaPlot, MathCad, Compaq Visual Fortran, MiKTEX, BibTEX
- **Operating Systems:** Windows 9X/NT4/NT4 Server/2000/2000 Server/XP

Awards

- Hasan Orbey Award in Graduate Studies (Ph.D. Award), Department of Chemical Engineering, Middle East Technical University, 2004.

Refereed International Journal Articles

[1] Selçuk, N., Değirmenci, E. and Göğebakan, Y., *Assessment of Catalyst Deactivation Model for Sulfur Retention in Fluidized Bed Combustors*, Combustion Science and Technology, Vol. 153, pp. 95-111, 2000.

[2] Selçuk, N., Değirmenci, E. and Göğebakan, Y., *Modeling of a Bubbling AFBC with Volatiles Release*, Journal of Energy Resources Technology, Vol. 125, pp. 72-81, 2003

[3] Göğebakan, Y. and Selçuk, N., *Assessment of a Model with Char Attrition for a Bubbling AFBC*, Combustion Science and Technology, Vol. 176, pp. 799-818, 2004.

[4] Selçuk, N., Göğebakan, Y., Harmandar, H. and Altındağ, H., *Effect of Recycle on Combustion and Emission Characteristics of High Sulfur Lignite*, Combustion Science and Technology, Vol. 176, pp. 959-975, 2004.

[5] Altındağ, H., Göğebakan, Y. and Selçuk, N., *Modeling of Sulfur Capture for Fluidized Bed Combustion of High Sulfur Content Lignites and Its Validation*, Applied Energy, Vol. 79/4, pp. 403-424, 2004.

[6] Selçuk, N., Göğebakan, Y., and Göğebakan, Z., *Partitioning Behavior of Trace Elements During Pilot-Scale Fluidized Bed Combustion of High Ash Content Lignite*, Journal of Hazardous Materials, Vol. B137, pp. 1698-1703, 2006.

[7] Afacan, O., Göğebakan, Y. and Selçuk, N., *Modeling of NOx Emissions from Fluidized Bed Combustion of High Volatile Lignites*, Combustion Science and Technology, Vol. 179, pp. 1-21, 2007.

Refereed Papers in International Conference Proceedings

[1] Selçuk, N., Değirmenci, E. and Göğebakan, Y., *Assessment of Catalyst Deactivation Model for Sulfur Retention in Fluidized Bed Combustors*, Proceedings of the 1^{st} Mediterranean Combustion Symposium (Ed. Beretta, F.), Antalya, Turkey, pp. 798-812, 1999.

[2] Selçuk, N., Değirmenci, E. and Göğebakan, Y., *Modeling of a Bubbling AFBC with Volatiles Release*, Proceedings of the 16^{th} International Conference on Fluidized Bed Combustion (Ed. Bonk, D. L. and Geiling, D. W.), ASME, Reno, Nevada, USA, Paper No:134 in CD-ROM, 2001.

[3] Göğebakan, Y. and Selçuk, N., *Assessment of a Model with Char Attrition for a Bubbling AFBC*, Proceedings of the 3^{rd} Mediterranean Combustion

Symposium (Ed. Beretta, F. and Bouhafid, A.), Marrakesh, Morocco, pp. 164-175, 2003.

[4] Selçuk, N., Göğebakan, Y., Harmandar, H. and Altındağ, H., *Effect of Recycle on Combustion and Emission Characteristics of High Sulfur Lignite*, Proceedings of the 3^{rd} Mediterranean Combustion Symposium (Ed. Beretta, F. and Bouhafid, A.), Marrakesh, Morocco, pp. 227-236, 2003.

[5] Selçuk, N., Göğebakan, Y., and Altındağ, H. *Co-Firing of Steam Coal with High Sulfur Content Lignite in a Bubbling Fluidized Bed Combustor*, Proceedings of the 18^{th} International Conference on Fluidized Bed Combustion (Ed. Lufei, J.), ASME, Toronto, Ontario, Canada, Paper No: FBC2005-78067 in CD-ROM, 2005.

[6] Selçuk, N., Göğebakan, Y., and Göğebakan, Z., *Partitioning of Trace Elements During Fluidized Bed Combustion of High Ash Content Lignite*, Proceedings of the 18^{th} International Conference on Fluidized Bed Combustion (Ed. Lufei, J.), ASME, Toronto, Ontario, Canada, Paper No: FBC2005-78068 in CD-ROM, 2005.

[7] Selçuk, N., Ayrancı, I. and Göğebakan, Y., *Effect of Recycle on Radiative Heat Transfer in the Freeboard of a Fluidized Bed Combustor*, Proceedings of the 18^{th} International Conference on Fluidized Bed Combustion (Ed. Lufei, J.), ASME, Toronto, Ontario, Canada, Paper No: FBC2005-78069 in CD-ROM, 2005.

[8] Afacan, O., Göğebakan, Y. and Selçuk, N., *Modeling of NOx Emissions from Fluidized Bed Combustion of High Volatile Lignites*, Proceedings of the 4^{th} Mediterranean Combustion Symposium (Ed. Beretta, F. and Costa, M.), Lisbon, Portugal, Paper No: 78 in CD-ROM, 2005.

Research Projects

[1] Selçuk, N., Göğebakan, Y., Tarhan, T., Batu, A., Ayrancı, I., Harmandar, H. and Altındağ, H.,*Clean and Efficient Energy Production from Turkish Lignites Using Fluidized Bed Combustion Technologies*, TÜBİTAK, MİSAG-159, Ankara, January 2003.

[2] Selçuk, N., Göğebakan, Y., Göğebakan, Z., Uygur, A. B., Afacan, M. O., Kürkçü, M., Karaismail, E., Çayan, F. N., *Co-firing of Biomass with Coal in Fluidized Bed Combustors*, TÜBİTAK, MAG-104M200 (Continuing).

Contract Research Projects

[1] Selçuk, N., Göğebakan Y. and Tarhan T., *Generation of Database Related to Steam Generation in Coal-Fired Fluidized Bed Combustion Systems*, METU, AGUDOS 2003-03-04-03, February 2002, Ankara.

[2] Selçuk, N., Göğebakan, Y., Altındağ, H., Tarhan, T. and Uygur, A. B., *Determination of Combustion and Sulfur Capture Performance for Imported Coal and Imported Coal/Lignite Mixture in Fluidized Bed Combustor*, METU, AGUDOS 2003-03-04-04, July 2003, Ankara.

[3] Selçuk, N. and Göğebakan Y., *Development of a Limestone Reactivity Determination Procedure*, METU, AGUDOS 2004-03-04-2-00-03, July 2004, Ankara.

[4] Selçuk, N. and Göğebakan Y., *Technical Studies for 2x160 MWe Çan Circulating Fluidized Bed Power Plant and New Power Plants*, METU, AGUDOS 2004-03-04-2-00-01, December 2005, Ankara.

Hobbies

- Software development and computer programming
- Amateur photography
- Formula 1